

https://dspace.org/

Inhibition of sonic hedgehog pathway by small molecule inhibitors: Targeting colon cancer stem cells

Omar, Aadilah

2016-02-19
http://hdl.handle.net/10539/19630

Downloaded from a DSpace repository. https://dspace.org/

INHIBITION OF SONIC HEDGEHOG PATHWAY BY SMALL MOLECULE INHIBITORS: TARGETING COLON CANCER STEM CELLS

Aadilah Omar

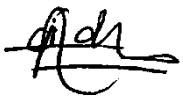
A dissertation submitted to the Faculty of Health Sciences, University of the Witwatersrand, in fulfillment of the requirements for the degree of Doctor of Philosophy (Internal Medicine).

Johannesburg, 2015

DECLARATION

I declare that this Dissertation is my own, unaided work. It is being submitted for the Degree of Doctor of Philosophy in Internal Medicine at the University of the Witwatersrand, Johannesburg. It has not been submitted before for any degree or examination at any other University.

Please see Appendix D for Turnitin report and Appendix E for ethics waiver.



_____

17th day of November 2015

ABSTRACT

Introduction, Methods, Results and Discussion/Conclusion

The existence of Cancer Stem Cells (CSC's) has been proven extensively in recent years. CSC's have been positively identified in, and isolated from colon cancer. They have been found to be resilient to therapy and are highly metastatic and it has been suggested that this could be attributed to the presence of CSC's expressing cell surface CD133. An active Hedgehog-Gli pathway has been detected in human colon carcinoma cells as well as their stem cells. Sonic Hedgehog (Shh) inhibitors such as cyclopamine have been successful in the treatment of other cancer types.

CSC's were isolated from HT29 and DLD1 cells using the CD133 surface protein and these cells were further characterized via their expression of key stem cell markers using fluorescence microscopy. These markers included c-Myc, KLF4 and alkaline phosphatase, all of which showed elevated expression levels in the CSC fraction. The growth pattern of CSC's in comparison to non-CSC's was analyzed using cell-impedance (xCELLigence) assays, with clear differences noted in their growth rates. Adhesion assays revealed that although CSC's have a lower proliferation rate, their adhesive potential proved to be greater, possibly due to them being highly metastatic. The effects of the Shh inhibitors cyclopamine and SANT-2 on cellular adhesion of colon CSC's were compared to the Shh pathway control molecule tomatidine, and a marked decrease in adhesion potential was noted. With regard to cell invasion, this was significantly decreased when CSC's were treated with the small molecule inhibitors. In cell migration/scratch assays a similar trend was seen, wherein cell migration was retarded by Hh pathway inhibition. Using confocal microscopy, the cell surface expression of Shh and CD133 was observed following treatment with cyclopamine and while found to significantly reduce Shh expression, CD133 expression remained unaffected.

Considering these *in vitro* results small molecule inhibitors targeting the Shh pathway appear to be promising therapeutic tools for the treatment of metastatic colon CSC's. Further investigation into the genes involved using PCR arrays would provide more detailed information on the drug action and allow for the development of an enhanced therapeutic.

ACKNOWLEDGEMENTS

I would like to thank Dr. Clement Penny for giving me this wonderful opportunity and also for all his advice, guidance and time, ensuring that my project was a success and my results submitted for the degree of Doctor of Philosophy.

For financial aid, I would like to acknowledge the University of the Witwatersrand for the Postgraduate Merit Award Scholarship and the National Research Foundation of South Africa for the Prestigious and Equity Scholarship.

Thanks to the members of the Penny laboratory, it was lovely to work with you all. A special thank you to my dear friend Katarina for always having faith in me and taking the time to proof read my thesis from the other side of the world!

I would like to thank the Almighty for without Him none of this would have been possible. All my success is due to his Will and I am very grateful for all that He has blessed me with.

Last but not least I would like to thank my parents for all the prayers and for cheering me on, and my partner and best friend Zaheer 'Boo' Abdulla ☺ for his words of encouragement. Without your support this work would not have been possible, your optimism and inspiration kept me going and I will always be grateful for this. Love you lots!

RESEARCH OUTPUT

Conference contributions:

- Omar A and Penny C. Inhibition of Sonic Hedgehog pathway with small molecule inhibitors: targeting colon cancer stem cells. Molecular Biology Research Thrust (MBRT) conference at The University of the Witwatersrand Postgraduate Development Hub, December 2013 – Second prize winner

- Omar A and Penny C. Inhibition of Sonic Hedgehog pathway with small molecule inhibitors: targeting colon cancer stem cells. South African Society of Biochemistry and Molecular Biology Congress, Goudini Spa Stellenbosch, July 2014.

- Omar A and Penny C. Inhibition of Sonic Hedgehog pathway with small molecule inhibitors: targeting colon cancer stem cells. Health Sciences Research Day at The University of the Witwatersrand, September 2014.

- Omar A and Penny C. Inhibition of Sonic Hedgehog pathway with small molecule inhibitors: targeting colon cancer stem cells. The University of the Witwatersrand Cross-faculty Symposium at the University of the Witwatersrand, October 2014.

LIST OF FIGURES

Figure 1: Illustration of the classical CSC concept 3

Figure 2: Shh pathway reactivation 8

Figure 3: Chemical structure of cyclopamine 9

Figure 4: Chemical structure of SANT-2 10

Figure 5: Chemical structure of tomatidine 11

Figure 6: Shh pathway inhibition 11

Figure 7: Shh pathway inhibition strategies 13

Figure 8: Basic principle of magnetic separation 22

Figure 9: Basic principle of adhesion assay 28

Figure 10: Basic principle of invasion assay 29

Figure 11: Basic principle of scratch/migration assay 30

Figure 12: Flow cytometry analysis charts 32

Figure 13: CD133+ spheroid growth 33

Figure 14: xCELLligence CI optimization charts 34-35

Figure 15: xCELLigence CI using optimal concentration 36-37

Figure 16: CD133 expression in DLD1 non-permeabilized cells 40-41

Figure 17: CD133 expression in HT29 non-permeabilized cells 42-43

Figure 18: CD133 expression in DLD1 permeabilized cells 44

Figure 19: CD133 expression in HT29 permeabilized cells 46

Figure 20: Graph summarizing CD133 expression in DLD1 and HT29 cells 47

Figure 21: Z-stack images of CD133+ non-permeabilized/permeabilized DLD1 cells 48

Figure 22: Z-stack images of CD133+ HT29 non-permeabilized/permeabilized cells 49

Figure 23: c-Myc expression in DLD1 cells 50-51

Figure 24: c-Myc expression in HT29 cells 52

Figure 25: Graph summarizing c-Myc expression in DLD1 and HT29 cells 53

Figure 26: KLF4 expression in DLD1 cells 54

Figure 27: KLF4 expression in HT29 cells 56

Figure 28: Graph summarizing KLF4 expression in DLD1 and HT29 cells 57

Figure 29: Alkaline phosphatase expression in DLD1 cells 58

Figure 30: Alkaline phosphatase expression in HT29 cells 60

Figure 31: Graph summarizing alkaline phosphatase expression in DLD1 and HT29 cells 61

Figure 32: Graphs illustrating adhesion potential results 62

Figure 33: Graphs illustrating effect on cell adhesion by cyclopamine 63

Figure 34: Graphs illustrating effect on cell adhesion by SANT-2 63

Figure 35: Graphs showing dose dependency assay with SANT-2 64

Figure 36: Graphs illustrating lack of effect on adhesion by tomatidine 64

Figure 37: Graphs illustrating effect on cell invasion by cyclopamine 65

Figure 38: Graphs illustrating effect on cell invasion by SANT-2 66

Figure 39: Graphs illustrating lack of effect on invasion by tomatidine 66

Figure 40: Images/graphs of scratch assay in DLD1 cells using cyclopamine 68-69

Figure 41: Images/graphs of scratch assay in HT29 cells using cyclopamine 70-71

Figure 42: Images and graphs of scratch assay in DLD1 cells using SANT-2 72-73

Figure 43: Images and graphs of scratch assay in HT29 cells using SANT-2 74-75

Figure 44: Microscopy images illustrating scratch assay using SANT-2 76

Figure 45: Images/graphs of scratch assay in DLD1 cells using tomatidine 77-78

Figure 46: Images/graphs of scratch assay in HT29 cells using tomatidine 79-80

Figure 47: Expression of Shh in DLD1 cells with application of cyclopamine 82

Figure 48: Expression of Shh in HT29 cells with application of cyclopamine 83

Figure 49: Graph illustrating effect of cyclopamine on Shh expression 84

Figure 50: Expression of Shh and CD133 in DLD1 cells with cyclopamine treatment 85

Figure 51: Expression of Shh and CD133 in HT29 cells with cyclopamine treatment 86

Figure 52: Graph illustrating effect of cyclopamine on Shh and CD133 expression 87

Figure 53: Acquired capabilities of cancer 97

Figure 54: Tumorigenic cell attachment and migration 98

Figure 55: Shh pathway activation, inhibition and mutations 102

LIST OF TABLES

Table 1: Dukes' classification for colon cancer staging 2

Table 2: Cell lines used and their origin 17

Table 3: Antibodies used in analyses 20

Table 4: CTCF of DLD1 CD133+ non-permeabilized cells 41

Table 5: CTCF of DLD1 CD133+ non-permeabilized cells negative control 42

Table 6: CTCF of DLD1 CD133- non-permeabilized cells 42

Table 7: CTCF of HT29 CD133+ non-permeabilized cells 43

Table 8: CTCF of HT29 CD133- non-permeabilized cells 43

Table 9: CTCF of DLD1 CD133+ permeabilized cells 45

Table 10: CTCF of DLD1 CD133- permeabilized cells 45

Table 11: CTCF of HT29 CD133+ permeabilized cells 47

Table 12: CTCF of HT29 CD133- permeabilized cells 47

Table 13: CTCF of DLD1 CD133+ cells stained with c-Myc antibody 51

Table 14: CTCF of DLD1 CD133- cells stained with c-Myc antibody 51

Table 15: CTCF of HT29 CD133+ cells stained with c-Myc antibody 53

Table 16: CTCF of HT29 CD133- cells stained with c-Myc antibody 53

Table 17: CTCF of DLD1 CD133+ cells stained with KLF4 antibody 55

Table 18: CTCF of DLD1 CD133- cells stained with KLF4 antibody 55

Table 19: CTCF of HT29 CD133+ cells stained with KLF4 antibody 57

Table 20: CTCF of HT29 CD133- cells stained with KLF4 antibody 57

Table 21: CTCF of DLD1 CD133+ cells stained with Alkaline phosphatase antibody 59

Table 22: CTCF of DLD1 CD133- cells stained with Alkaline phosphatase antibody 59

Table 23: CTCF of HT29 CD133+ cells stained with Alkaline phosphatase antibody 61

Table 24: CTCF of HT29 CD133- cells stained with Alkaline phosphatase antibody 61

Table 25: CTCF of DLD1 CD133+ cells stained with Shh antibody following treatment with cyclopamine 82

Table 26: CTCF of HT29 CD133+ cells stained with Shh antibody following treatment with cyclopamine 83

Table 27: CTCF of DLD1 CD133+ cells stained with Shh antibody following treatment with cyclopamine 85

Table 28: CTCF of DLD1 CD133+ cells stained with CD133 antibody following treatment with cyclopamine 85

Table 29: CTCF of HT29 CD133+ cells stained with Shh antibody following treatment with cyclopamine 86

Table 30: CTCF of HT29 CD133+ cells stained with CD133 antibody following treatment with cyclopamine 86

LIST OF ABBREVIATIONS

CSC	Cancer Stem Cell
EMT	Epithelial to Mesenchymal Transition
Shh	Sonic Hedgehog
Hh	Hedgehog
ALDH	Aldehyde dehydrogenase
EpCAM	Epithelial Cell Adhesion Molecule
KLF4	Kreuppel-like Factor 4
Hh	Hedgehog
Smo	Smothened
Ptch1	Patched1
FGF	Fibroblast Growth Factor
PCR	Polymerase Chain Reaction
miRNA	Micro Ribonucleic Acid
TGF	Transforming Growth Factor
FDA	Food and Drug Administration
ATCC	American Type Culture Collection
RPMI	Roswell Park Memorial Institute Media
DMEM	Dulbecco’s Modified Eagle Medium
FCS	Fetal Calf Serum
HEPES	Hydroxyethylpiperazineethanesulfonic acid
BSA	Bovine Serum Albumin
EGF	Epidermal Growth Factor
DMSO	Dimethyl Sulfoxide
TC	Tissue Culture
PBS	Phosphate Buffered Saline

IgG	Immunoglobulin
PE	Phycoerythrin
FcR	Fragment crystallizable Receptor
DAPI	Diaminophenylindole
CI	Cell Index
CTCF	Corrected Total Cell Fluorescence
ECM	Extracellular Matrix
DIC	Differential Interference Contrast
ITS	Insulin Transferrin Selenium
SuFu	Suppressor of Fused

Contents

DECLARATION ii
ABSTRACT iii
ACKNOWLEDGEMENTS iv
RESEARCH OUTPUT v
LIST OF FIGURES vi
LIST OF TABLES ix
LIST OF ABBREVIATIONS xi
1. Introduction 1
1.1 Colon cancer 1
1.2 Cancer stem cell theory 2
1.3 CD133 receptor 4
1.4 Other stem cell markers 5
1.5 Sonic hedgehog pathway 6
1.6 Shh and epithelial to mesenchymal transition (EMT) 8
1.7 Shh inhibtion with cyclopamine 9
1.8 Shh inhibitors 9
1.9 The primary cilium 12
1.10 Evaluation of non-CSC's versus CSC's 14
2. Hypothesis 15
3. Objectives 15
4. Materials 17
4.1 Cell culture 17
4.1.1 Cell lines 17
4.1.2 Cell culture media 17
4.1.3 Additional supplements for cell culture and assays: 19
4.2 Cell counting 19
4.3 Microscopy 19
4.4 Small molecule inhibitors 19
4.5 Antibodies 20
5. Methods 21

5.1 Cell culture 21
5.1.1 Thawing of cells 21
5.1.2 Cryopreservation of cells 21
5.1.3 Determination of cell count 21
5.2 Isolation of CSC's from parent cancer cell population 22
5.2.1 Magnetic Cell Separation 22
5.2.2 Flow cytometric confirmation of the isolated cell population 23
5.3 Cell Impedance Assays 24
5.4 Fluorescence microscopy 25
5.5Assays 27
5.5.1Cell Adhesion assays 27
5.5.2 Invasion assay 28
5.5.3 Migration/Scratch assay 30
5.6 Statistical analysis 31
6. Results 32
6.1 Flow cytometry confirmation isolated of CD133+ cells 32
6.2 Spheroid formation of CD133+ cells 33
6.3 Cell proliferation assays- xCELLigence 34
6.4 Confocal microscopy characterization 39
6.4.1 CD133 localization in non-permeabilized CD133+ and CD133- cell fractions 39
6.4.2 CD133 localization in permeabilized CD133+ and CD133- cell fractions 44
6.4.3 Immunofluorescence localization of c-Myc in CD133+ and CD133- cells 50
6.4.4 Immunofluorescence localization of KLF4 in CD133+ and CD133- cells 54
6.4.5 Immunofluorescence localization of alkaline phosphatase in CD133+ and CD133- cells 58
6.5 Cell adhesion assays 62
6.6 Cell invasion assays 65
6.7 Cell migration/scratch assays 67
6.8 Expression of Shh 82
6.9 Expression of CD133 and Shh 85
6.10 Correlation of metastatic properties 88
7. Discussion 89
7.1 Introduction 89
7.2 Isolation of CSC's 90

7.3 CSC growth profiles 91
7.4 Stem cell marker expression 93
7.4.1 CD133 93
7.4.2 c-Myc 94
7.4.3 KLF4 94
7.4.4 Alkaline phosphatase 95
7.5 Therapeutic development 96
7.6 Assessment of physiological properties of CSC's 97
7.6.1 Cell adhesion 98
7.6.2 Cell invasion 99
7.6.3 Cell migration 100
7.6.4 Inhibition of Shh; relationship to CD133 expression 102
7.7 Future directions 103
7.8 Outlook 104
8. References 105
9. APPENDIX 114
Appendix A 114
Appendix B 117
Appendix C 127
Appendix D 128
Appendix E 130

1. INTRODUCTION

1.1 COLON CANCER

Colorectal cancer, commonly known as colon cancer or bowel cancer is a cancer from uncontrolled cell growth in the colon or rectum that forms part of the large intestine and usually develops from dysplastic adenomatous polyps[1]. This type of cancer was ranked as the fifth most common among males and third most common among females[2] with 41 000 new cases reported in 2012[3]. With a lifetime risk of 1 in every 98 males in South Africa the urgency for therapeutics is clear. Risk factors include increasing age[4-6], males[7], excessive intake of alcohol and red meat, obesity, smoking and a sedentary lifestyle[8]. Adenocarcinomas make up more than 95% of all cases with the remaining 5% being neuroendocrine tumours and small cell carcinomas[9].

Single-base pair mutations within the *ras*-gene[10,11] or allelic deletion of chromosome 5[12] are the two prominent genetic alterations that occur in colorectal neoplasia. These in combination with losses in the chromosome 17 and 18 *ras* sequences have been found to result in the formation of colorectal adenomas[13,14]. The Vogelstein model suggests that for colorectal tumorigenesis to progress there must be mutational activation of an oncogene in conjunction with the loss of tumour suppressor genes[15]. The three dominant conditions that are thought to influence the development of colorectal cancer include polyps, familial polyposis and ulcerative colitis. The polyp-cancer sequence suggests that the majority of colorectal neoplasia form as a result of adenomatous polyps and villous adenomas[16].

The key factors that distinguish malignant tumours from benign tumours include the ability to infiltrate surrounding tissue, the destructive nature of the cells as well as its highly metastatic potential. Colon cancer is classified according to the Dukes' system which gives an indication of the degree of invasion and can be useful in treatment planning. Early detection is key as it then allows for successful surgery and curative treatment, however, unfortunately in most cases at diagnosis the advanced disease results in an estimated 5-year survival rate of merely 8% [9]. The prominent prognostic factor is the stage of the tumour with the degree of bowel wall invasion, lymph node metastasis and distant metastases negatively affecting the prognosis of the patient[17].

Table 1: Dukes' classification for colon cancer staging

Stage	Criterion
A	Tumour confined to the intestinal wall
B	Tumour invading through the intestinal wall into muscle layer
C	Lymph node(s) involvement (this is further subdivided into C1 lymph node involvement where the apical node is not involved and C2 where the apical lymph node is involved)
D	Distant metastasis to other organs

Currently, several modes of treatment are available such as surgery, chemotherapy, radiation therapy, immunotherapy and monoclonal antibody therapy. Other novel approaches include gene therapy[18], non-pathogenic bacteria and telomerase therapy[19]. In cases where the tumour has become metastatic, treatment is challenging since various tissues are affected. In this study, colon cancer cell lines derived from tumours classified as Dukes' stages B and C will be used for the *in vitro* testing of several therapeutic agents.

1.2 CANCER STEM CELL THEORY

In recent years an increasing amount of evidence supports the theory of human cancer being considered as a stem cell disease[20-23]. The theory suggests that the formation of solid tumours is not simply the result of monoclonal expansions of transformed cells but instead the tumour consists of tissue displaying abnormal growth caused by a group of Cancer Stem Cells (CSC's) (Figure 1). This theory was proven in solid tumours when human breast cancer cells were grown in immuno-compromised mice; and it was noted that only a small population of breast cancer cells were capable of forming new tumours[24]. CSC's have been positively identified in, and isolated from various human solid cancers including, breast[24], brain[25,26], colon[27,28], head and neck[29]and pancreatic cancer[30].

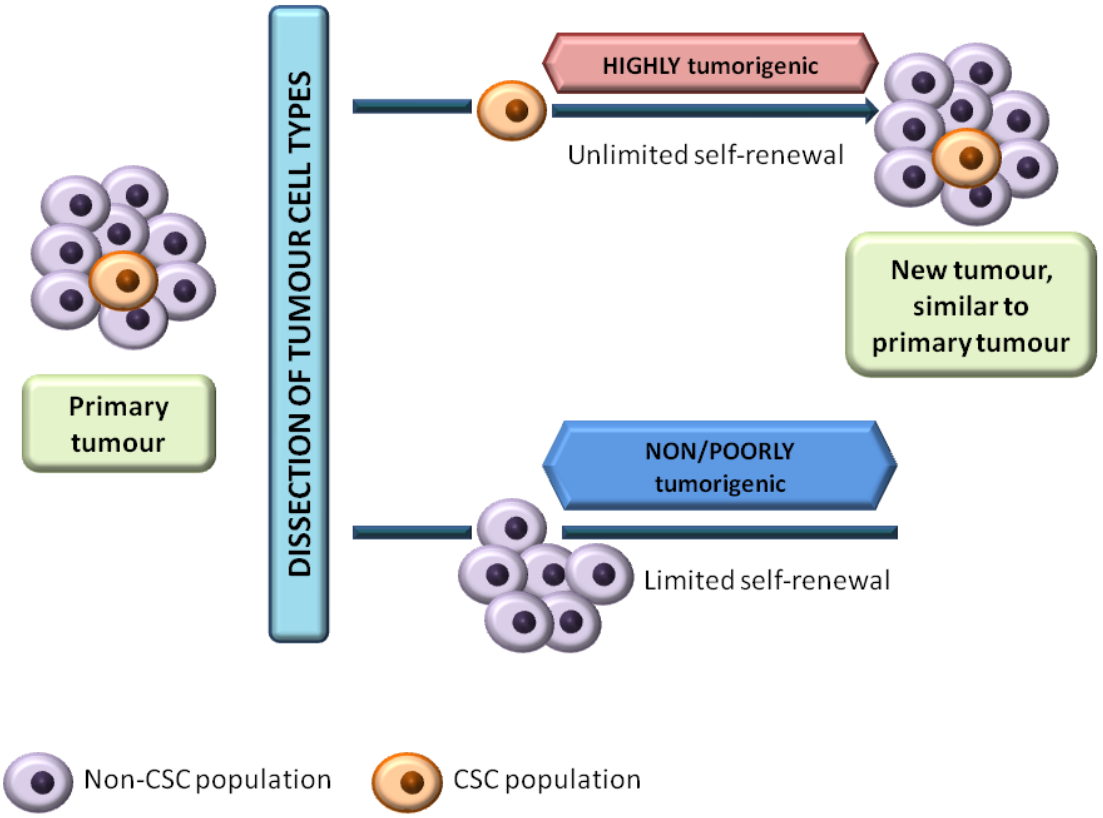


Figure 1: An illustration of the classical CSC concept. It is believed that tumours are heterogeneous and upon dissociation and transplantation into an immune-compromised mouse model, human CSC's are able to reinitiate and form a similar heterogeneous tumour *in vivo* (own figure).

Three important observations have been made proving the existence of CSC's in solid tumours:

1. Not all cancer cells possess the ability to form new tumours upon transplantation into immune-deficient mice, it is only a small population of the cancer cells that contain this tumorigenic potential.
2. This special subpopulation of cancer cells can be identified by a distinctive profile of surface markers such as CD29, CD34, CD90, CD117 and CD133[31]. In this study CSC's will be isolated from a population of cancer cells by magnetic cell separation using the CD133 marker.
3. The secondary tumours formed from the CSC's comprise of non-tumorigenic cancer cells as well as tumorigenic cancer cells that are further able to produce more tumours. In this way, the full phenotypic heterogeneity of the primary tumour is re-created.

In adult tissue while normal adult stem cells assist in the maintenance of tissue that continuously regenerate, for example skin and gastrointestinal mucosa, regeneration also occurs in response to disease or injury[32]. Their capacity to self-renew is lifelong; they are multipotent and have the ability to switch between dormant and active states providing a level of resistance against cytotoxic drugs. CSC's display similar characteristics and are able to self-renew and thereby form a new tumour from a small number of cells. In comparison with other cancer cells, CSC's posses a lower proliferation rate and have also been found to be more resistant to chemotherapy and radiation treatments, due to the increased activity of membrane transporters[31]. The survival of even a few CSC's following treatment poses a major health risk since these could result in a relapse of the tumour. This emphasizes the need to develop effective therapeutics targeting these cells. Currently several approaches for the eradication of these CSC's are being explored[33], including:

- Targeting altered genetic signalling pathways by blocking specific cell surface molecules
- Altering the cancer microenvironments that nurture CSC's
- Inducing differentiation of CSC's
- Immunotherapy based on CSC associated antigens
- Exploiting metabolites to kill CSC's
- Designing small interfering RNA/DNA molecules that especially target CSC's

1.3 CD133 RECEPTOR

Although there are a several markers that are helpful for the isolation of CSC's from solid tumours, including CD133, CD44, EpCAM and ALDH activity, none of these markers are expressed exclusively by CSC's [34]. CD133 also known as Prominin-1 is a cell surface protein and will be used as a CSC marker in this study, being one of the prominent markers of CSC's in colorectal cancer[35]. It is expressed in endothelial progenitor cells[36], glioblastoma multiforme[25], hematopoietic stem cells[37], neuronal stem cells, glial stem cells[38], as well as brain tumours [39]. CD133 is also expressed in various other normal tissues including the trachea, salivary glands, digestive tract, kidney as well in reproductive organs such as the placenta, mammary glands and testes[40,41]. The expression and utility of CD133 has been well established in a number of colorectal cancer cell lines within the Oncology Laboratory. Furthermore, the expression of CD133 in patients with Dukes' stages B and C cancer has been linked to the recurrence of tumours following therapy and a poor prognosis[35]. Presently

whilst the exact function of CD133 remains unknown, its expression during the production of the plasma membrane, and more specifically epithelial microvilli, indicates a possible role in this context. Recent literature has suggested that CD133 directly interacts with plasma membrane cholesterol and is predominantly found in plasma membrane protrusions[42]. Due to this association, it has been proposed that the functional role of CD133 is that of an "organizer" of the plasma membrane topology[43-45]. This interaction with cholesterol also infers that it may play a role in maintaining lipid composition within the plasma membrane. Cells expressing CD133 are thought to possess stemness properties which include their ability to self-renew, differentiate and form tumours in xenografts[46]. As further confirmation of the stem cell properties of cells expressing CD133, the expression of a number of additional markers will be assessed and these are described below. With regards to cell terminology, please note that **CD133+** refers to cells that express cell surface CD133 (CSC's: positive fraction from magnetic separation) and **CD133-** refers to cells that do no express surface CD133 (non- CSC's: negative fraction from magnetic separation).

1.4 OTHER STEM CELL MARKERS

The use of CD133 as a definitive marker for CSC's is debatable and some studies have shown that CD133 expression in colon cells is not necessarily restricted to stem cells, as it is also expressed on differentiated colonic epithelium[47]. It can therefore be suggested that CD133+ cells could very well contain stem cell like potential. Since CD133 may not exclusively be expressed by CSC's, following the separation of cells using the CD133 marker, they will then be further characterized using other markers.

The Myc Oncogene

The regulator gene Myc codes for a transcription factor and in certain cancer types this gene has been found to be mutated causing its continuous expression. Myc is also activated upon several mitogenic signals, including Shh. Myc plays an active role in various processes such as cell proliferation, regulation of cell growth, apoptosis, differentiation and stem cell self-renewal[48], thereby making it an ideal CSC marker. Myc is also a key factor required for the induction of pluripotential stem cells that are required for stemness.

Krueppel-like factor 4 (KLF4)

Another marker that will be considered is the KLF4 gene that encodes for Krueppel-like factor 4 (KLF4), a zinc-finger protein that contributes to the progression of gastric carcinoma by promoting tumour growth, invasion and metastasis[49]. It is thought to serve as a good indicator of stem-like capacity in embryonic stem cells and possibly even in mesenchymal stem cells. KLF4 was found to be one of the four genes essential for pluripotency in stem cells, others included Oct-3/4, SOX2 and as mentioned previously c-Myc[50].

Alkaline phosphatase

The hydrolase enzyme alkaline phosphatase which is responsible for the removal of phosphate groups in nucleotides, proteins and alkaloids, will also be employed as a biomarker in this study. Alkaline phosphatase staining has been used in many instances to detect undifferentiated pluripotent stem cells as there are elevated levels contained on their cell membrane[51]. This method of staining is also implemented when the level of pluripotency is being evaluated and to positively identify embryonic stem cells[52]. Its utilization in detecting cancer stem cells is well established in various cancer cell lines including melanomas[53] and ovarian cancer[54].

1.5 SONIC HEDGEHOG PATHWAY

The Hh (Hedgehog) signalling pathway was named due to the appearance of the polypeptide ligand and intercellular signalling molecule Hh. Three Hh homologues have been identified in humans, Desert Hh, Indian Hh and the most widely studied Sonic Hedgehog (Shh)[55]. During embryonic development this pathway is a key regulator and ensures that symmetry as well as the correct distribution of cell types is maintained[56]. In knockout mice that lacked components of the pathway, it is of particular interest here that abnormalities were observed in the gastrointestinal tract, as well as brain, lungs, skeleton and musculature. In adult tissue the Hh pathway is mainly inactive[57], but is thought to play a role in regulating adult stem cells which consequently maintain and regenerate old or damaged tissue. Moreover it is expressed in human adult gut epithelium[58].

Reactivation of the Hh pathway in adult tissues may be linked to the development of some cancers (Figure 2). This may occur via genetic alterations in Hh pathway components or excessive secretion of Hh ligands. Certain cancers including basal cell carcinoma, medulloblastoma and rhabdomyosarcoma are attributed to mutations that either causes the activation of Smoothened (proto-oncogene) or the inactivation of Patched (tumour suppressor)[59]. These two proteins play an imperative role in regulating the cellular response that occurs as a result of Hh. Oncogenic mutations in either Ptch (Patched) or Smo (Smoothened) could result in an increased activity of the Hh pathway[60,61]. As a result of the Smo suppression, the full length Gli1 translocates to the nucleus. This in turn causes the transcription of downstream genes including vascular endotheial growth factor (VEGF) and c-Myc[62]. Dependence of basal cell carcinomas and medulloblastomas on the Hh pathway has provided new targets for treating these cancers by targeting components of the pathway. In several cancer types including lung[63,64], ovarian[65], prostate[66], breast[67], endometrial[68], skin[69] and gastrointestinal[70-72], the pathway was found to be reactivated.

Shh is believed to play an early and imperative role in the genesis of pancreatic cancer and is over-expressed in pancreatic adenocarcinoma as well as its precursor lesions[73]. It was also found that inhibition of this pathway by cyclopamine was able to induce apoptosis and hinder proliferation both *in vitro* and *in vivo*. With regards to colorectal cancer studies have indicated that Shh expression may prompt the adenoma-carcinoma sequence[74]; the Shh ligand as well as its downstream targets (Gli) are over-expressed in human colorectal cancer tissue[75]. An active Hh-Gli pathway was also positively identified in human colon carcinoma cells as well as its stem cells[76]. It is proposed in the present study that inhibiting the Shh pathway in colorectal CSC's may be a novel approach leading to new treatments for colorectal cancer.

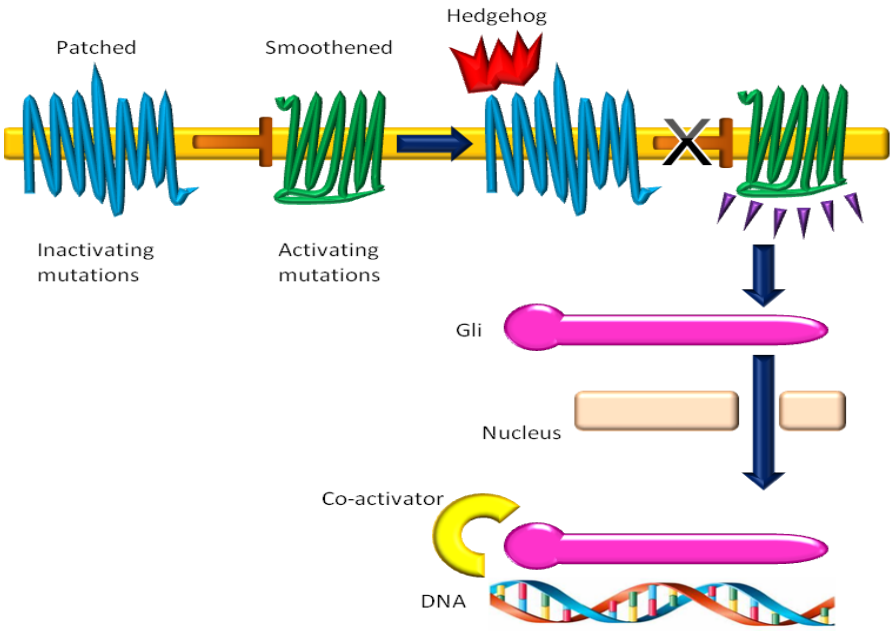


Figure 2: The mechanism by which the Shh pathway is reactivated: Ptch suppresses the activity of Smo, however, following the binding of the Hh ligand to Ptch, this suppression is then inhibited allowing for the activation of downstream targets through the Gli transcription factors. When a ligand is absent it results in the phosphorylation and cleavage of Gli; however, in the presence of a ligand, Gli is not cleaved and the full length Gli translocates to the nucleus where it exhibits transcriptional activity (own figure).

1.6 SHH AND EPITHELIAL TO MESENCHYMAL TRANSITION (EMT)

A key process in metastatic cancer is the so-called Epithelial to Mesenchymal Transition (EMT), wherein epithelial cells loose the expression of E-cadherin and express N-cadherin, typical of motile mesenchymal cells[77]. Hh signalling activation results in EMT through FGF, Notch, TGF beta signalling cascades, and indirectly through miRNA regulatory networks[77]. A study by Higgins et al, suggested that Shh induces EMT *in vitro* and results in gene expression changes[78]. This was proven by inducing EMT in lung, breast and prostate cancer cells. Real-time PCR as well as immunofluorescence indicated that EMT had taken place and Matrigel™ assays confirmed the invasive potential of the phenotype present. Gene expression analysis using real-time PCR indicated the up-regulation of EMT genes, in particular an increase in the expression of N-cadherin, Gli2 and Shh genes. It was seen that the cells had undergone the switch to N-cadherin and these cells showed an increased ability to invade. In the same study it was demonstrated that the application of cyclopamine impeded this increased expression of N-cadherin, Shh as well as Gli2. In combination, these results imply that Shh is a crucial mediator of EMT in human tumours[78].

1.7 SHH INHIBTION WITH CYCLOPAMINE

The discovery of cyclopamine dates to the 1950's with the occurrence of congenital abnormalities in newborn lambs in the highland areas of the Western United States. It was found that pregnant ewes that had grazed on the plant Corn Lily (*Veratrum californicum*) during day 14 of gestation would most likely result in newborn lambs with cyclopia, a single central eye. The compound responsible for these malformations was identified as an alkaloid, named cyclopamine (Figure 3).

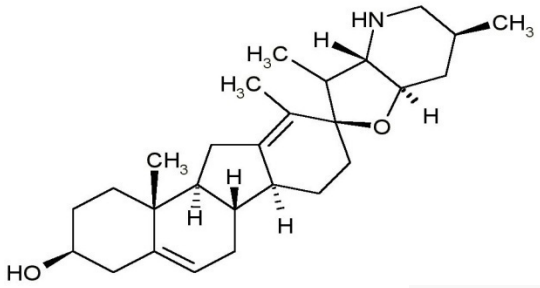


Figure 3: Chemical structure of cyclopamine with IUPAC name (3β,23*R*)-17,23-Epoxyveratraman-3-ol and chemical formula $C_{27}H_{41}NO_2$.

Cyclopamine is thought to specifically inhibit the Hh response[79,80], and may also play a role in the balance between active and inactive forms of Smo, making it suitable for the treatment of cancers dependent on Smo activation (Figure 6). In a study using gastric primary cancer cells GAM-016 and MKN-45, it was found that cyclopamine successfully inhibited gastric cancer cell proliferation by inducing cell cycle arrest and apoptosis[81]. Cyclopamine acts as an antagonist of the Hh signalling pathway by directly binding to the Smo heptahelical domain[82] and in this way is able to induce apoptosis and block proliferation making it a potent cancer therapeutic. Other Shh inhibitors are discussed below.

1.8 SHH INHIBITORS

Current approaches for the treatment of cancer are limiting due to the cytotoxic effects that these therapeutics have on healthy proliferating tissue[59]. Ideally the most efficient drug would be one that is broad spectrum but non-toxic to healthy tissue. Therefore, alternatives such as 'mechanism-based' therapies that are specific in targeting abnormally active signalling pathways could provide a solution with less collateral damage. In this case, targeting the Shh pathway is highly promising since its primary function is during the period of embryonic development and is not essential for survival in adults. The drugs evaluated in the present study include cyclopamine (see above), SANT2 and tomatidine.

SANT-2

The cell-permeable SANT-2 molecule (Figure 4) being a potent antagonist of the Hh pathway is a useful tool for investigating Hh signalling. It acts by antagonizing the Smo receptor (K_D= 12nM) activity and inhibits SAG (Smo agonist) activity. Other Smo inhibitors such as GANT58 and JK184 were considered but proved to be unsuitable for this study as their effect is downstream of Smo and therefore, could not be used in comparison to cyclopamine. SANT-2 was selected from a range of cyclopamine analogues and will be used in this study and its effect or lack thereof, on cell invasion, adhesion and migration will be analyzed.

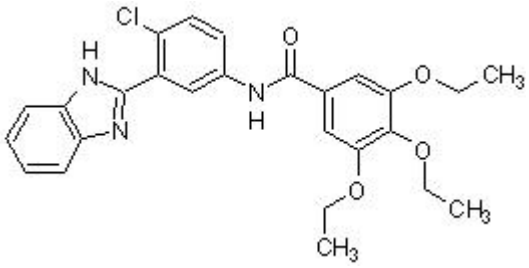


Figure 4: Chemical structure of SANT-2

Currently the only FDA approved drug targeting the Hh signalling pathway is Vismodegib (Erivedge). It has found to be effective in the treatment of basal-cell carcinoma and is undergoing clinical trials for implementation in the treatment of colorectal cancer, small-cell lung cancer, stomach cancer, pancreatic cancer and medulloblastoma[55,83-86]. In studies done to assess its efficacy as an advanced basal-cell carcinoma therapeutic, it was concluded to be a safe (FDA approved) and effective small molecule inhibitor of Smo[87]. Disease development in this case resulted from mutations in the Hh pathway leading to a loss in Ptch function. Cyclopamine as well as Vismodegib act on Smo directly, however other Shh inhibitors such as robotnikinin[88] have an effect on the motor protein dynein (ciliobrevin A)[89] or are able to hinder DNA-Gli interactions[90](Figure 7).

Tomatidine

Many Shh studies make use of a steroidal alkaloid such as tomatidine (Figure 5) which is found in the skins of unripe tomatoes. They are structurally similar to cyclopamine but are non-teratogenic and have no effect on the Hh pathway[91] making it useful as a negative control[73].

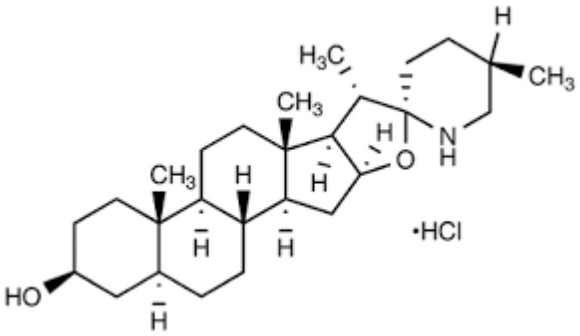


Figure 5: Chemical structure of tomatidine

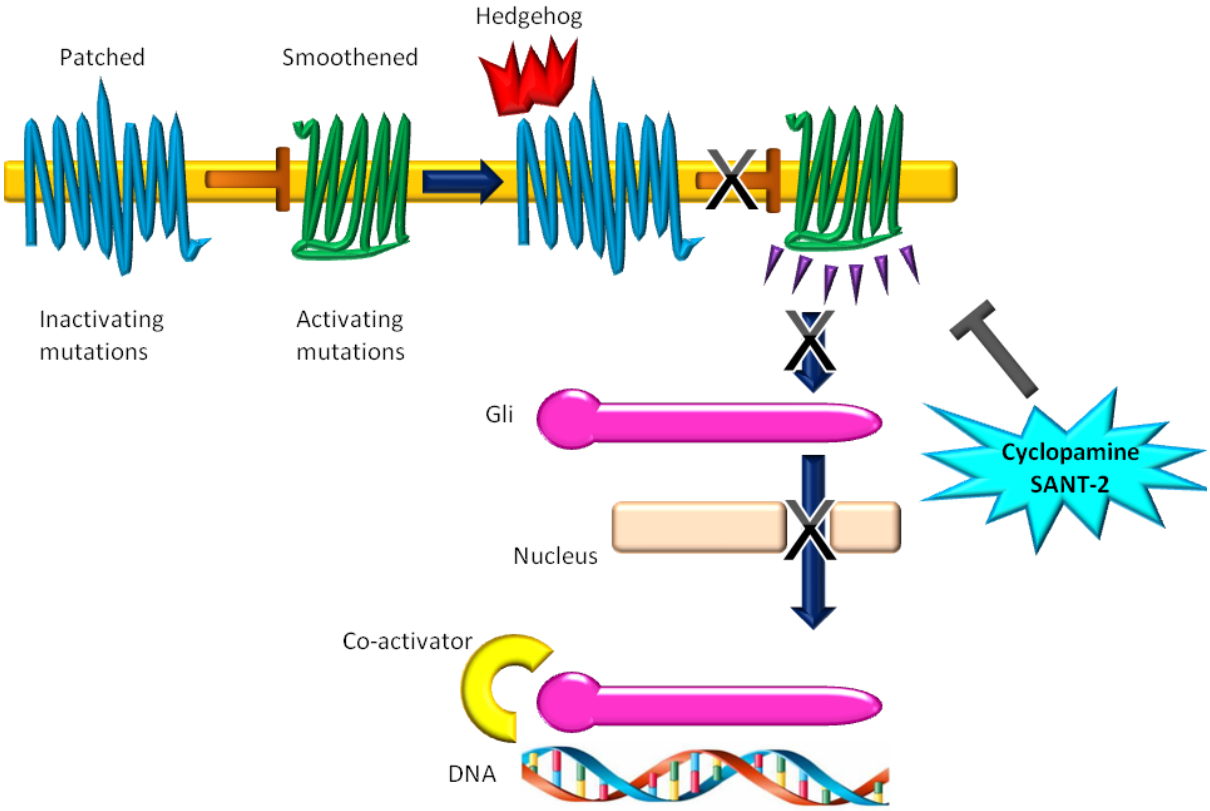


Figure 6: The pathway inhibition induced by cyclopamine and SANT-2: both small molecules act as antagonists of Smo, preventing the activation of Gli and its movement into the nucleus, thereby preventing the transcription of oncogenes (own figure).

1.9 THE PRIMARY CILIUM

It is important to discuss the primary cilium, since it has been found to be a central organelle in Hh signal transduction[92]. Moreover, it is the central location for many Hh pathway components including Shh, Ptch1, Smo and Gli transcription factors. Since the primary cilium acts as a sensory organelle, it is able to receive both mechanical as well as chemical signals and convey these to the nucleus, inducing a cellular response. As a result, any disruption in the localization of these proteins within the primary cilium would lead to an impedance of the signal. Overall, a functional and intact primary cilium is required for the modulation of the Shh pathway[93].

Cyclopamine and SANT-2 have differing effects on the primary cilium, in a study on NIH3T3 cells, cyclopamine treatment (10μM) caused localization of Smo to the primary cilium, while SANT-2 prevented the Shh-dependent translocation of the protein Smo to the primary cilium[93]. The same paper also discussed how SANT-2 was able to inhibit both a dominant active form of Smo (SmoA1) as well the wild-type Smo at comparable doses whereas cyclopamine was required at far higher doses to attain a similar inhibitory effect with SmoA1[59]. On the contrary, in the present study, SANT-2 was required at comparatively higher concentrations than cyclopamine to induce an inhibitory effect on cell adhesion and invasion.

In considering the aforementioned effects of SANT-2 and cyclopamine on Smo, together with their structural differences, it is thought that their binding to Smo occurs at differing sites. Furthermore, following their binding the conformational changes that are induced in Smo also differ, as well as the manner in which they hinder Smo interaction with other cellular factors[93]. It has also been shown that SANT-2 competes with cyclopamine for Smo binding, indicating that SANT-2 functions at the level of Smo which is upstream of SuFu[94]. The mechanism whereby cyclopamine inhibits the Shh pathway has been elucidated, being able to bind directly to the heptahelical bundle of Smo (Figure 7), possibly altering the Smo protein conformation[82]. This protein conformation is structurally similar to that of the surface protein Ptch. This understanding of the mode of action that cyclopamine has would allow for the progression in the therapeutic development of this small molecule since it may explain the trends noticed in this study.

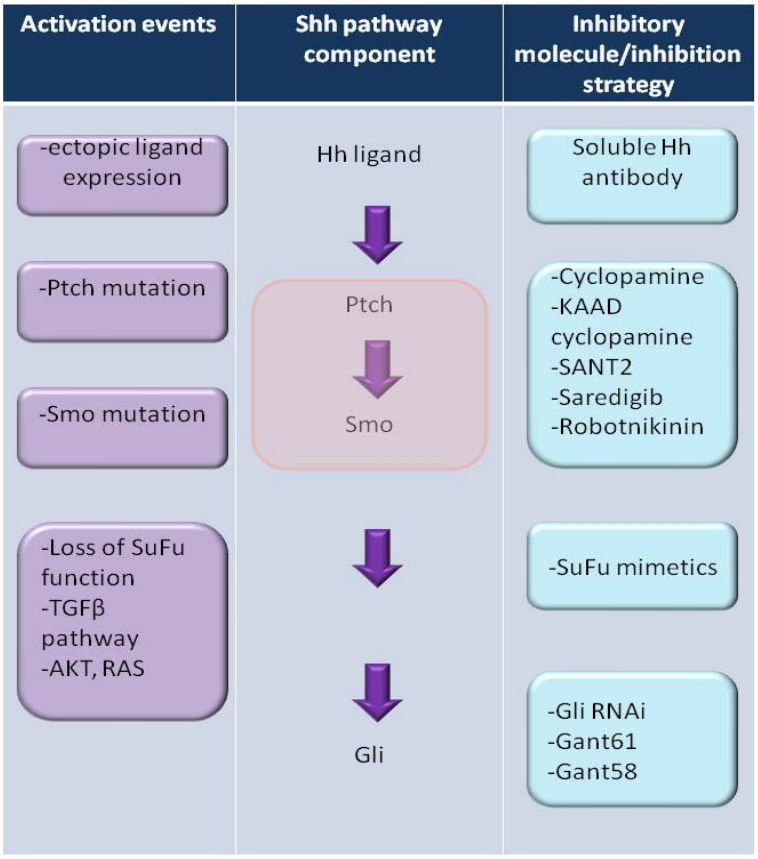


Figure 7: Inhibition strategies targeting the aberrant activation of the Shh pathway. Known activation events resulting in oncogenic development (purple boxes) juxtaposed with potential inhibition strategies (blue boxes). An appropriate inhibition strategy is key to successful treatment with small molecule inhibitors. The inhibitors utilized in this study specifically target Smo mutations (pink box) (Adapted from Figure 3, Drug Discovery Today, Therapeutic Strategies[95]).

1.10 EVALUATION OF NON-CSC'S VERSUS CSC'S

It has been proposed that there are 6 distinct characteristics or hallmarks of cancer[96] and these include:

- Evasion of apoptosis
- Insensitivity to anti-growth signals
- Infinite replicative potential
- Self-sufficiency in growth signalling
- Induction and sustainment of angiogenesis
- Ability to metastasize and invade surrounding tissue

Similarly, cancer stem cells possess the following key properties[97]:

- Ability to differentiate and give rise to all cell types
- Ability to self-renew
- Tumorigenic
- Slow cycling and therefore resilient to conventional therapeutics
- Resistance to therapy due to activation of several signalling pathways, such as Notch, Wnt/β-catenin, TGF-β, Hh, PI3K/Akt/mTOR and JAK/STAT pathways[33]
- Highly metastatic[33]

Several of these physiological traits can be evaluated *in vitro* using various assays including, invasion, adhesion, colony formation, proliferation and scratch assays. The efficacy of drugs on inhibiting these properties may be assessed using these same assays[98]. In this study several of these assays will be employed to either ascertain the differences between normal cancer cells and CSC's or to evaluate the ability to inhibit the Shh pathway in CSC's specifically.

2. HYPOTHESIS

Considering the need for targeted therapy against CSC's and their occurrence in colon cancers, as well as the role of Shh in EMT and metastasis, we therefore hypothesize that disrupting this pathway using small molecule inhibitors would be effective in impeding the invasive and adhesive potential of colorectal CSC's.

3. OBJECTIVES

1. Isolation of a specific population of CSC's from 3 colorectal cancer cell lines representing the middle and late stages of disease:
   a. By magnetic separation using the cell surface marker, CD133
   b. Confirmation of the CD133 stem cell isolation/population using flow cytometry

   Evaluation of the expression of the key stem cell markers, c-Myc, KLF4 and alkaline phosphatase in CSC's and non-CSC's using confocal microscopy.

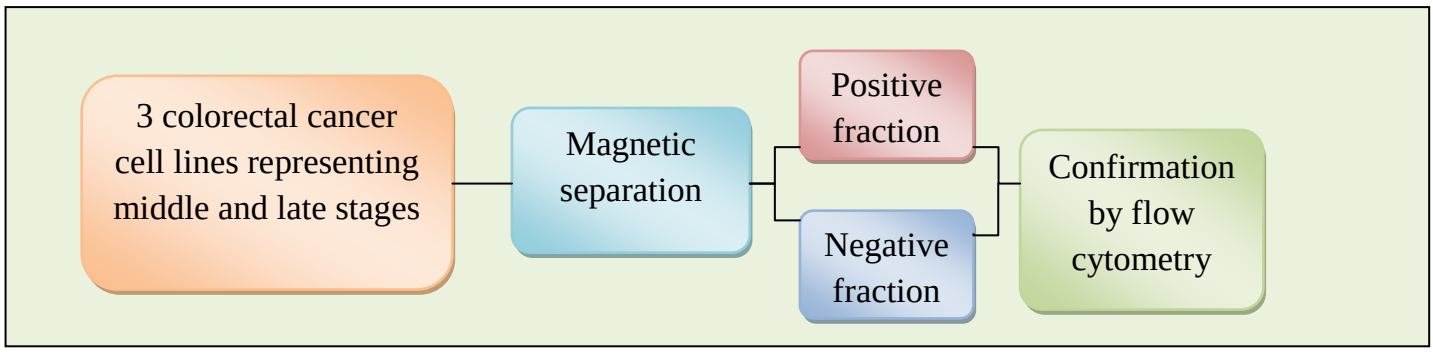
A real-time assessment of CSC proliferation relative to non-CSC's with regards to:

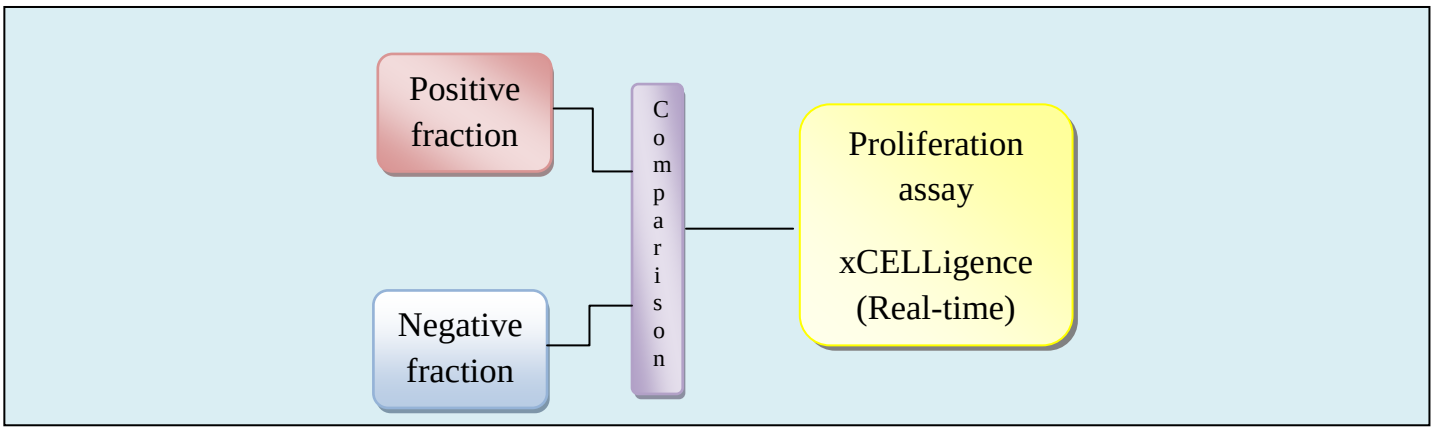
   a. Time to confluency (proliferation rate)
   b. Number of cells required to reach confluency
   c. Growth pattern profiling

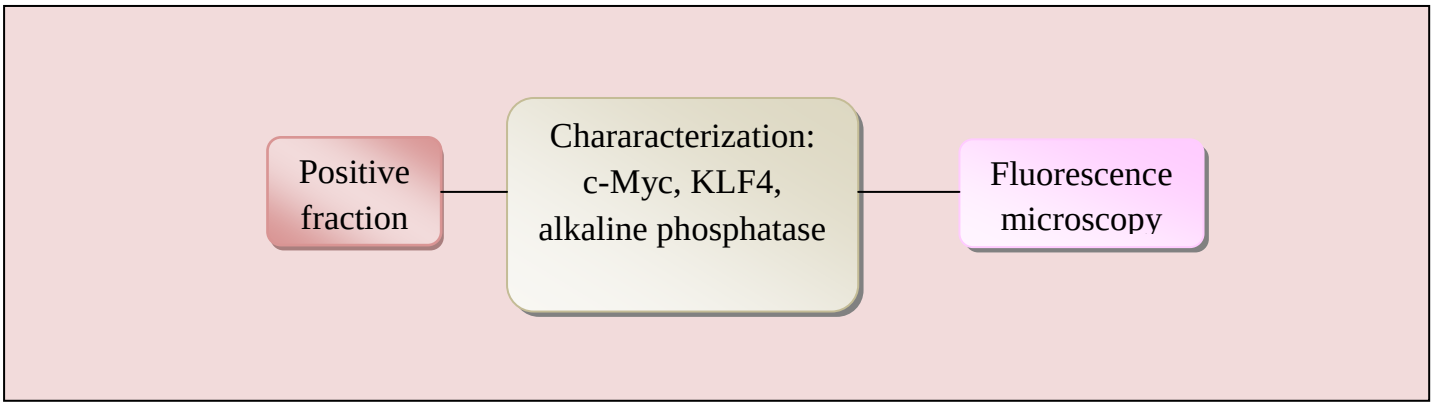
2. Inhibition of the Shh pathway in colon CSC's using the Smo inhibitors cyclopamine and SANT-2. The effects of these compounds was analyzed with regard to the following cellular parameters:
   →cell adhesion
   →cell invasion
   →cell migration

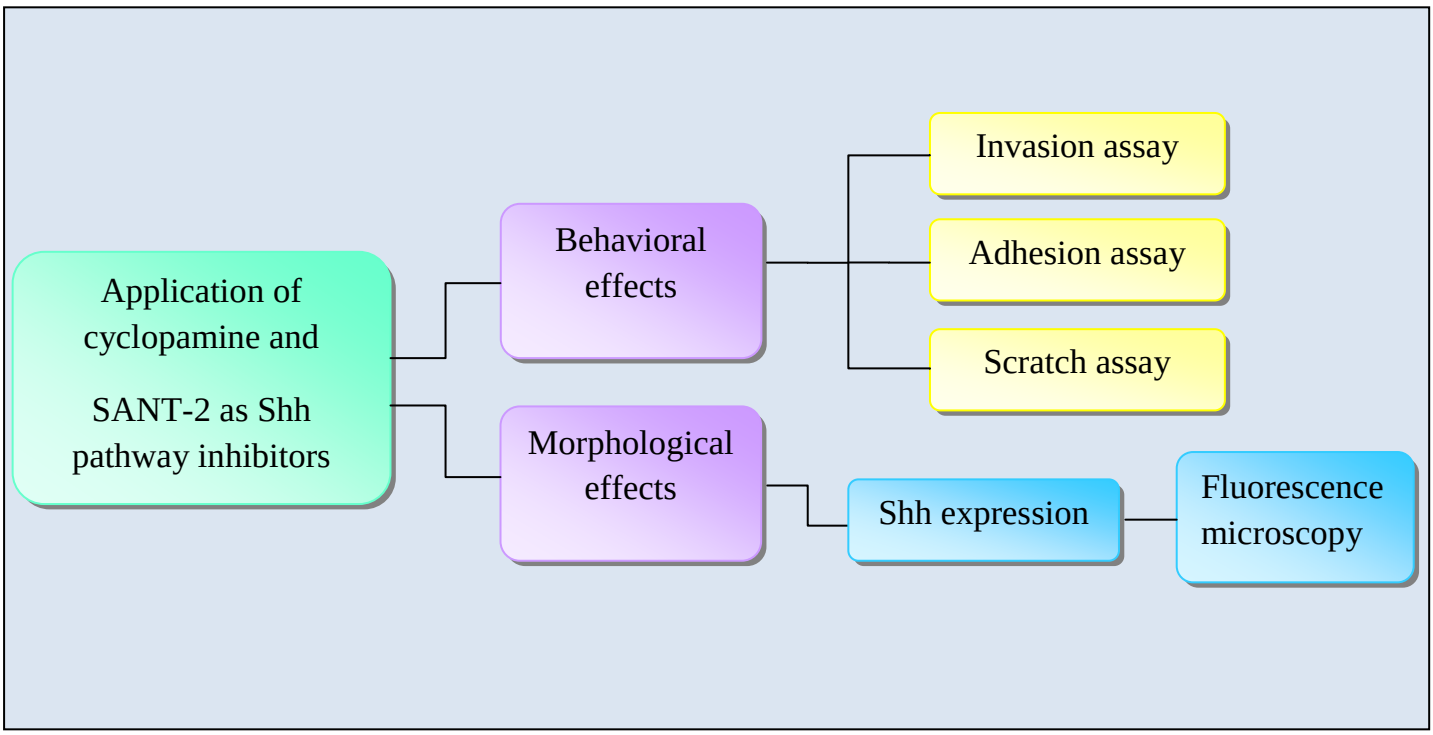
Evaluation of CD133 and Shh expression following Shh pathway inhibition, using fluorescence.

(See flow diagram)


3 colorectal cancer cell lines representing middle and late stages
Magnetic separation
Positive fraction
Negative fraction
Confirmation by flow cytometry


Positive fraction
Negative fraction
Comparison
Proliferation assay
xCELLigence (Real-time)


Positive fraction
Chararacterization: c-Myc, KLF4, alkaline phosphatase
Fluorescence microscopy


Application of cyclopamine and SANT-2 as Shh pathway inhibitors
Behavioral effects
Morphological effects
Invasion assay
Adhesion assay
Scratch assay
Shh expression
Fluorescence microscopy

4. MATERIALS

4.1 CELL CULTURE

4.1.1 Cell lines

Table 2: Cell lines used and their origin

Cell line/Source	Disease
Neoplastic	
DLD1 (ATCC CCL-221™)	Human colorectal adenocarcinoma Dukes' type C (late)
HT29 (ATCC HTB-38™)	Human colorectal adenocarcinoma suspected Dukes' type B
SW480 (ATCC CCL-228™)	Human colorectal adenocarcinoma Dukes' type B (early)

Note: For more detailed information on cell lines see Appendix A.

An ethics waiver for the use of the abovementioned cell lines was obtained, see Appendix E.

4.1.2 Cell culture media

The mixed cell populations require different media prepared from the following components:

- Dulbecco´s Modified Eagle'sMedium (DMEM) and Ham's F-12(1:1 mix) (1x), (HT29 and DLD1) (Biowhittaker® Lonza #BE12-719F).
- RPMI 1640 (SW480) (Biowhittaker® Lonza)

The above culture media was supplemented with:

- 10% fetal calf serum (FCS) (heat inactivated) (HYCLONE® #SV30160.03).
- 1% Penicillin/Streptomycin (Biowhittaker® Lonza #17-602E).

The stem cell populations require media containing the following components (according to Mather, 2008):

- 6mg/ml glucose
- 1mg/ml $NaHCO_3$
- 2mM L-glutamine
- 5mM HEPES

- 4µg/ml Heparin
- 4mg/ml BSA (bovine serum albumin)
- 10ng/ml βFGF (fibroblast growth factor)
- 20ng/ml EGF (epidermal growth factor)
- 100µg/ml apotransferrin
- 25 µg/ml insulin
- 9.6 µg/ml putrescine (diaminobutine)
- 30nM sodium selenite anhydrous
- 20nM progesterone

The following stock solutions were prepared for the stem cell media:

❖ Glucose 10% solution
10g in 100ml sterile H_2O

❖ $NaHCO_3$ 7.5% solution
7.5g in 100ml DMEM F12

❖ Heparin 50mg/ml solution
56mg in 1.12ml sterile H_2O (mass may vary depending on batch)

❖ EGF 1mg/ml solution
2mg in 2ml acetic acid

The stem cell media was prepared as follows:

- DMEM F12 (1x), for (HT29 and DLD1)
- RPMI 1640 (SW480)

The above culture media was supplemented with (for 50ml media): *DMEM F12 contains HEPES, therefore none was added

- 1% Penicillin/Streptomycin
- 3ml Glucose (10% solution) (Merck)
- 666 µl $NaHCO_3$ (7.5% solution) (Merck)
- 500µl Glutamine (Sigma #G7513)

- 4µl Heparin (50mg/ml solution) (Sigma #H3149-10KU)
- 8µl FGF (Invitrogen)
- 8µl EGF (1mg/ml solution) (Gibco #PHG0314)
- 500µl Insulin-Transferrin-Selenium (Gibco #51500-056)
- 9.6µl Putrescine (Sigma)
- 4.62µl Progesterone (Sigma)
- 0.2g BSA (Santa Cruz #sc-2323)

4.1.3 Additional supplements for cell culture and assays:

- Phosphate-Buffered Saline (PBS) (1 tablet in 200ml H_2O) (Sigma #P4417-100TAB)
- Trypsin/EDTA (1x)
- Fixing solution: 3% Paraformaldehyde in PBS (Merck)
- Blocking buffer: 0.5% BSA in DMEM F12
- Washing buffer: 0.1% BSA in DMEM F12
- Crystal violet stain: 5mg/ml in 2% ethanol (Sigma)
- Toluidine blue stain: 1% in 50% isopropanol (Sigma)
- Extraction solution: 2% SDS in H_2O

4.2 Cell counting

- Trypan Blue stain (Sigma)
- Counting Slides (dual chamber)(Bio-Rad #145-0011)

4.3 Microscopy

- Permeabilisation solution/Buffer: 0.25% (v/v) of t-Octylphenoxypoly ethoxyethanol (TritonX-100) (#T-9289; Sigma) was dissolved in PBS/BSA.
- F-actin cytoskeleton staining solution: (1X Phalloidin conjugate working solution) 1µl of 1000X Cyto-painter Phalloidin iFluor 488 Reagent (# ab176753; ABCAM ®) conjugate DMSO solution into 1ml PBS/BSA.
- Nuclear stain: 4',6-diamidino-2-phenylindole (DAPI) (#236276 ; Cell Biology Boehringer Mannheim , Germany) was received in a 10mg crystalized form and was dissolved in N,N-Dimethylformamide (DMF) to make up a stock solution of 5mg/ml.
- DAPI working solution: 1µl of stock solution in 10ml PBS.

4.4 Small molecule inhibitors

- Cyclopamine (BioVision #1578-5)
- SANT-2 (WhiteSci #3617150)
- Tomatidine (BioVision #1893-25)

4.5 ANTIBODIES

Table 3: Different antibodies were used in the various analyses

Cancer Stem Cell separation		
Primary Antibody (MACS Miltenyi)	Microbeads (magnetic) conjugated to monoclonal anti-human CD133 antibodies (isotype: mouse IgG1, clone AC133).	
Flow cytometry		
Detection of CD133		
Primary Antibody (Biolegend)	PE conjugated anti-mouse CD133 antibody (isotype: Rat IgG2a, clone 315-2C11)	
Fluorescence microscopy		
Detection of CD133		
Primary Antibody (MACS Miltenyi)	CD133/1 (AC133) purehuman antibody (mouse monoclonal)	1:400
Secondary Antibody	Alexa Fluor 532 anti-mouse IgG (Invitrogen)	1:200
Detection of c-Myc		
Primary antibody	Mouse polyclonal IgG c-Myc (Abcam)	
Secondary antibody	Alexa Fluor 660 anti-mouse IgG (Invitrogen)	
Detection of KLF4		
Primary Antibody	Rabbit polyclonal IgG KLF4 200µg/ml (Santa Cruz)	
Secondary Antibody	Alexa Fluor 594 anti-rabbit IgG (Invitrogen)	
Detection of Alkaline Phosphatase		
Primary Antibody	Anti-human IgG Alkaline phosphatase γchain (sigma)	
Secondary Antibody	Alexa Fluor 647 anti-goat IgG (Invitrogen)	
Detection of Shh		
Primary Antibody	Rabbit polyclonal IgG (Abcam)	
Secondary Antibody	Alexa Fluor 594 anti-rabbit IgG (Invitrogen)	

5. METHODS

5.1 CELL CULTURE

The three cell lines were cultivated in the appropriate medium containing Penicillin/Streptomycin (10000 IU/ml), FCS (10%) and incubated at 37°C in 5% CO_2 (ThermoForm series ll water jacketed CO_2 Incubator [HEPA FILTER])., using tissue culture treated dishes. The cell lines used were SW480, DLD1 and HT29 which represent early and middle to late stage colon cancer respectively. Cell lines were sub-cultured upon reaching confluency (approximately every 3-4 days), whereby media was aspirated off and cells rinsed with PBS. Thereafter 1ml Trypsin-EDTA was added to cells to facilitate detachment and cells were incubated for 5 minutes in the CO_2 incubator. The resulting cell suspension was resuspended with 9ml media and an appropriate aliquot was placed into a new cell culture dish. Complete media was then added to the cells and they were returned to the incubator.

5.1.1 Thawing of cells

Frozen cells were removed from -80°C and thawed on ice. Thawed cells were transferred to a 15 ml tube containing 5ml of the appropriate media supplemented with 1% Penicillin/Streptomycin and 20% FCS. This was then centrifuged at 800rpm for 5 minutes and the pellet re-suspended in the appropriate media. Each cell suspension was transferred to a cell culture dish and incubated at 37°C, 5% CO_2. The growth of the cells was monitored over the next 5 hours and the media changed to 10% FCS upon cell attachment.

5.1.2 Cryopreservation of cells

The adherent cells were trypsinized and the resultant suspension centrifuged at 800rpm for 5 minutes. The supernatant was discarded and the cell pellet re-suspended in the appropriate media supplemented with 1% Penicillin/Streptomycin, 20% FCS and 10% DMSO. 1ml of this solution was added to labelled cryovials and maintained at -20°C overnight; thereafter the vials were transferred to the -80°C freezer for long term storage.

5.1.3 Determination of cell count

A TC10 automated cell counter (Bio-Rad) was employed to determine the number of cells used in all experiments. 10µl of cell suspension (neat from trypsinized plate) was mixed with 10µl of Trypan Blue dye in an Eppendorf tube. 10µl of this suspension was then carefully applied into a well on a dual chamber counting slide and inserted into the cell counter chamber. A total number of cells were determined as well as the number of live cells, this calculated as cells/ml and as a percentage of the total number of cells.

5.2 ISOLATION OF CSC'S FROM PARENT CANCER CELL POPULATION

5.2.1 Magnetic Cell Separation

Magnetic activated cell sorting allows cells to be separated following incubation with magnetic nanoparticles coated with antibodies against a particular surface antigen. In this study, the cell surface biomarker CD133 was used. The Miltenyi Biotec CD133 Cell Isolation kit was employed for magnetic separation (depicted in Figure 8).

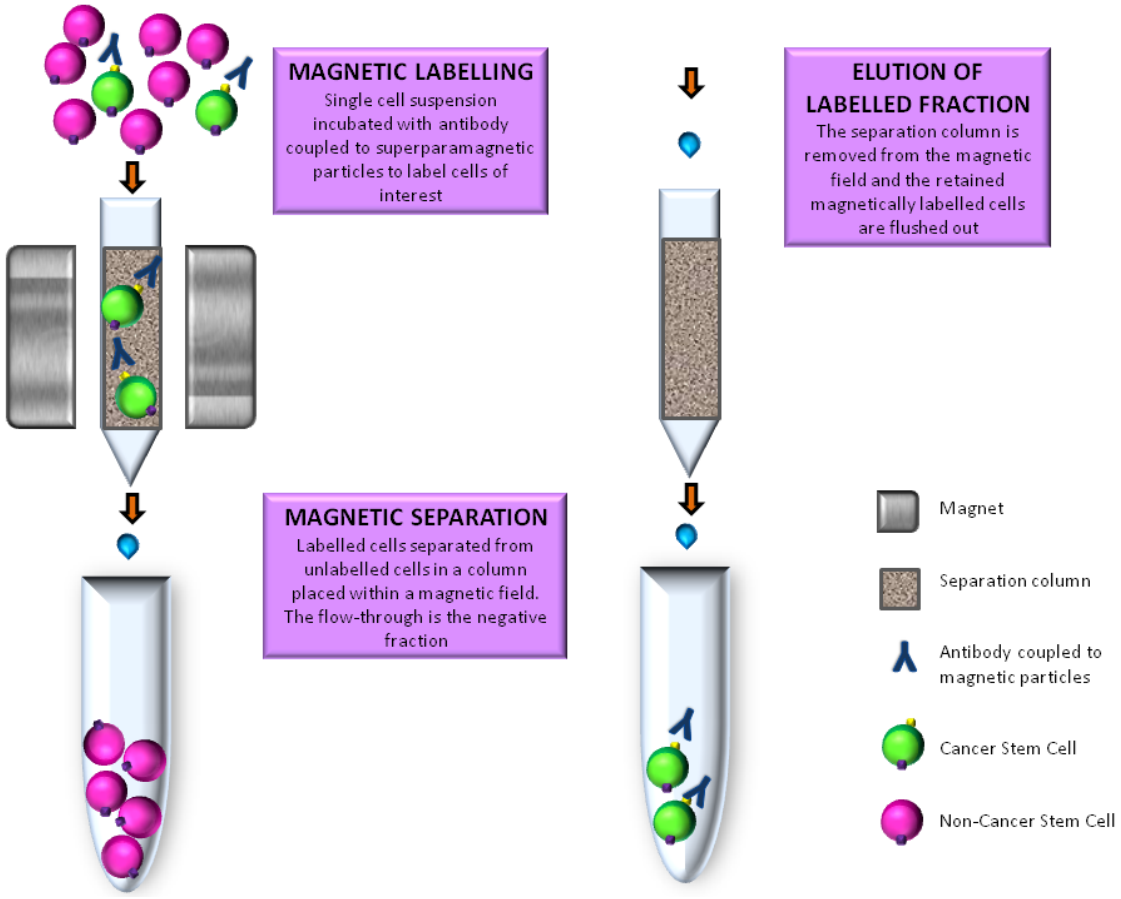


Figure 8: Basic principle of magnetic separation. Cells are first magnetically labelled and thereafter undergo magnetic separation whereby cells of interest remain in the column. The cells are then eluted from the column and collected for further experimentation (own figure).

Prior to magnetic labelling, the cell number was determined by counting, with an optimal range of between $1x10^5$ -$1x10^6$cells/ml. The cells were centrifuged at 800rpm for 10 minutes and the pellet then re-suspended in 300µl separation buffer: 2mmol EDTA, 0.5% BSA in PBS. 100µl of FcR Blocking Reagent was then added to this, together with 100µl of CD133 MicroBeads; this was mixed well and incubated for 30 minutes at 4°C. Cells were then washed with 2ml separation buffer and centrifuged as before, but with the supernatant being

aspirated off and the cells finally re-suspended in 500µl of separation buffer. The separation column was placed within the magnetic field and prepared by rinsing with 500µl separation buffer; and once this had completely run through, the cell suspension was applied and the flow-through collected as the negative fraction. The column was washed 3 times with 500µl of separation buffer each time and this too was collected as part of the negative fraction. The column was removed from the magnetic field and placed into a Falcon tube, 1ml of separation buffer was added and immediately the plunger was firmly depressed to flush the magnetically labelled cells into the collecting tube.

5.2.2 Flow cytometric confirmation of the isolated cell population

Flow cytometry was employed to confirm the CSC population by the expression level of CD133 on the cell surface. The laser in the flow cytometer distinguishes between the labelled and unlabelled cells due to the fluorescence emitted by the dye. Positive and negative fractions eluted from the magnetic separation were evaluated for purity by flow cytometry. Both the positive and negative fractions were set to $1x10^6$cells/100µl. 2µl of a conjugated antibody specific for CD133 (Miltenyi Biotech) was used and detected specifically using the FL2 laser, as it was tagged with a PE fluorochrome. Following a 20 minute incubation period in the dark, the cells were washed twice with separation buffer and finally re-suspended in 100µl of buffer. Control mouse beads (BD CompBead Plus anti-mouse IgG κ) were also used with one drop of negative control added to each of the negative and positive beads, respectively; and with one drop of positive control solution added to positive beads. The positive beads were also incubated with 2µl of antibody for 20 minutes. The mouse beads were run first on the flow cytometer and the peaks obtained were used as a reference for the experimental samples and is used to optimize fluorescence compensation settings for multicolor flow cytometric analyses. Here, a shift in the peaks signifies a positive population that is able to emit fluorescence due to the presence of cell surface associated CD133. A linked marker was used to measure this shift in peaks, together with a dot plot to illustrate the percentage of cells that emitted fluorescence. This analysis represents the separation efficiency and therefore the purity of the CD133 positive fraction.

5.3 Cell Impedance Assays

These assays were carried out with the "xCELLigence" real time cell analyzer (RTCA) (Roche).The E-plates are coated with gold electrodes that detect impedance (resistance) as the cells attach and grow towards confluence. The cells in suspension are applied to these wells and the software set to perform sweeps every 30 minutes. Therefore a measurement of the resistance/attachment is made once the plates are loaded and thereafter every 30 minutes. An increase in measured resistance in each culture well indicates increased cell attachment and growth with the resistance measured as the cell index (CI).

Optimization of cell densities

Prior to evaluating experimental conditions, appropriate cell densities need to be determined for each cell line. The number of cells added to each well in the E-plates is crucial to the success of the experiment as there needed to be enough cells for them to reach confluency but not too many as confluency will be reached too quickly and fair assessment of the proliferative properties cannot be made. The number of cells added will differ between cell lines and types depending on their growth rate and the appropriate quantity can be determined using titration assays. The titration assay performed was according to the manufacturer's guidelines and the following densities were recommended:

- 6250 cells/ml
- 12 500 cells/ml
- 25 000 cells/ml
- 50 000 cells/ml

The cells were first washed with PBS and then trypsinized, the cell number was then determined using the Bio-Rad cell counter. The number of cells was adjusted by serial dilution in order to reach the optimal amount (this was optimized in another assay with varying cell quantities. The baseline was then calculated by adding 100µl of the appropriate media to each well that will be used and running this for 1 minute with 1 sweep. The subsequent steps were then programmed and 100µl of cell suspension added to the wells accordingly (total of 200µl per well), then left to stand for 30 minutes. The E-plate was then inserted into the xCELLigence instrument and the program set to run for 500 hours, performing a sweep every 30 minutes. This was stopped once the confluence plateau was reached. Plots were generated automatically by the RTCA software.

5.4 FLUORESCENCE MICROSCOPY

Immunofluorescence is a technique which takes advantage of the highly specific binding of an antibody to its antigen in order to label particular proteins or other molecules within the cell. Cells are grown and then fixed on to coverslips prior to staining with a primary antibody, binding specifically to the protein or marker. This is then detected with a secondary antibody that is bound to a fluorophore and is referred to as indirect immunofluorescence. This complex fluoresces when excited with the correct excitation wavelength under the microscope, allowing for the visualization of the target proteins. This enables the precise sub-cellular localization of proteins in relation to both the cytoplasm and the nucleus and allows one to elucidate likely interactions of proteins based on their localization. In this study, the products of the Myc and KLF4 genes will be analyzed as well as the marker alkaline phosphatase.

Immunofluorescence staining of cells requires cell attachment and growth on sterile glass cover slips. CD133+ and CD133- cells of approximately 70% confluency were rinsed with PBS, trypsinized and thereafter re-suspended in the appropriate media. A heat sterilized glass cover slip was placed in a petri dish and the cell suspension was carefully aspirated only onto a cover slip, to ensure that the cells attached only to the cover slip. The plates were gently placed in an incubator at 37°C in a 5% humidified chamber overnight allowing the cells to attach to the cover slip. Following an overnight incubation at 37°C the slides were viewed, and more media was added if further incubation was required. Once the cells were partially confluent, the media was removed and the cover slips were rinsed with PBS before 500µl of 3% paraformaldehyde (PFA) was added. Fixation was done for 30 minutes at room temperature, thereafter the PFA was removed, cover slips rinsed with PBS and once again placed in PBS, sealed with Parafilm® and stored at 4°C until staining.

For immunofluorescence staining, the antibodies were diluted in PBS containing 0.5% BSA in PBS (BSA prevents non-specific binding to antigenic sites). The previously fixed cover slips were incubated with 100µl of the respective primary antibodies (see Table 3), at an optimised concentration of 1:400. Slides that were used as a negative staining control did not have primary antibody applied to them, instead 100 µl of the PBS/BSA solution was added. The slides were placed in container with a high moisture content provided by filter paper soaked in water, to reduce evaporation; and were incubated overnight at 4°C.This procedure provides sufficient time for the antibodies diluted at lower concentrations to identify and bind to their epitopes. Following primary antibody staining the cover slips were washed by

dipping 10 times in a beaker containing 0.5% PBS/BSA, followed by dipping 10 times in a second beaker of 0.5%PBS/BSA. The cover slips were placed on glass slides facing upward and 100µl of the secondary antibody solution (see table) was then applied and the slides once again incubated in a moist container in the dark for 1 hour. The negative control slides were only incubated with the secondary antibody and not the primary antibody.

Further fluorescent staining was done in order to localise the nuclei and the actin cytoskeleton. The nuclei were stained with diamidino-phenylindole (DAPI-blue fluorescence), a fluorescent nucleic acid intercalator, which stains DNA and thus localises the nucleus. Slides were removed from the dark following secondary antibody staining and cover slips were rinsed in each of the 2 beakers of 0.5% PBS/BSA by dipping. 100µl of DAPI was applied to the cover slip and incubated for 5 min in the dark at room temperature.

Phalloidin binds to F-actin filaments and allows for the cytoskeletal structure of the cell to be observed. Slides were once again rinsed in each of the 2 beakers following DAPI staining and 100 µl of diluted Phalloidin488 was added and this was allowed to bind for 30 minutes in the dark. Finally the stained cover slips were then mounted on to slides (cell surface down) using Fluoromount® and this was left to dry for 2-3 hours at room temperature in the dark before viewing on the Zeiss LSM 780 confocal microscope.

The captured images were then analysed using ImageJ software 1.47V where the cell of interest was first selected and the measurements set to include area, integrated density and mean grey value. Once this was determined the background fluorescence was measured thrice. Three cells within the region of interest were selected and measured and the CTCF (corrected total cell fluorescence) was then calculated according to the following formula:

CTCF = Integrated density – (area of selected cell x mean fluorescence of background readings)

These results are displayed in tables in the Results section 6.4.

5.5 Assays

5.5.1 Cell Adhesion assays

To determine the ability of a certain cell line to adhere to a specific adhesive substrate, the adhesion assay was performed in 12 well plates coated with Geltrex™ (Invitrogen) (depicted in Figure 9). 250µl of the neat Geltrex™ solution is applied to wells and allowed to set at 37ºC for 30 minutes in order to form a soft gel. The wells are then washed with 200µl of washing buffer and blocked with 200µl of blocking buffer for a further 30 minutes (see Materials section 4.1.3 for composition of buffers and solutions). To evaluate the efficacy of the Shh inhibitors, the cells were pre-incubated with the various small molecule inhibitors for 10 minutes (see Materials section 4.4). The wells were then washed and the cells suspended in serum-free media were added to the wells at a concentration of $1x10^5$ cells/ml and incubated for 2 hours. After 2 hours of incubation the attached cells were washed, fixed for 10 minutes at room temperature, washed again and then stained with crystal violet for 10 minutes. Following a thorough wash the plates were left to dry for 10 minutes and the dye was extracted with 1ml SDS solution and the absorbance measured at 550 nm. This absorbance acted as an indicator of cells attached to the Geltrex™ and the control wells were used to calibrate the spectrophotometer and set the reference point. The adhesion of CD133 positive cells and CD133 negative cells was compared in terms of their ability to adhere to the Geltrex™ in this assay and was performed in triplicate. The adhesion potential of CSC's is thought to be greater than that of differentiated cancer cells, and this was confirmed. Moreover, the ability of the small molecules to inhibit the attachment of CSC's was also ascertained.

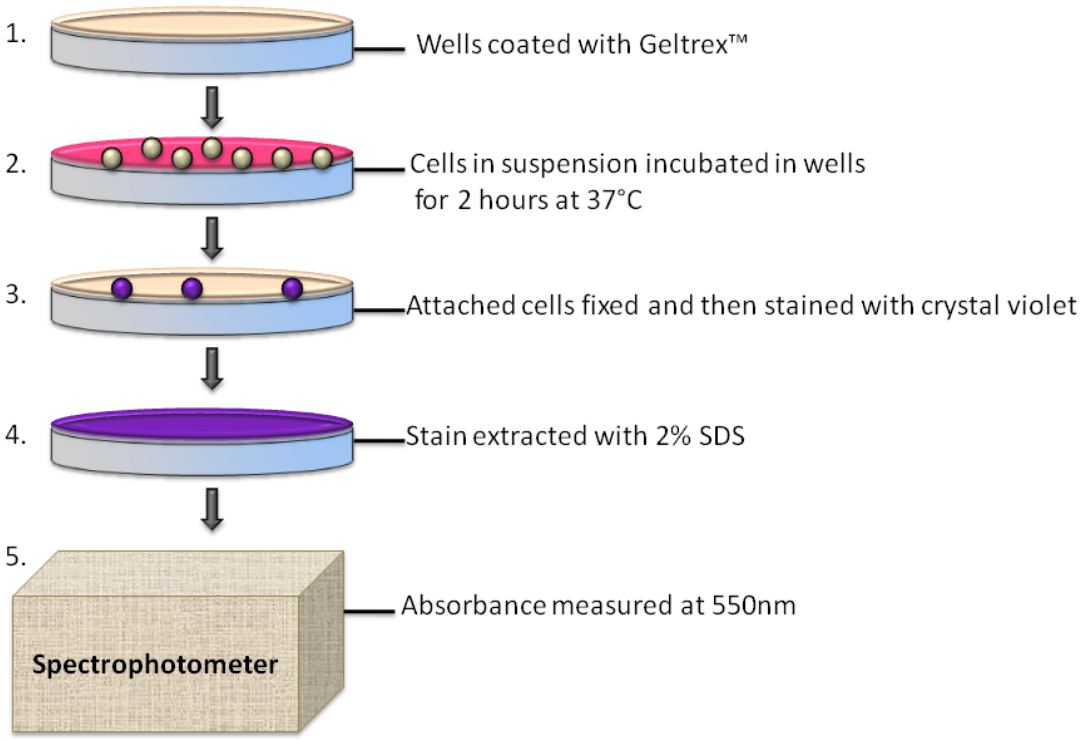


Figure 9: Basic principle of adhesion assay, whereby 1-3.)The ability of cells to adhere to wells coated with Geltrex™ (mimicking the ECM) is assessed and quantified following 3-4.) crystal violet staining and 5.) measurement by a spectrophotometer (own figure).

5.5.2 Invasion assay

The *in vitro* experimental approach to determine the potential of cells to invade an extracellular matrix (ECM) is the chemo-invasion assay. It makes use of a chemo-attractant on the lower site of a polycarbonate filter to induce cell invasion through an upper layer of extracellular matrix and subsequently through the pores of the filter membrane by chemotaxis (Figure 10). The pore size has to be large enough to allow for active cell ingression through the pores, but must not permit them to simply fall through. Geltrex™, the extracellular matrix which will be used contains components of the basement membrane, these mostly being laminin, collagen IV, and heparan sulfate proteoglycans. Prior to commencing the assay the cells were nutrient starved overnight using DMEM F12 with Penicllin/Streptomycin at a confluency of 70%. The following day the Transwell inserts were prepared by applying 50µl of neat Geltrex™ to each well and allowing this to set at 37ºC for 30 minutes. The cell suspension was then made up (concentration of approximately $1x10^6$ cells/ml) by trypsinizing the cells and suspending them in the nutrient free media containing the small molecule inhibitors and allowing this to stand for 10 minutes. 300µl of CSC media (containing nutrients) was added to the lower chamber of the well while 100µl of the cell suspension was

added to the upper chamber. The upper chamber was then inserted into the lower chamber and this was incubated at 37ºC for 20 hours. Following incubation the media from the upper chamber was removed, then rinsed with PBS and cells in the lower chamber were fixed with 300µl of fixing solution for 15 minutes (with upper chamber inserted). Next, the lower chamber and insert were rinsed three times and 300µl of Toluidine Blue stain was added to the lower chamber (with upper chamber inserted) and left to stand for 2 minutes. The lower chamber and insert was rinsed once again and 1ml of SDS extraction solution was added and left for 1 hour. The extracted dye was then measured using a spectrophotometer set at 620nm relative to controls used to set the reference point. The effects of the small molecule inhibitors directed against the Shh pathway was assessed using this assay.

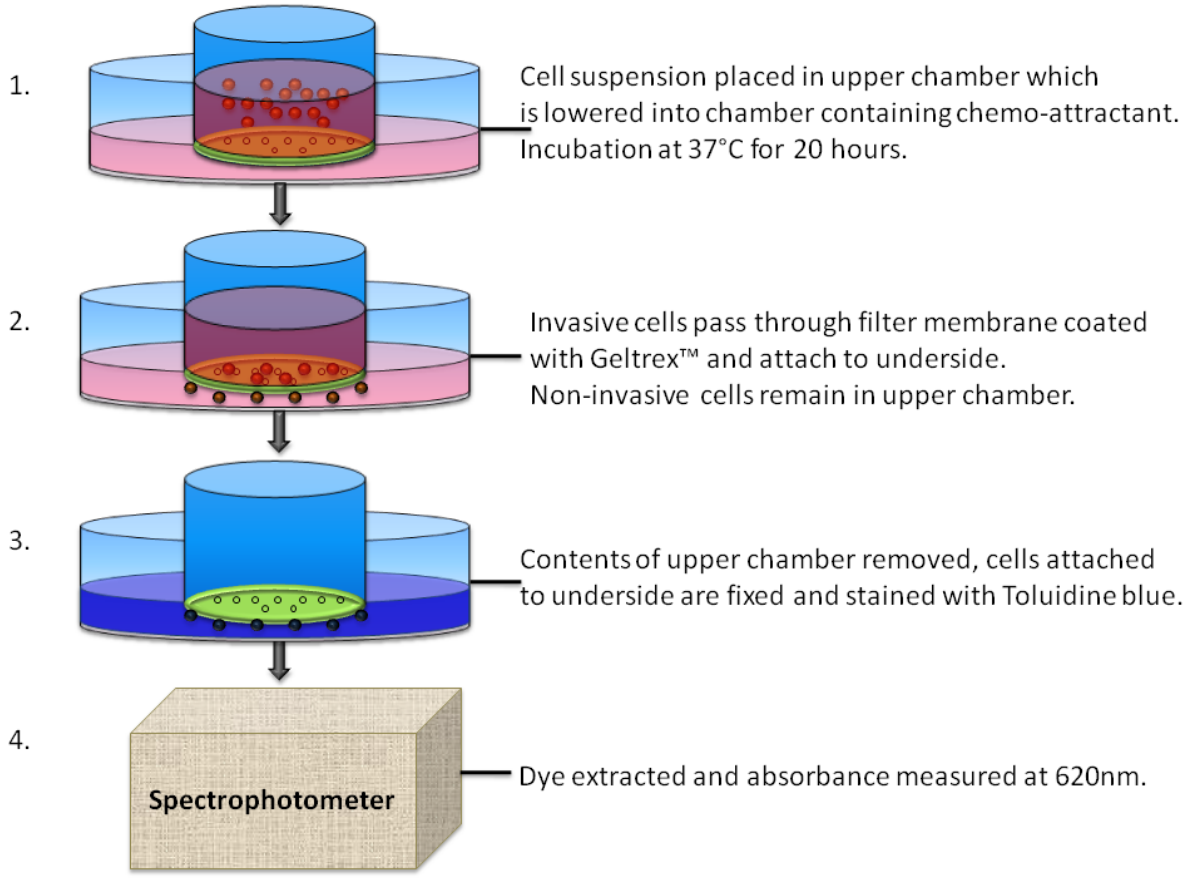


Figure 10: Principle of invasion assay – 1.) Cell suspension applied to upper chamber with polycarbonate membrane coated with Getrex™. This is then lowered into another chamber containing a chemo-attractant (nutrients). 2.) Cells invading transwell insert with membrane (8µm pore size) and Geltrex™. This system serves as a model to mimic the interaction with the basement membrane. Cells with invasive potential are able to move through the pores and the Geltrex™ as they are drawn toward the chemo-attractant. 3.) Cells attached to the underside of the membrane are fixed with PFA and stained with Toluidine Blue. The dye extracted from attached cells is then measured at 620nm with a spectrophotometer (own figure).

5.5.3 Migration/Scratch assay

Scratch/migration assays can be carried out in tissue culture to estimate the migration and proliferation rates of different cell types, as well as to evaluate the effect of potential inhibitors or promoters on cell proliferation. In this experiment the focus will be on the cell migration ability. These assays generally involve first growing a confluent cell monolayer within a cell culture plate (Figure 11). Next, a cell-free area is created by scoring a line through the confluent monolayer. The cells are then incubated with the test drug and a control in parallel. The closure of the open gap by cell migration and/or proliferation is then monitored microscopically over a 24 hour period (every 2 hours for the first 6 hours thereafter at the 24 hour mark). Ten measurements were made at each time interval and the average gap calculated. The rate at which the gap closes was then measured and used to determine the rate of migration following treatment with the small molecule inhibitors in comparison to the control.

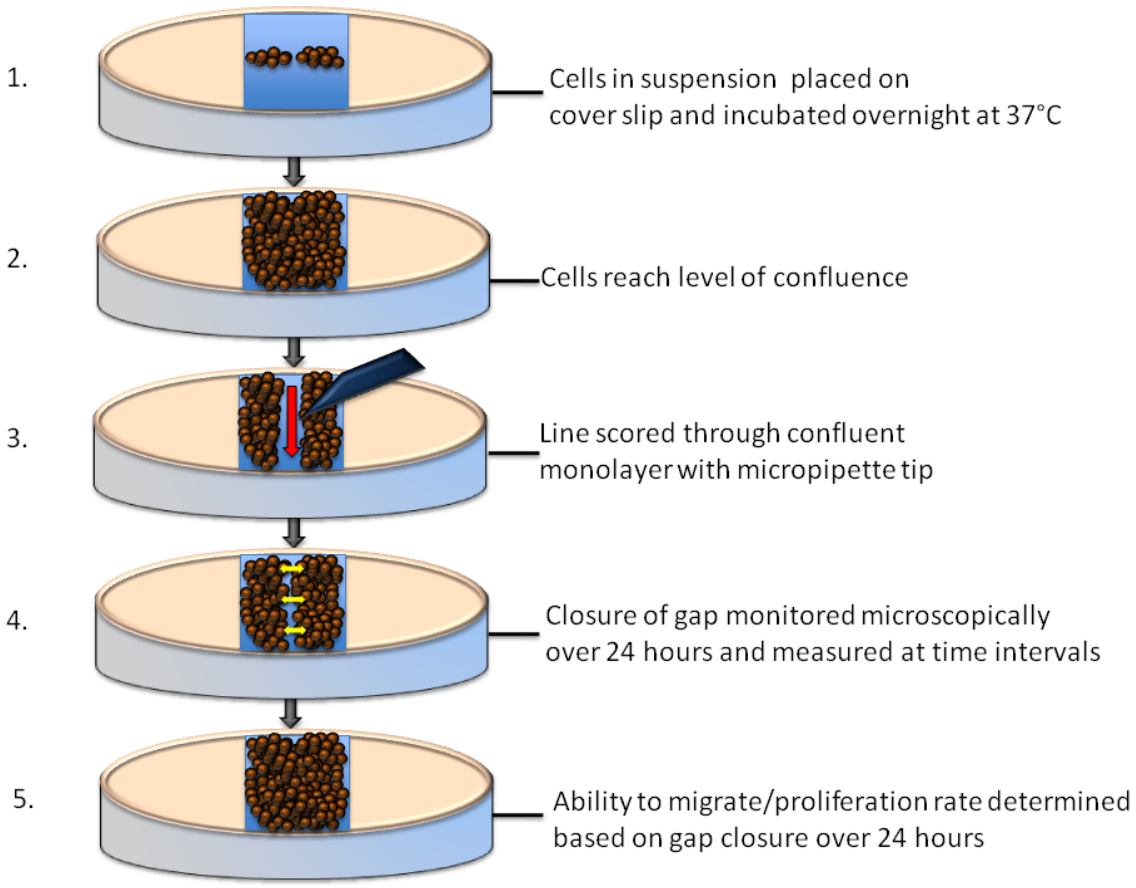


Figure 11: Basic principle of scratch/migration assay – 1.) Cell suspension placed on glass cover slip and incubated until, 2.) a confluent monolayer is grown . 3.) A line or scratch is scored through the monolayer. 4.) Closure of the gap is monitored over a 24 hour period with measurements of the gap taken periodically. 5.) The ability of cells to migrate or proliferate is measured, in some instances the gap closes completely while in others a gap remains (own figure).

5.6 STATISTICAL ANALYSIS

Statistical evaluations of the following data were performed:

- Comparison of the expression of CD133 and other stem cell markers by positive and negative fractions using two-tailed Student's *t*-test with a 95% confidence interval. *p* – values of less than 0.05 were considered significant.

- The expression of Shh and CD133 following treatment with cyclopamine was compared to an untreated control using two-tailed Student's *t*-test with a 95% confidence interval. *p* – values of less than 0.05 were considered significant.

- Comparison of the positive and negative fractions in the adhesion assay using two-tailed Student's *t*-test with a 95% confidence interval. *p* – values of less than 0.05 were considered significant.

- Comparison of the treated and untreated cells in adhesion, invasion, and scratch assays: Upon application of the small molecule inhibitors, their effects on invasion and adhesion will be evaluated using a two-tailed Student's *t*-test with a 95% confidence interval. *p* – values of less than 0.05 were considered significant.

- Linear dependency between two variables was expressed using Pearson's (*r*) correlation coefficient. The correlation between invasion and adhesion was determined, as well as the correlation between adhesion and migration (migration/scratch assay).

6. RESULTS

6.1 FLOW CYTOMETRY CONFIRMATION ISOLATED OF CD133+ CELLS

Flow cytometry was performed on a BD Accuri™ C6 flow cytometer following staining with a PE-conjugated CD133 antibody. Fluorescence was detected by the FL2 laser and using forward scatter plots cells were gated on the majority cell population using BD Accuri™ C6 software. Outlying cells and debris were excluded and peaks were generated after counting 10 000 cells. From the flow cytometry plots below, clear shifts in a specific cell population to the right (red peak) relative to the control (blue peak) are seen with both the DLD1 (Figure 12.a) and HT29 (Figure 12.c) cell lines. The shift of 70% or more shows a successful magnetic separation of CD133+ cells from the general cell population. Increased purity of the CD133+ population is possible with a further magnetic separation. This was not employed in this situation since the specified CSC media would result in the selection and survival of CSC's only. Due to the absence of FBS, differentiation of stem cells is discouraged. Furthermore, following the initial separation as a relatively low number of CD133+ cells are isolated, this would be an insufficient amount to perform another separation immediately without allowing the cells to proliferate. For successful isolation to be achieved, a minimum number of $1x10^8$ cells/ml is recommended according to the manufacturer's guidelines.

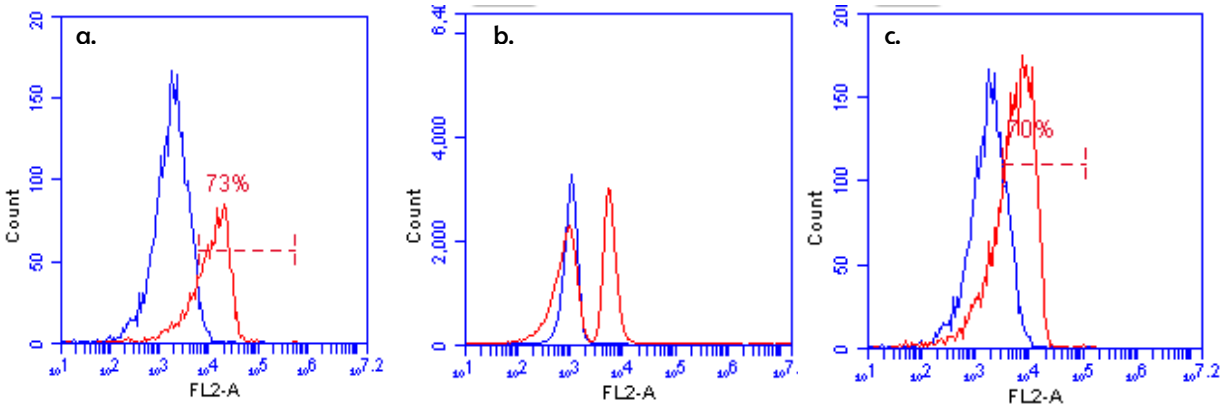
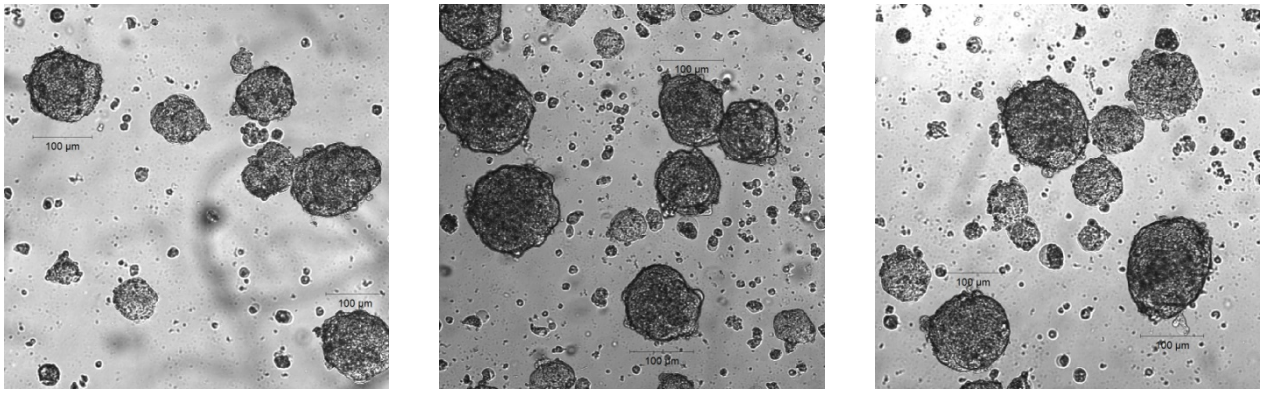


Figure 12: CSC's were successfully isolated using the CD133 receptor as a definitive marker. The Miltenyi Biotec CD133 Cell Isolation kit was employed for magnetic separation of cells; which was then confirmed by flow cytometry using a PE conjugated CD133 antibody. The blue peak represents the cells lacking CD133 expression, while the red peak represents those expressing CD133 on their cell surface. a.) DLD1 CSC's with 73% of the population expressing CD133, b.) BD™ CompBeads Set Anti-Mouse Ig, κ/negative control compensation microparticles used to optimize fluorescence compensation settings, c.) HT29 CSC's with a level of 70% cells expressing CD133.

6.2 SPHEROID FORMATION OF CD133+ CELLS

Following magnetic separation the CD133+ fractions were then cultured in a serum-free stem cell specific medium supplemented with various growth factors (see Materials section 4.1.2). The omission of FBS encourages stem cell growth without inducing differentiation. Initial cultures of separated stem cells grow as spheroids which were viewed in glass bottom cell culture dishes on the confocal microscope, using differential contrast microscopy (see images below Figure 13). This spheroid growth, a distinctive feature of stem cells, indicates the presence of CSC's in these cultures.

a.) DLD1



b.) HT29

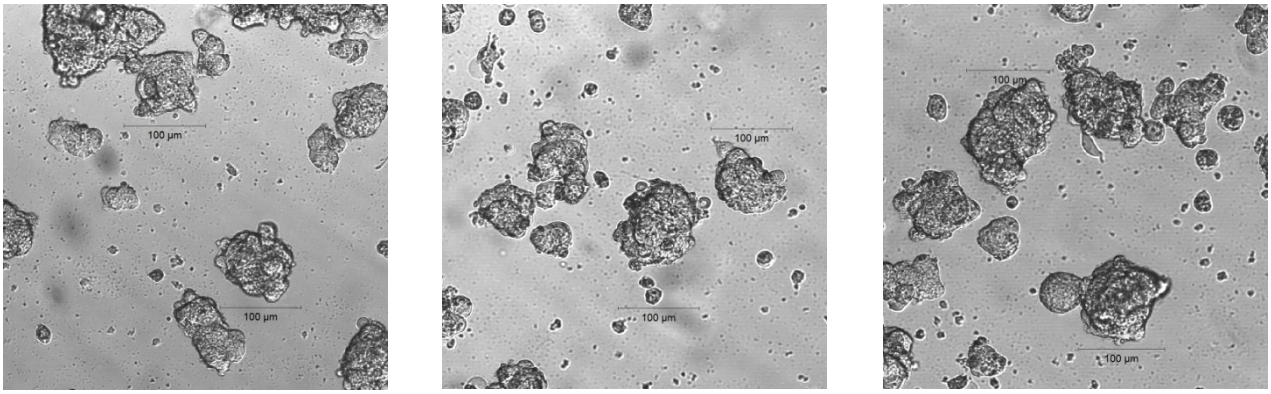
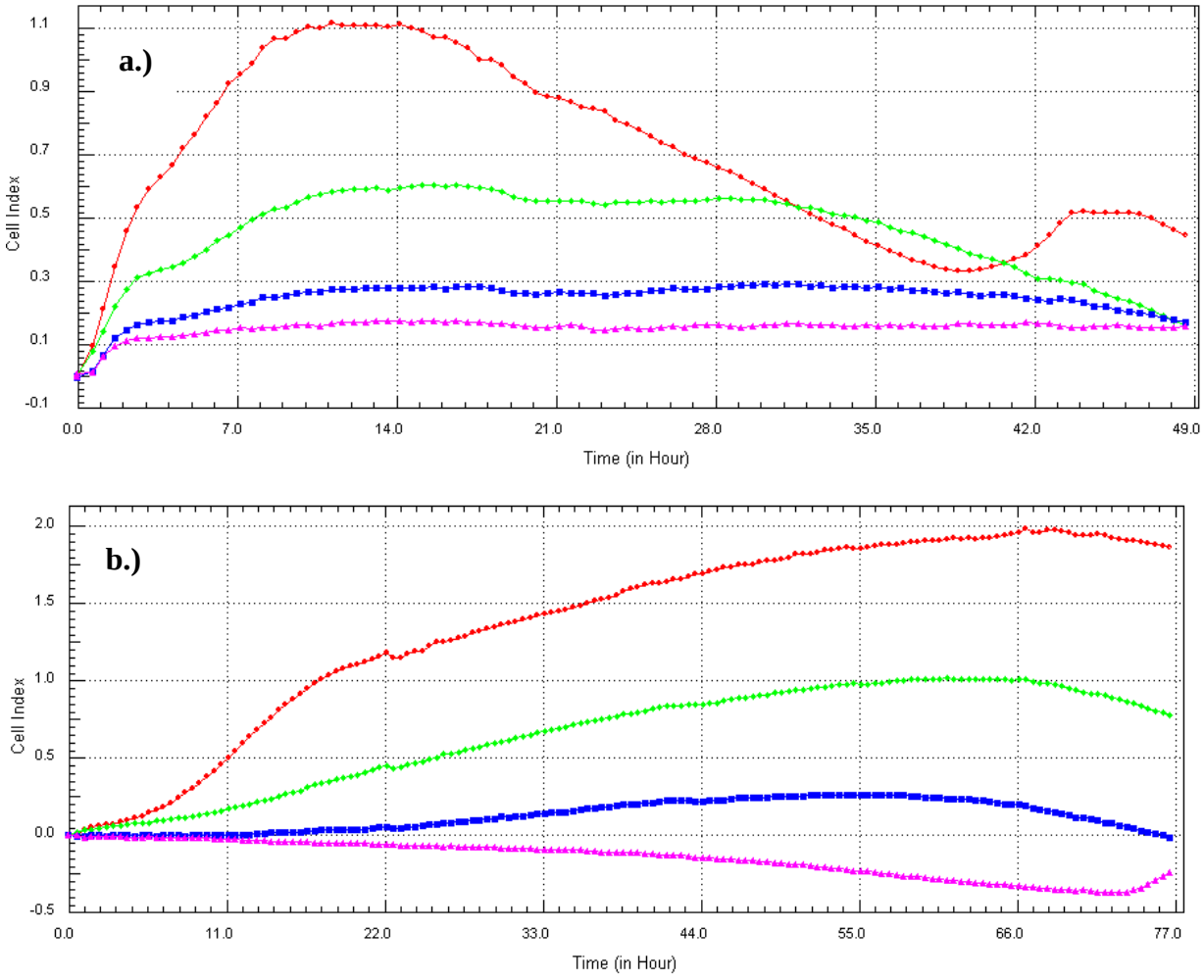


Figure 13: CD133+ cells showed spheroid growth typical of stem cells, of a.) DLD1 CSC's and b.) HT29 CSC's. Each cluster of cells measures approximately 100µm in diameter.

6.3 CELL PROLIFERATION ASSAYS- XCELLIGENCE

Optimal cell concentrations are imperative in xCELLigence proliferation assays and these were determined in a prior experiment since studies using CD133+ fractions of DLD1 and HT29 cells are not mentioned in literature. Concentrations ranging from 6250 cells/ml to 50 000 cells/ml were tested over a 100 hour period (Figure 14). This was in accordance with the manufacturer's guidelines and the cell titration protocol provided by Roche. The duration over which the experiment should be conducted was also determined and is vital to the study since it should allow sufficient time for cells to reach confluence but not to become over-confluent and detach. Another aspect taken into consideration was the limited volume the E-plate well could accommodate (100µl) as this would restrict the amount of media that could be added. The volume of media had to be adequate for the duration of the experiment, to ensure cell survival. Furthermore, media could not be added during the course of the experiment as the weight of the newly added media distorts the impedance value, or the Cell Index (CI) as measured by the instrument.



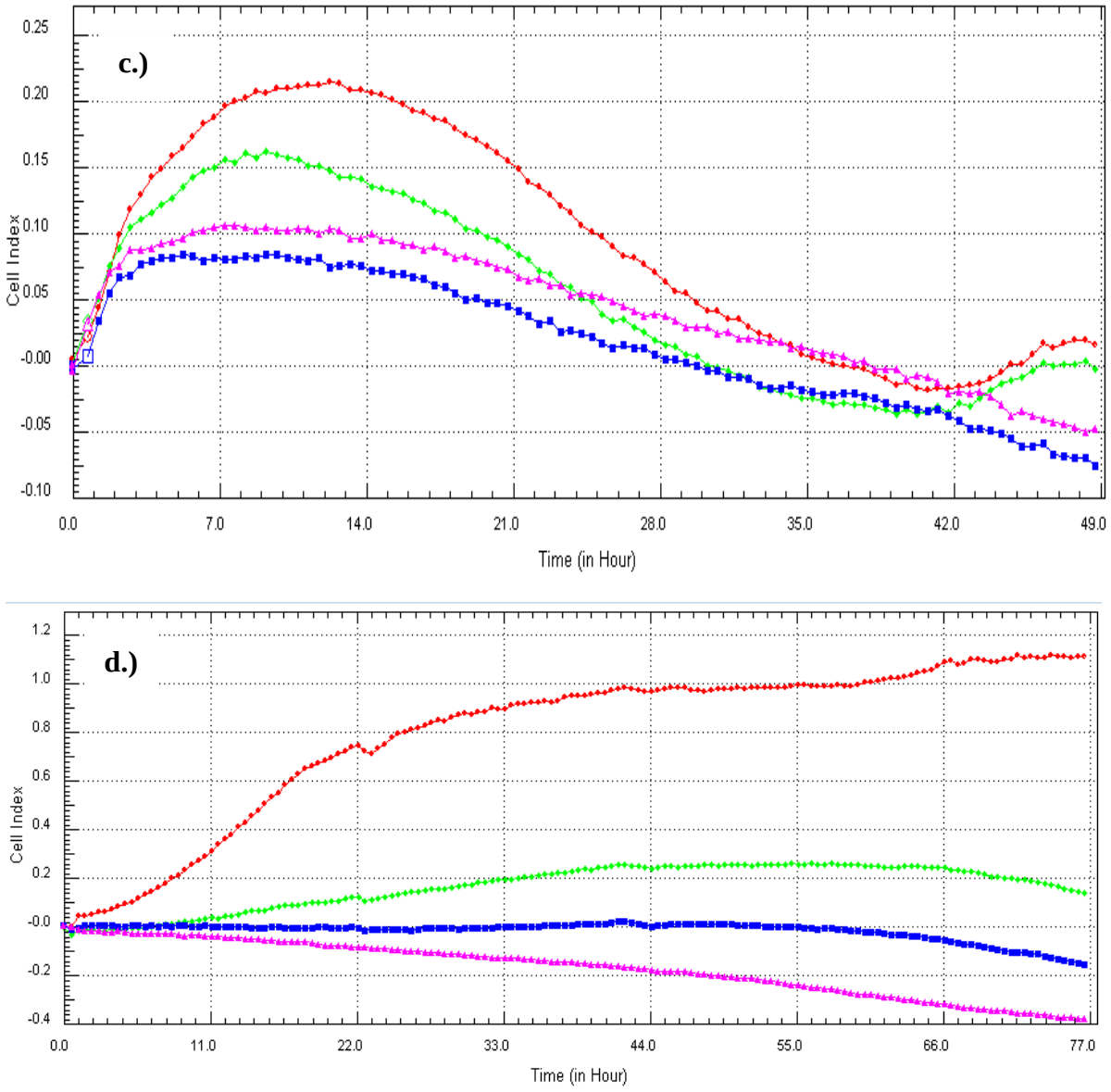
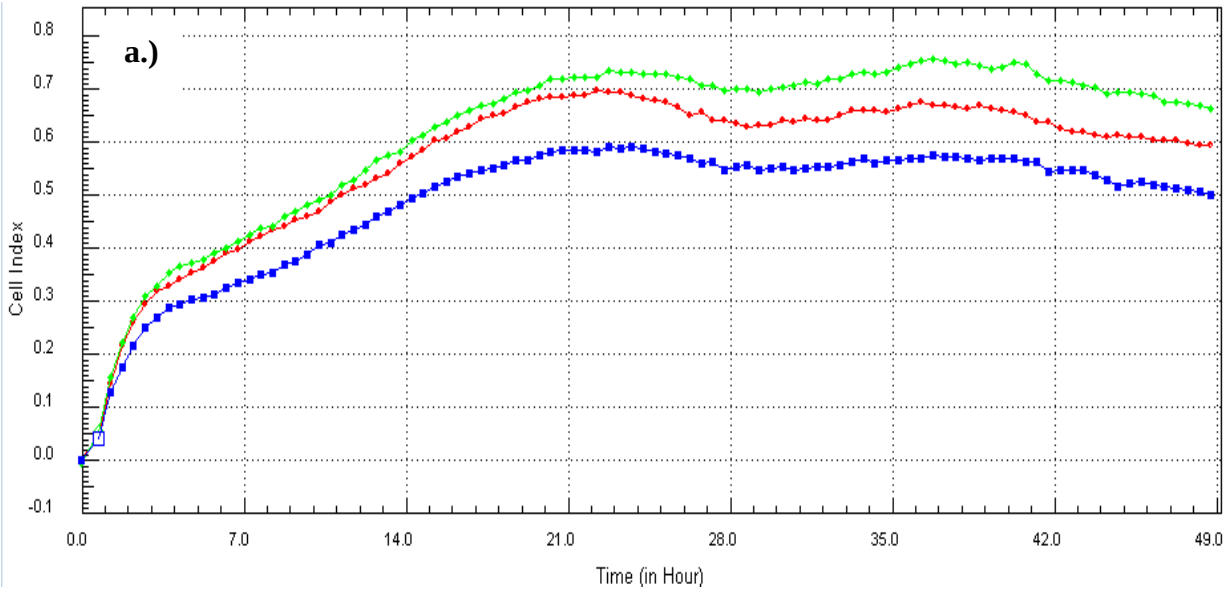
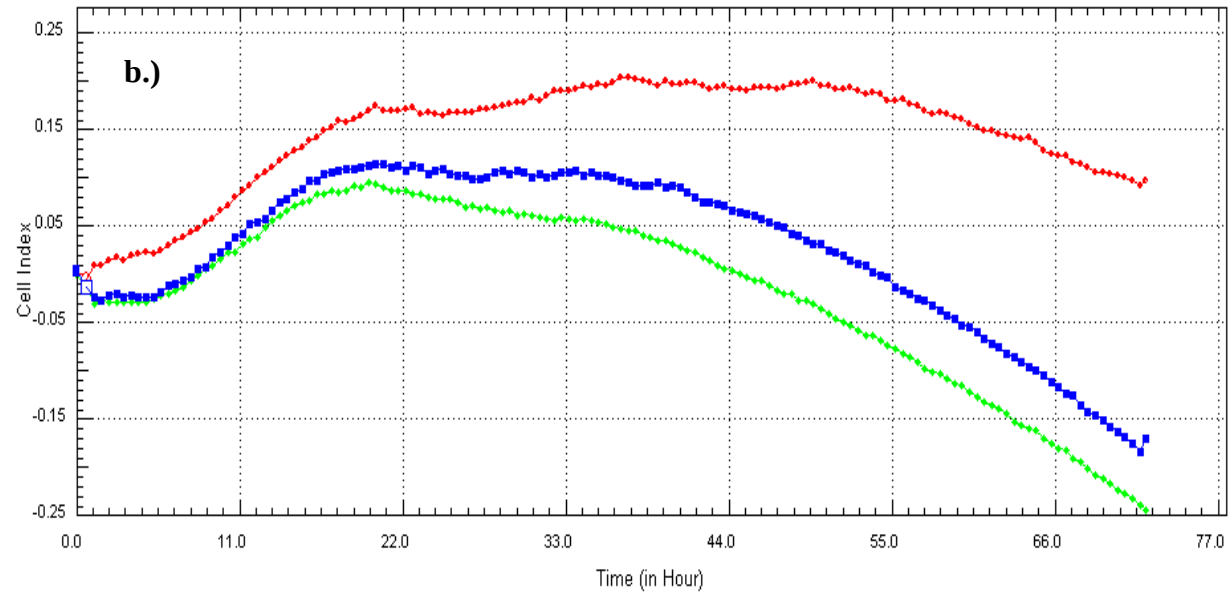
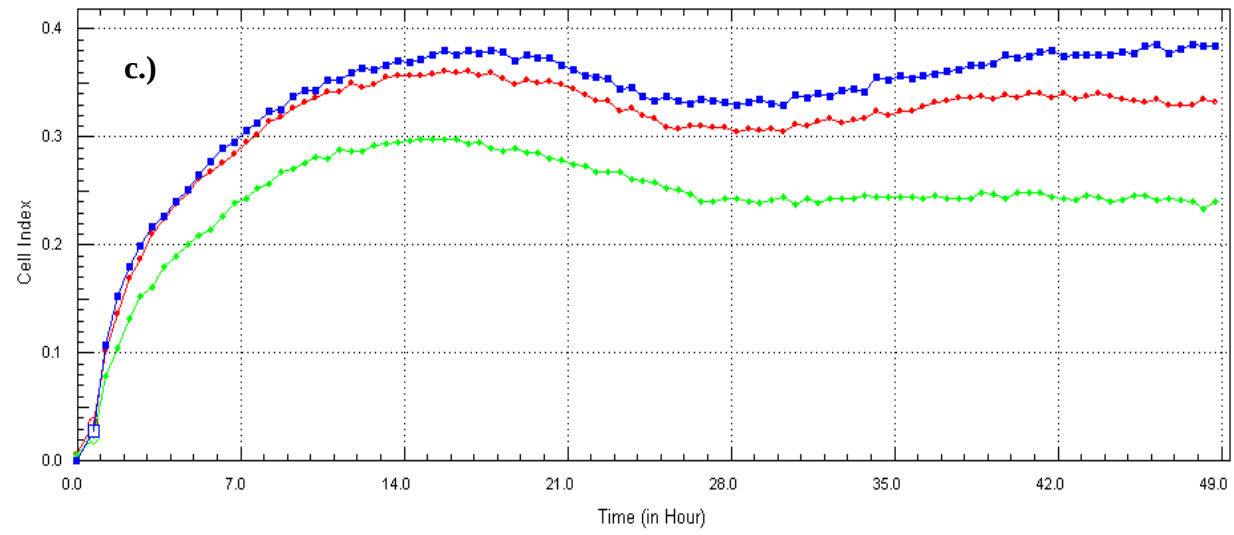


Figure 14: Cell Index (level of adherence) was measured by xCELLigence using E-plates, with sweeps every 30 minutes over a period of 100 hours, giving an indication of cell growth patterns and proliferation rates. Dilution tests were performed using 50 000 (red), 25 000 (green), 12 500 (blue) and 6250 (pink) cells/ml. a.) HT29 CD133- dilution test, b.) HT29 CD133+ dilution test, c.) DLD1 CD133- dilution test, d.) DLD1 CD133+ dilution test. From the graphs it can be deduced that the optimal concentration would be 25 000 cells/ml for CD133- fractions of both cell lines and 50 000 cells/ml for CD133+ fractions of both cell lines. This deduction was made based on the overall curve of the graph and if an ideal level of confluence is reached in the stipulated time of 72 hours. It was also noted that the CD133- fractions were able to reach this level at approximately 48 hours, whereas the CD133+ fractions required an additional 24 hours, to reach confluence at 72 hours. Graphs shown represent the CI over time (hours).

Following optimization:







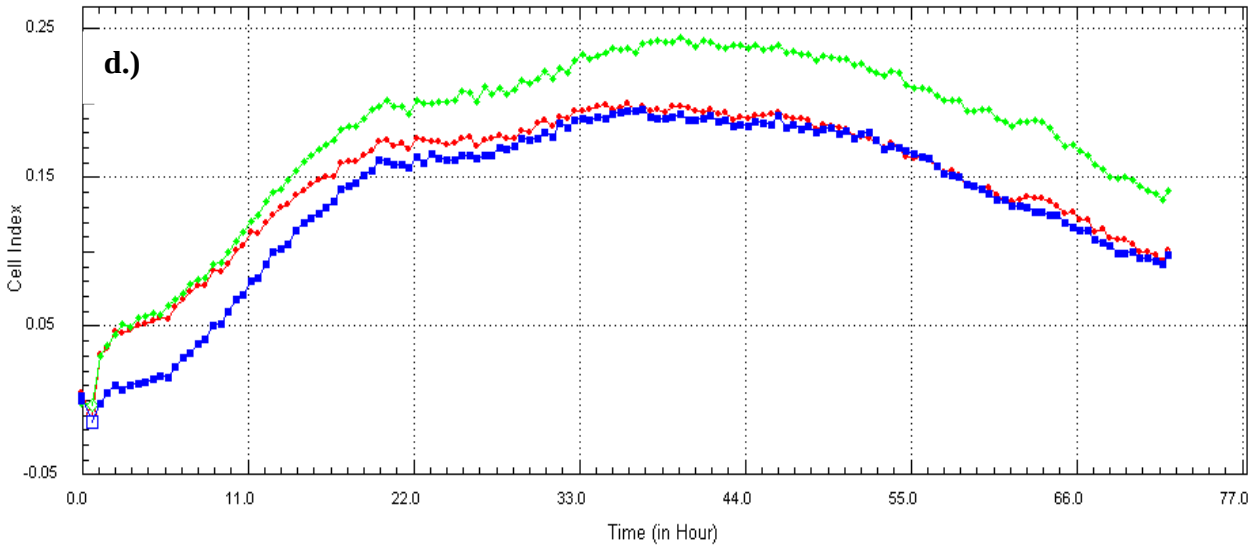


Figure 15: The optimal concentration previously determined was then used, 25 000 cells/ml CD133- and 50 000 cells/ml CD133+, which was performed in triplicate, shown here as the red, blue and green curves. a.) HT29 CD133- , b.) HT29 CD133+ , c.) DLD1 CD133- , d.) DLD1 CD133+. It was clear that the DLD1 cell growth pattern differed to HT29 pattern; and the DLD1 proliferation rate was slower than the HT29 cells. The CD133+ (CSC's) proliferation rate was slower than CD133- cells, with growth plateaus at 72 hours and 48 hours, respectively. It could be suggested that the CD133+ fractions would either require further time or a higher concentration of cells in order to reach a greater level of confluence, as indicated from the dilution experiments. The HT29 CD133- cells exceeded previous CI recordings at this starting concentration by reaching a value of 0.75. This exponential growth pattern was evident in the dilution tests where CI peaked at a value of 1.1, representing a concentration of 50 000 cells/ml. A further observation that can be made is the decline in CI following the growth plateau of the CD133+ fractions of both cell lines, with a shorter plateau period in comparison to the CD133- fractions. A slight lag phase is also seen in the CD133+ fractions, particularly in the HT29 cell line.

The HT29 CD133- exceeded previous CI recordings with a starting concentration of 25 000 cells/ml by reaching 0.75. This exponential growth pattern was evident in the dilution tests where CI peaked 1.1 at a concentration of 50 000 cells/ml (Figure 15). These HT29 non-CSC showed highly exponential growth in the first 7 hours, followed by further growth at a slightly lower rate in the subsequent 14 hours. After this, a plateau was then reached and the CI ranged between 0.6 and 0.7. This indicates that the HT29 cell line has a greater proliferation rate in comparison to the DLD1 cell line. In contrast the CSC of the same cell line showed a far less rapid growth over the initial 21 hour period, resulting in a plateau between 0.1 and 0.2 CI. Similarly, the DLD1non-CSC showed accelerated growth in the first 7 hours, followed by further growth till reaching a plateau at 14 hours; however, the CI reached a maximum of merely 0.35. As expected, the CSC counterpart subsequent to a 21 hour exponential growth phase, reached a plateau of 0.2 CI (please note that CI values given are approximate and provide an indication of average of 3 measurements). A further observation that can be made is the decline in CI following the plateau of the CD133+ fractions of both cell lines, with a shorter plateau period in comparison to the CD133- fractions. A slight lag phase is also seen in the CD133+ fractions, particularly in the HT29 cell line, this possibly being due to cancer stem cells being slow cycling[99]. Overall the trends noted are that the DLD1 cell line has a slower growth rate than that of the HT29 cell line and that in both cell lines the CSC's proved to have slower proliferation rates in comparison to their non-CSC counterparts. It could be suggested that the CD133+ fractions would either require further time or a higher starting concentration of cells in order to reach a greater level of confluency, as can be deduced from the dilution experiments.

6.4 CONFOCAL MICROSCOPY CHARACTERIZATION

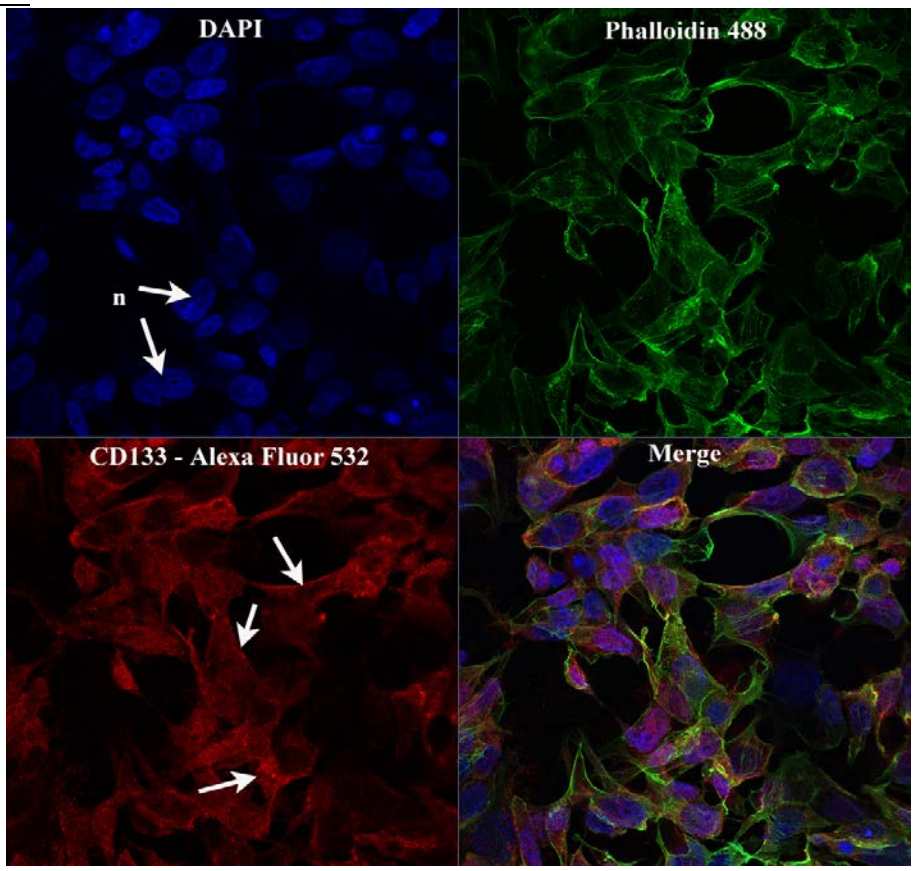
The positive and negative fractions collected from the magnetic separation using the marker CD133 were then further characterized using confocal microscopy. Several markers were selected based on their role in the Shh pathway, invasion and metastasis. These markers included c-Myc, KLF4 and alkaline phosphatase and are also thought to be indicators of stem-like capacity required for induced pluripotent stem cell production and are markers of embryonic stem cells. Positive and negative fractions were stained with primary antibodies specific for the respective marker and thereafter stained with secondary antibodies with conjugated fluorochromes. In the case of negative control slides the primary antibody was omitted and only secondary staining was performed to differentiate from non-specific binding. Fluorescence microscopy captured on Zeiss confocal microscope at 63X magnification provided an indication of the expression of cell surface markers.Using the confocal microscope the fluorescence was captured with Zeiss software (Carl Zeiss LSM 780), image gain was adjusted within certain bounds. The images were analyzed using ImageJ software in order to quantify the fluorescence emitted and 3 cells per captured field of view were selected for measurement. The CTCF was then calculated with the measured background fluorescence taken into consideration (see Methods section 5.4 for formula). The nuclei were stained with the DNA intercalating dye DAPI (blue), and f-actin filaments were stained with Phalloidin 488 to stain the cytoskeleton green. The respective antibody staining is indicated with red fluorescence. The three stains are shown separately as well as a final image overlaying them in order to visualize where the marker expression in relation to the cytoskeleton and nucleus as well as the number of cells and their orientation.
See Appendix B for all negative control images.

6.4.1 CD133 localization in non-permeabilized CD133+ and CD133- cell fractions

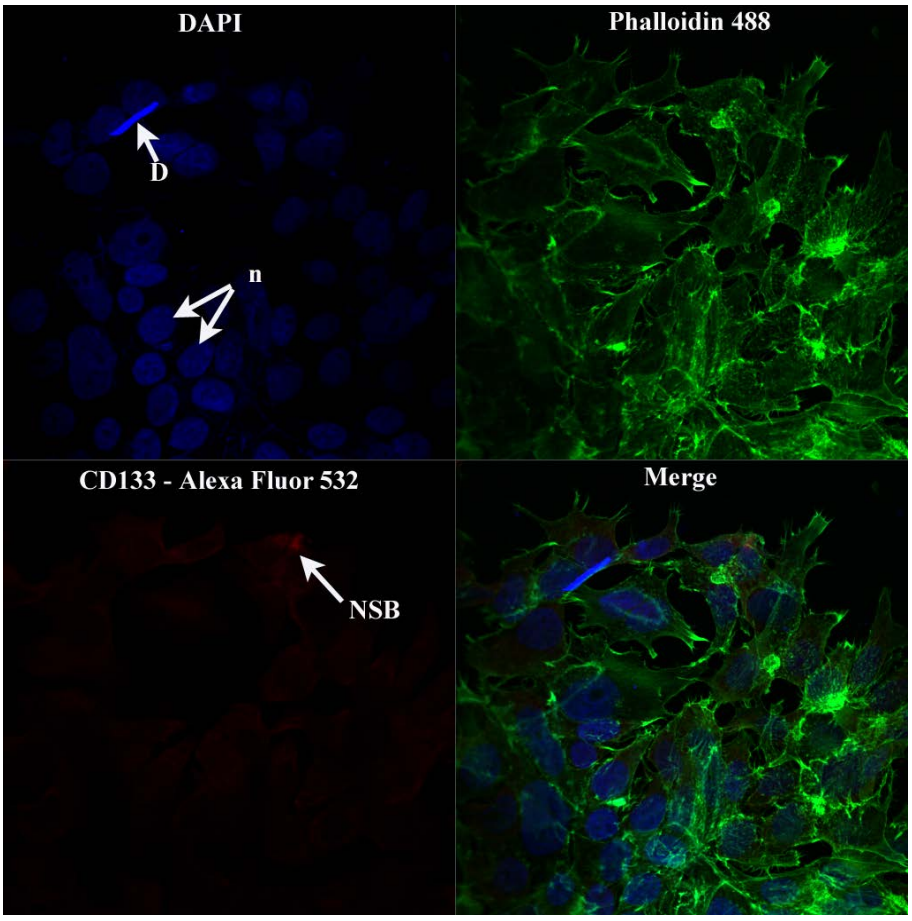
At the outset, CD133 expression was evaluated whereby fluorescence emitted from the positive fractions of both the DLD1 and HT29 cell lines was observed to be far greater than that of the negative cell fractions. This was to be expected since isolation of the CSC’s was done on the basis of this marker and cells not expressing CD133 would have passed through the column to comprise of the negative fraction.

a.) DLD1

CD133+



Control



CD133-

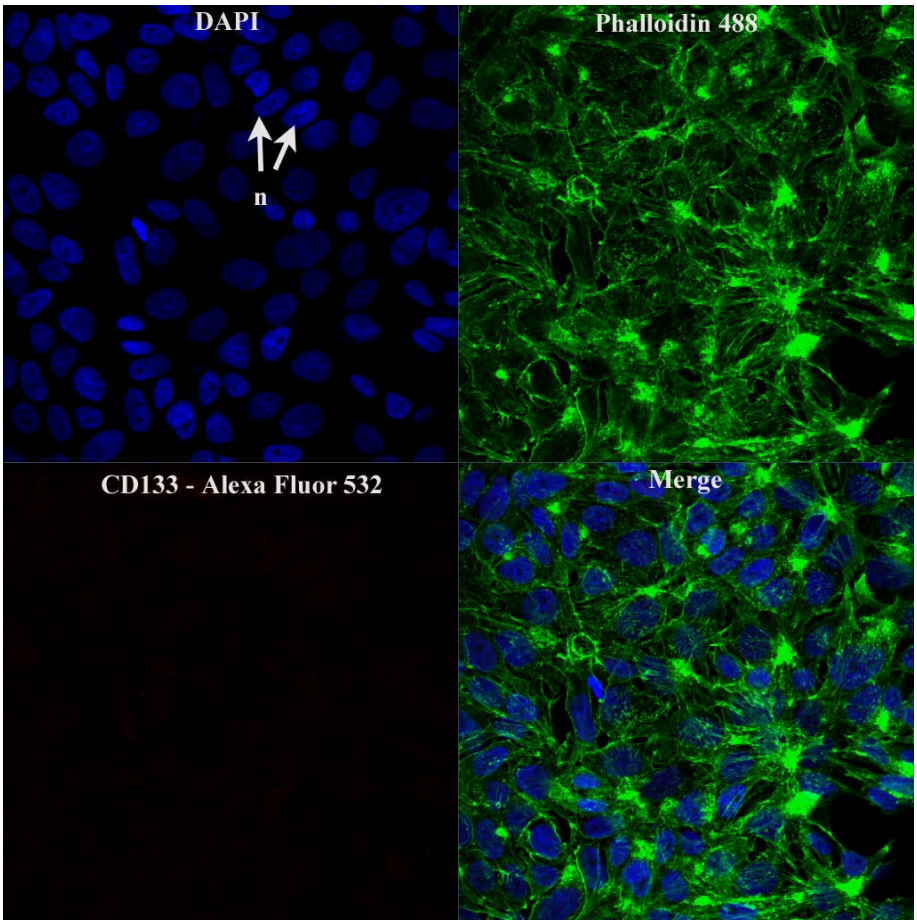


Figure 16: CD133 localization in non-permeabilized CD133+ and CD133- fractions of DLD1 cell line at 63x magnification with nuclei shown with (n) and debris (D). Arrows indicating the cell-surface CD133 on DLD1 cells. It is evident that the levels of CD133 are far higher in the DLD1 CD133+ cell fraction with no expression of CD133 seen in the negative fraction (Original Magnification 63X).

Table 4: Corrected Total Cell Fluorescence (CTCF) of DLD1 CD133+ cells (non-permeabilized), stained with an anti-CD133 antibody

	Integrated density	**Area of selected cell**	**Background fluorescence**	**CTCF**
	20279	1086	0.405	19839.17
	19842	1776	0.405	19122.72
	21985	1678	0.405	21305.41
Average CTCF				20089.1

Table 5: Corrected Total Cell Fluorescence (CTCF) of DLD1 CD133+ cells (non-permeabilized); negative control

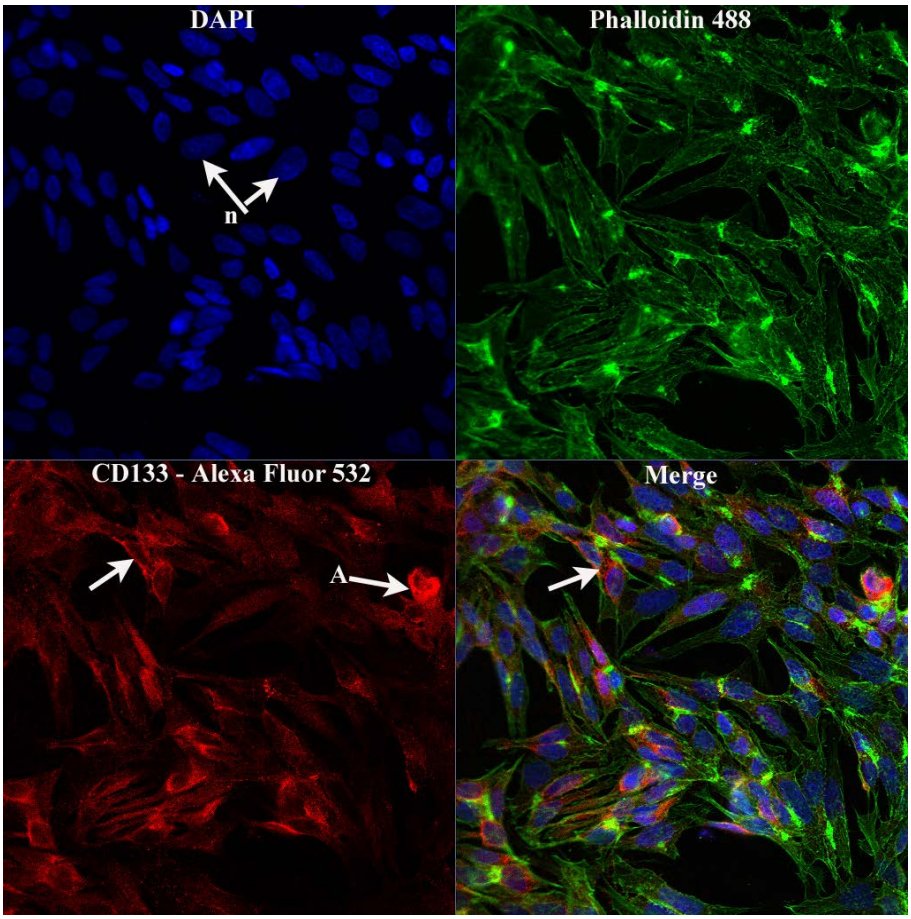
	Integrated density	Area of selected cell	Background fluorescence	CTCF
	1435	1025	0	1435
	1652	895	0	1652
	1524	939	0	1524
Average CTCF				1537

Table 6: Corrected Total Cell Fluorescence (CTCF) of DLD1 CD133- cells (non-permeabilized), stained with an anti-CD133 antibody

	Integrated density	Area of selected cell	Background fluorescence	CTCF
	4852	1296	1.387	3054.448
	4751	1485	1.387	2691.305
	4683	1346	1.387	2816.098
Average CTCF				2853.95

b.) HT29

CD133+



b.) CD133-

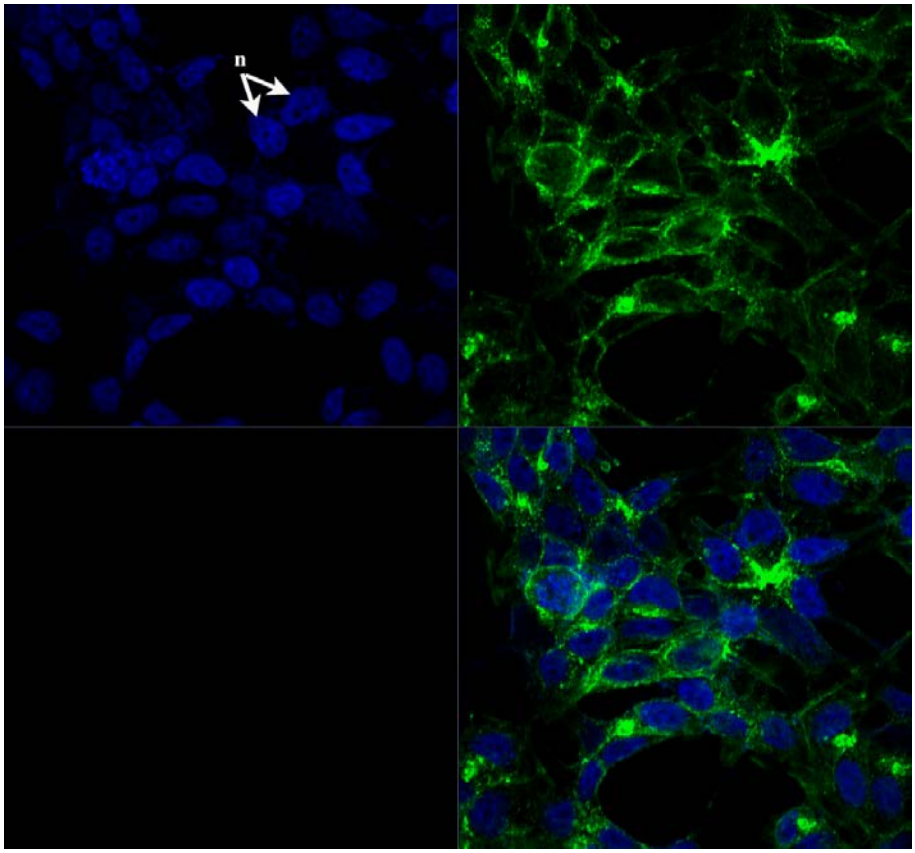


Figure 17: b.) CD133 localization in non-permeabilized CD133+ and CD133- fractions of HT29 cell line, nuclei shown with (n) and cell undergoing apoptosis (A). In non-permeabilized HT29 cells the CD133+ fraction displayed a greater fluorescence intensity indicated with arrows, in comparison to the CD133- fraction, which had little or no fluorescence when stained with the CD133 antibody (Original Magnification 63X).

Table 7: Corrected Total Cell Fluorescence (CTCF) of HT29 CD133+ cells (non-permeabilized), stained with an anti-CD133 antibody

	Integrated density	Area of selected cell	Background fluorescence	CTCF
	9963	639	0.169	9855.009
	10308	629	0.169	10201.7
	8805	661	0.169	8693.291
Average CTCF				9583.333

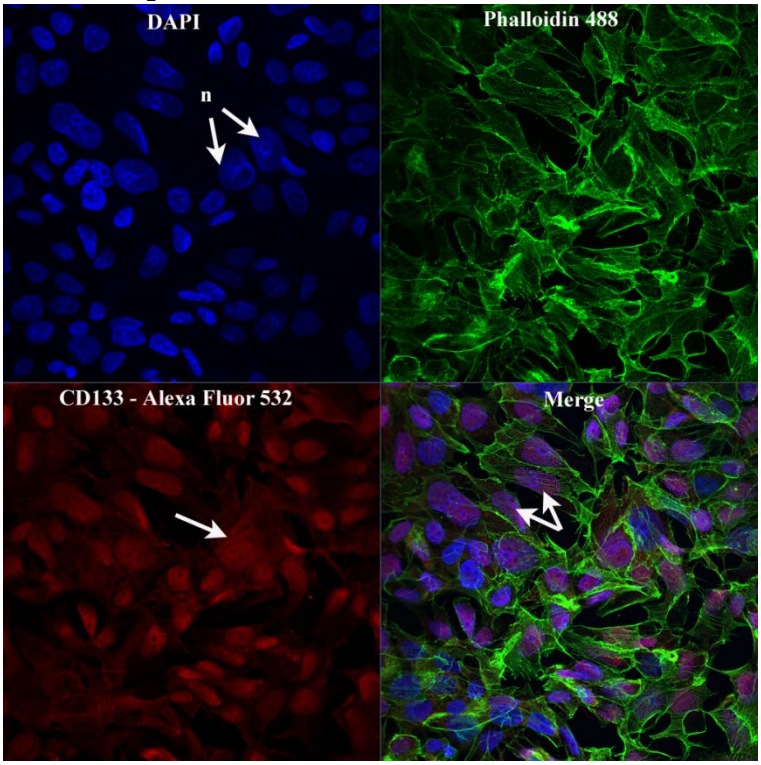
Table 8: Corrected Total Cell Fluorescence (CTCF) of HT29 CD133- cells(non-permeabilized), stained with an anti-CD133 antibody

	Integrated density	Area of selected cell	Background fluorescence	CTCF
	2068	571	0.386	1847.594
	2099	507	0.386	1903.298
	2263	667	0.386	2005.538
Average CTCF				1918.81

6.4.2 CD133 localization in permeabilized CD133+ and CD133- cell fractions

a.) DLD1

CD133+



CD133-

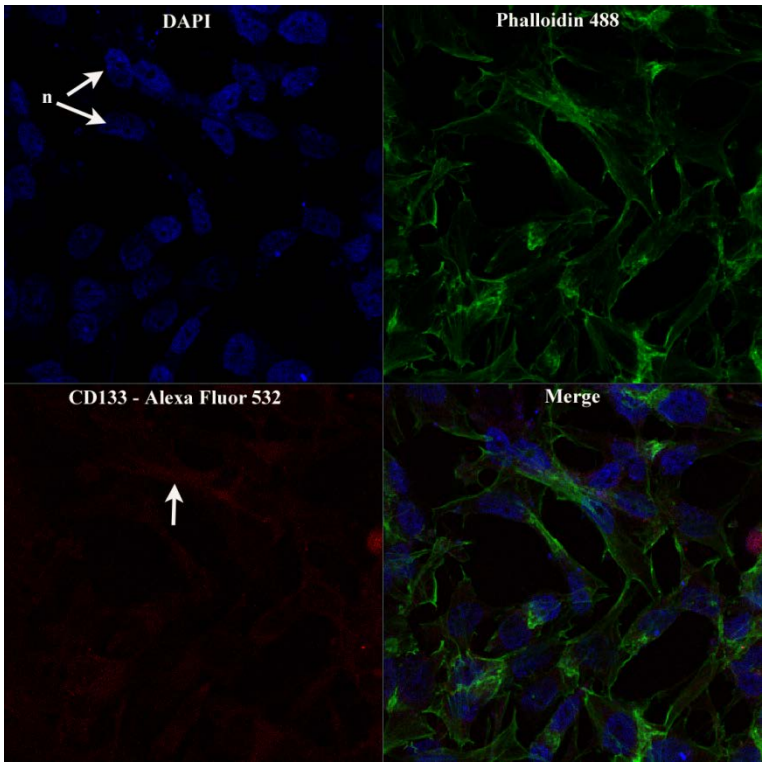


Figure 18: a.) CD133 localization in permeablized CD133+ and CD133- fractions of DLD1 cell line, nuclei indicated with (n). With the permeabilization of DLD1 cells, CD133 is additionally localized intracellularly within the CD133+ fraction. Based on the colour of the nucleus in the 2D image, pink, this indicates a co-staining of the nucleus (red+blue=pink), shown with arrows, indicating an association of CD133 with the nucleus or DNA. Although some fluorescence is visible in the CD133- cell fraction indicated with the arrow, it is to a much lesser extent (Original Magnification 63X).

Table 9: Corrected Total Cell Fluorescence (CTCF) of DLD1 CD133+ cells (permeabilized), stained with an anti-CD133 antibody

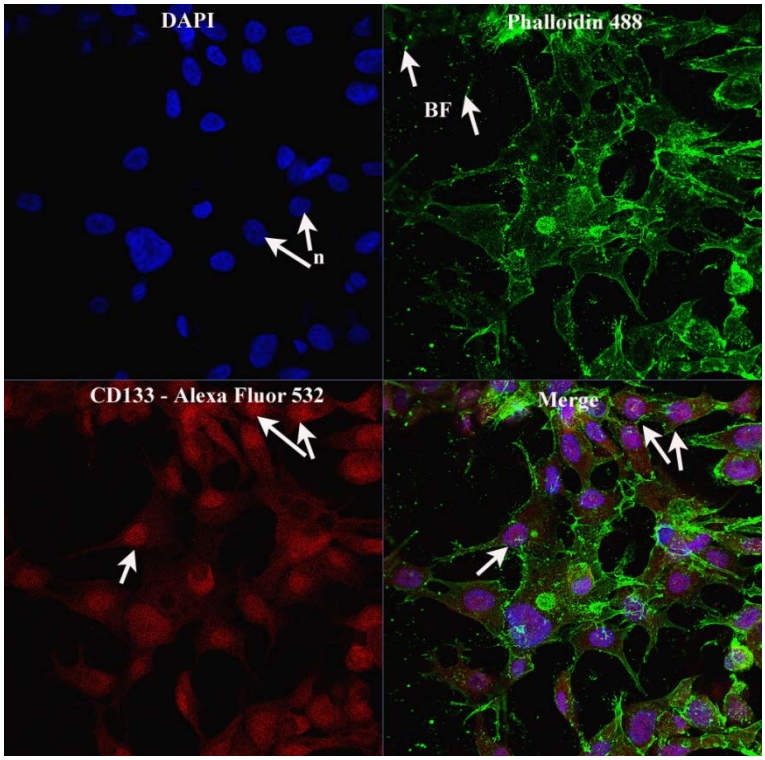
	Integrated density	Area of selected cell	Background fluorescence	CTCF
	12003	1948	0.054	11897.81
	13801	1517	0.054	13719.08
	12448	1577	0.054	12362.84
Average CTCF				12659.91

Table 10: Corrected Total Cell Fluorescence (CTCF) of DLD1 CD133- cells (permeabilized), stained with an anti-CD133 antibody

	Integrated density	Area of selected cell	Background fluorescence	CTCF
	608	237	0.512	486.656
	658	430	0.512	437.84
	733	354	0.512	551.752
Average CTCF				492.0827

b.) HT29

CD133+



CD133-

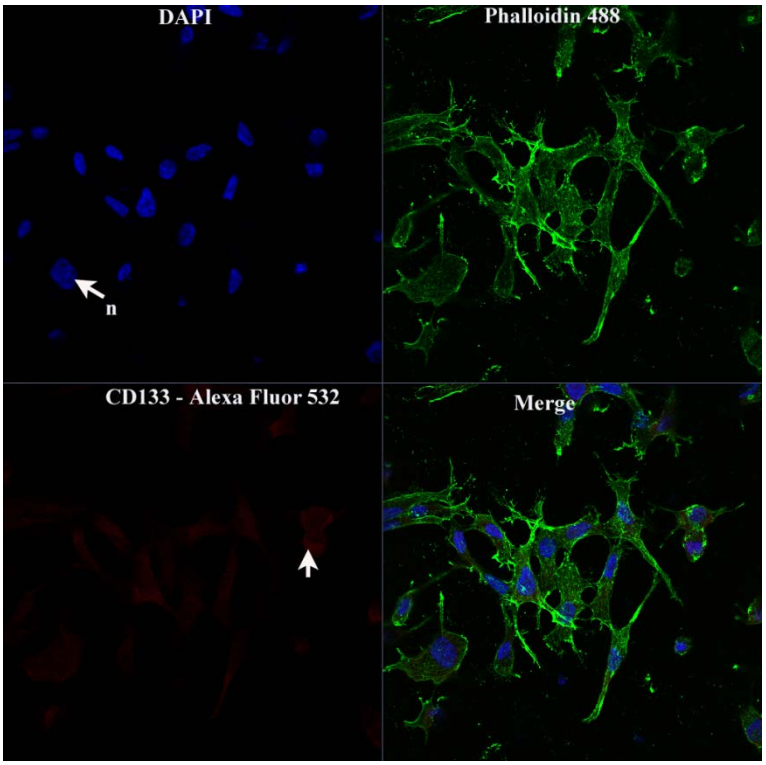


Figure 19: b.) CD133 localization in permeabilized CD133+ and CD133- fractions of HT29 cell line, nuclei indicated with (n) and background fluorescence (BF). CD133 was detected in the cytoplasm of CD133+ cells shown with arrows. The receptor seemed to be concentrated in some areas of the cell producing a more intense fluorescence emission- cytoplasmic and nuclear association. Nuclear association is apparent with pink colouration, shown with arrows. A low level of CD133 was detected in the cytoplasm of the CD133- cells indicated with the arrow. It is far les prominent in comparison to the CD133+ cells (Original Magnification 63X).

Table 11: Corrected Total Cell Fluorescence (CTCF) of HT29 CD133+ cells (permeabilized), stained with an anti-CD133 antibody

	Integrated density	Area of selected cell	Background fluorescence	CTCF
	9216	791	0.15	9097.35
	10401	811	0.15	10279.35
	10250	927	0.15	10110.95
Average CTCF				9829.217

Table 12: Corrected Total Cell Fluorescence (CTCF) of HT29 CD133- cells (permeabilized), stained with an anti-CD133 antibody

	Integrated density	Area of selected cell	Background fluorescence	CTCF
	342	108	0.02	339.84
	399	181	0.02	395.38
	422	365	0.02	414.7
Average CTCF				383.3067

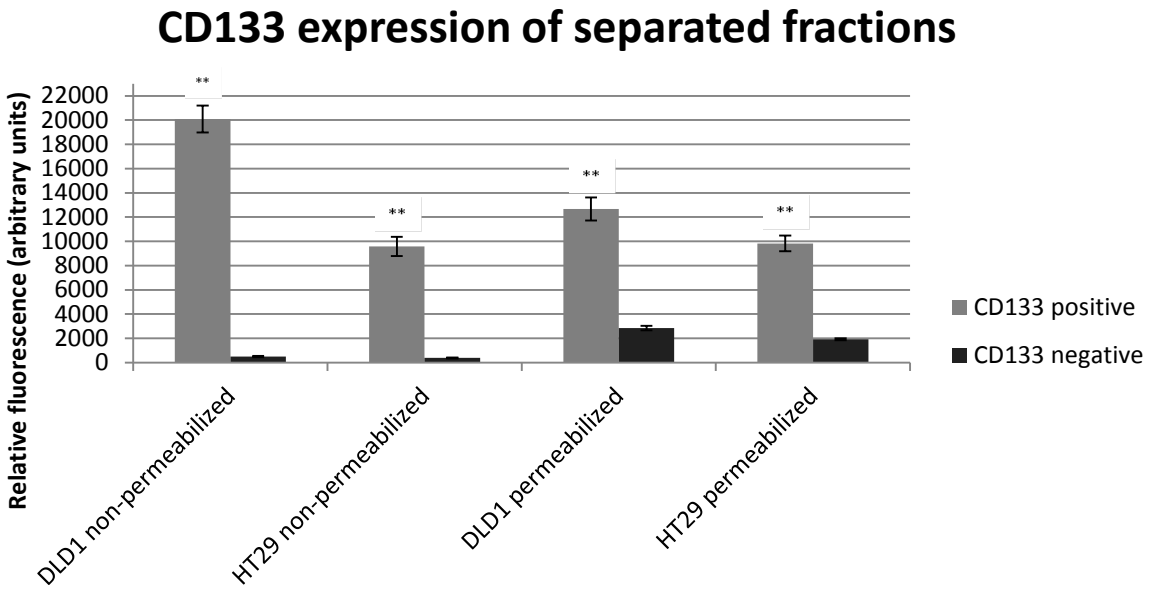
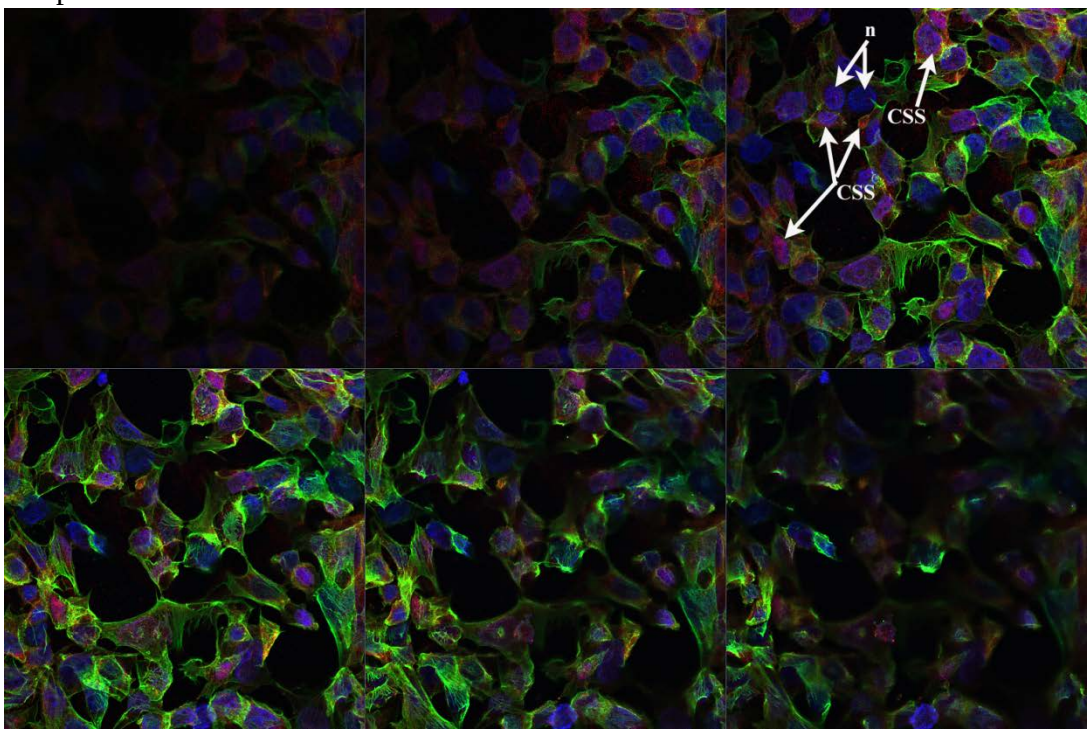


Figure 20: Graph summarizing the CD133 expression of separated cell fractions in non-permeabilized (surface expression) and permeabilized (cytoplasmic expression) cells derived from the DLD1 and HT29 cell lines. Significantly increased level of CD133 expression is seen in the CD133+ fractions of both cell lines of non-permeabilized cells with a relative fluorescence peaking at approximately 20 000 units in DLD1 non-permeabilized cells (p= 0.0014**). The lowest expression level of CD133 positive cells was seen on the cell surface of HT29 (non-permeabilized) cells (p= 0.0042**). A significant difference in the expression of CD133 in the permeabilized cells is also noted in both the DLD1 (p= 0.0022**) and HT29 cells (p= 0.0014**).

DLD1 CD133+ cells non-permeabilized and permeabilized Z-stack

a.) Non-permeabilized



b.) Permeabilized

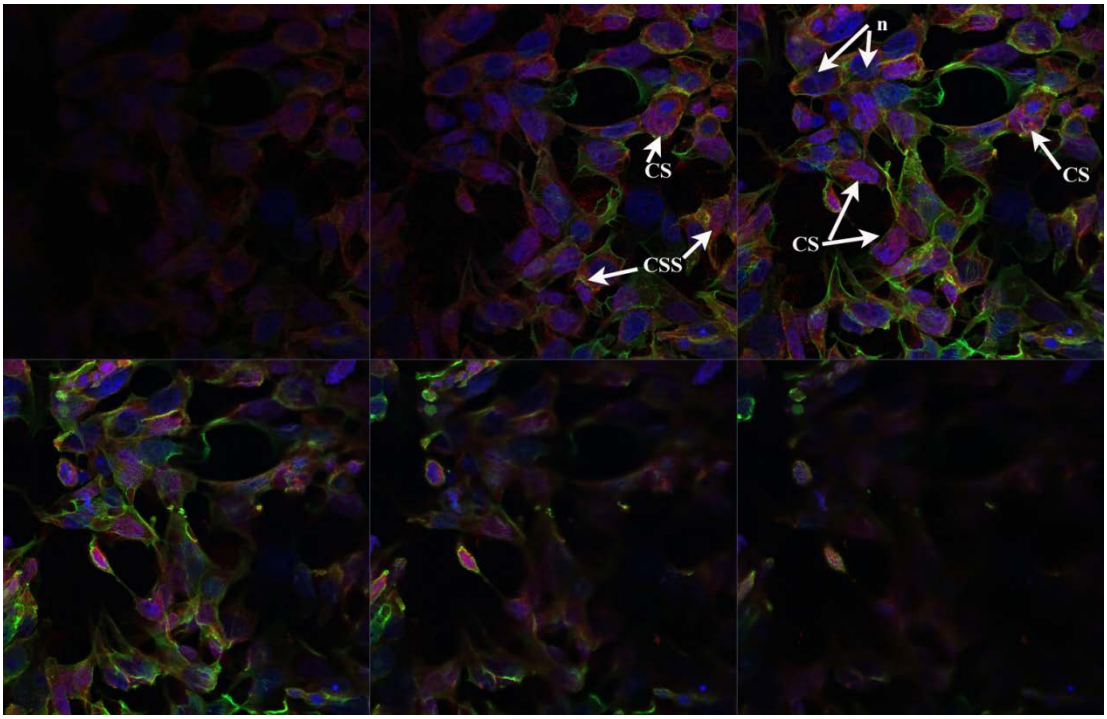
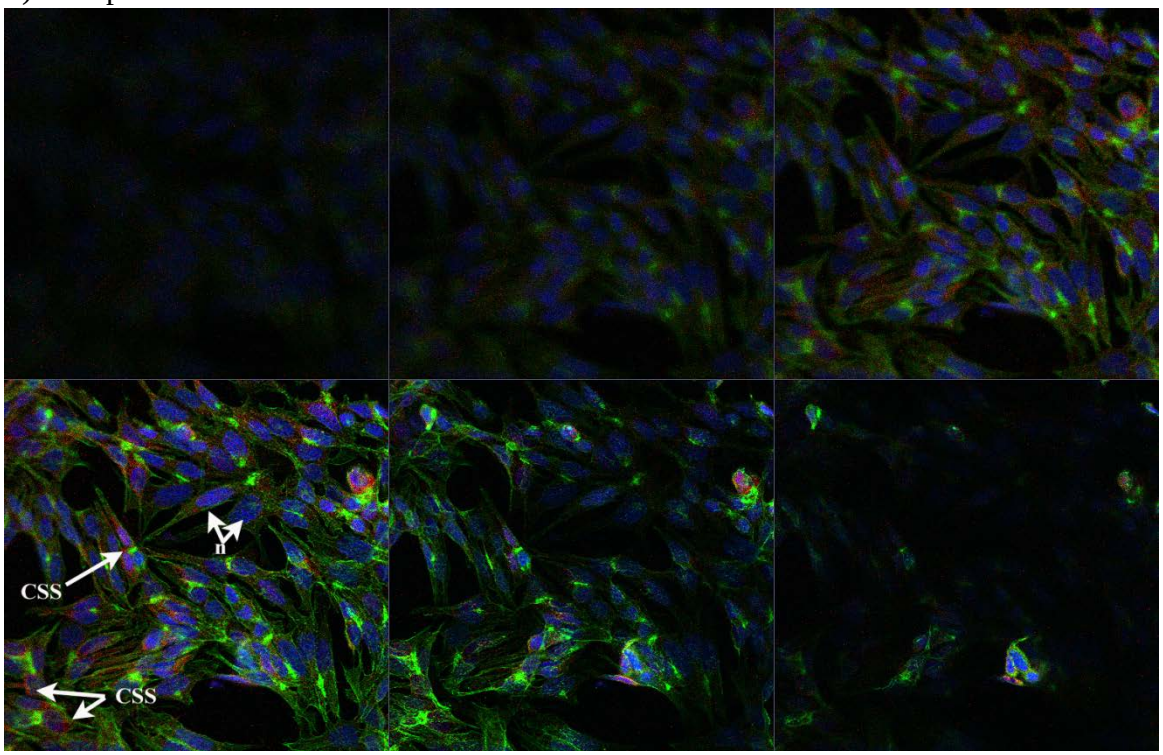


Figure 21: The Z-stack images show the expression of CD133 in non-permeabilized and permeabilized CD133 positive fractions of DLD1 cells. a.) Arrows indicate the nuclei (n) which appear blue and cell surface staining of CD133 (CSS) appears red. b.) When permeabilized CD133 is detected in the cytoplasm (CS) as well as the cell surface (CSS) it can be seen in the images as pink and red respectively (Original Magnification 63X).

HT29 CD133+ cells non-permeabilized and permeabilized Z-stack

a.) Non-permeabilized



b.) Permeabilized

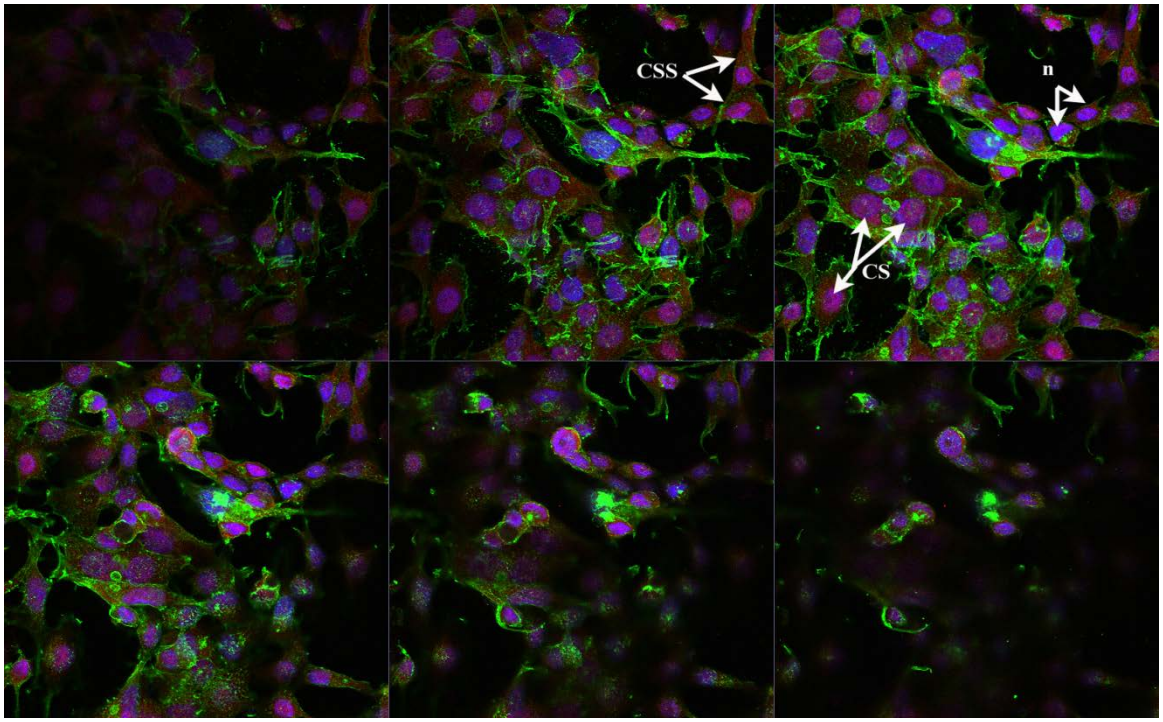


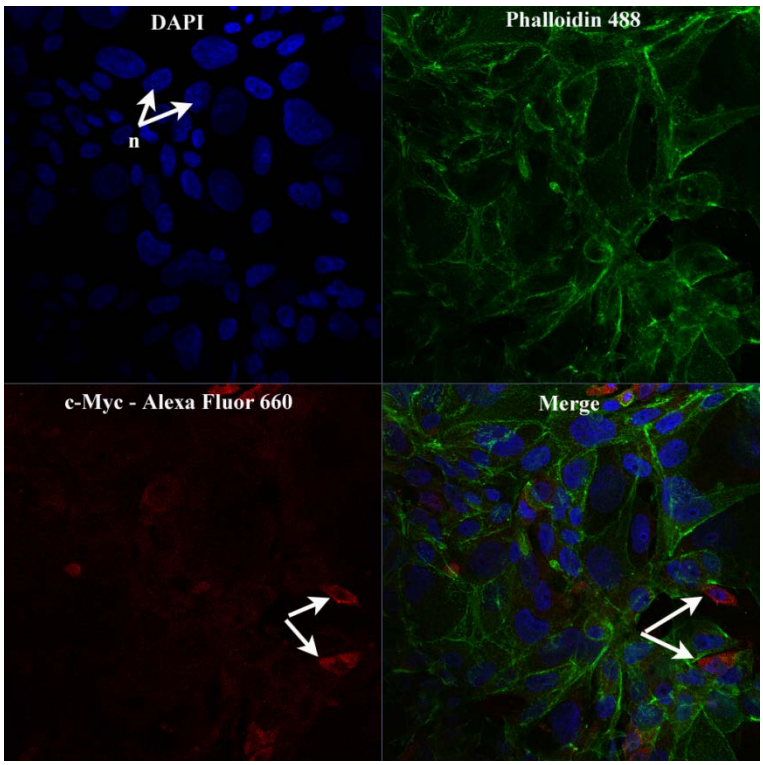
Figure 22: Z-stack images of non-permeabilized versus permeabilized HT29 CD133+ cells. a.) Nuclei are shown with (n) and arrows indicate the cell surface staining (CSS) which appears red. b.) A definite presence of CD133 is identified in the cytoplasm (CS) of the cells shown as pink (Original Magnification 63X).

The results above indicate that CD133 is strongly expressed by the CD133+ fractions of both the DLD1 and HT29 cell line (Figure 16-22). In the non-permeabilized cells the cell surface expression of CD133 is clearly evident.The permeabilized CD133+ cells of both cell lines stained with a CD133 antibody show a nuclear association with the protein. Permeabilized cells indicate the presence of CD133 in both the CD133+ and CD133- within the cytoplasm. Z-stack images were captured to confirm the cell surface expression of CD133 where the non-permeabilized CSC's did not display fluorescence in the cytoplasm but expression of CD133 is seen on the cell surface (red) as expected and the permeabilized fraction showed fluorescence on the cell surface as well as the cytoplasm (blue nuclei+red stain = pink). This localization is in accordance with the initial cell separation step as cells within this population were isolated based on their cell surface expression of CD133. Furthermore, it shows that CD133 is not only expressed on the cell surface, is also synthesized within the cell and due to the pink fluorescence an association with the nucleus is suggested.

6.4.3 Immunofluorescence localization of c-Myc in CD133+ and CD133- cells

a.)DLD1

CD133+



CD133-

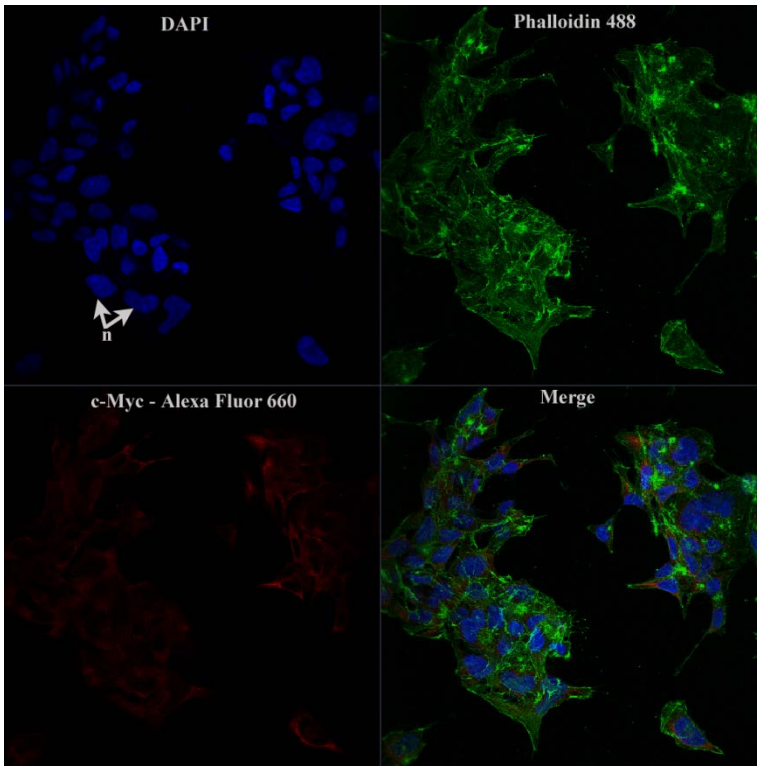


Figure 23: a.)Expression of c-Myc in CD133+ and CD133- fractions of DLD1 cell line; nulcei shown with (n). From the above images a subtle difference between DLD1 CD133+ and DLD1 CD133- is apparent. Both fractions showed cytoplasmic staining, often being associated with membrane protrusions in CD133+ cells (arrow). However, not all CD133+ cells showed consistent staining, instead a few cells within the population stained more intensely (Original Magnification 63X).

Table 13: Corrected Total Cell Fluorescence (CTCF) of DLD1 CD133+ cells that were stained with an anti-C-myc antibody

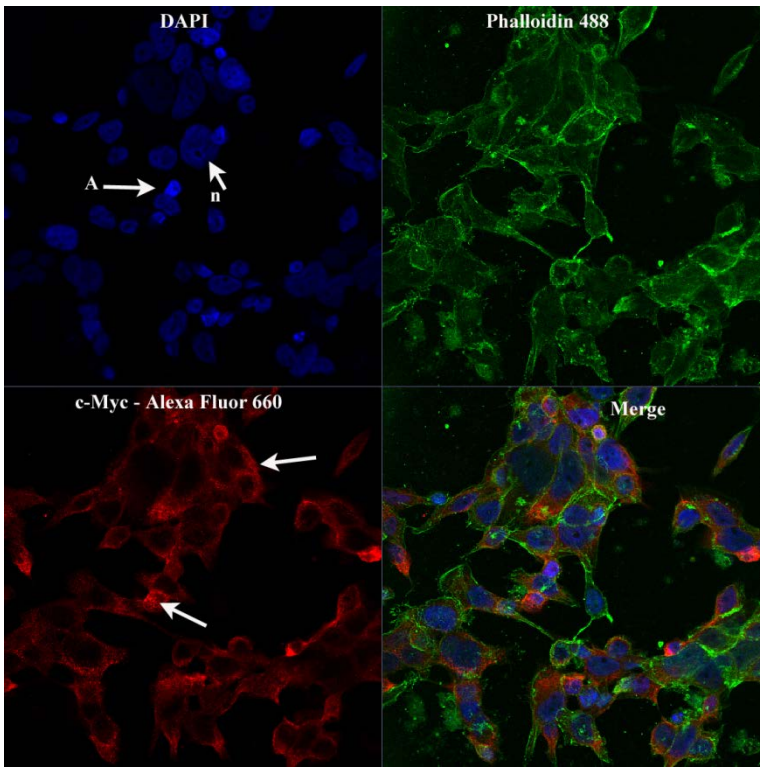
	Integrated density	Area of selected cell	Background fluorescence	CTCF
	1979	599	0.737	1537.537
	2615	697	0.737	2101.311
	2300	673	0.737	1803.999
Average CTCF				1814.282

Table 14: Corrected Total Cell Fluorescence (CTCF) of DLD1 CD133- cells, stained with an anti-C-myc antibody

	Integrated density	Area of selected cell	Background fluorescence	CTCF
	1169	480	0.106	1118.12
	1219	663	0.106	1148.722
	1244	533	0.106	1187.502
Average CTCF				1151.448

b.) HT29

CD133+



CD133-

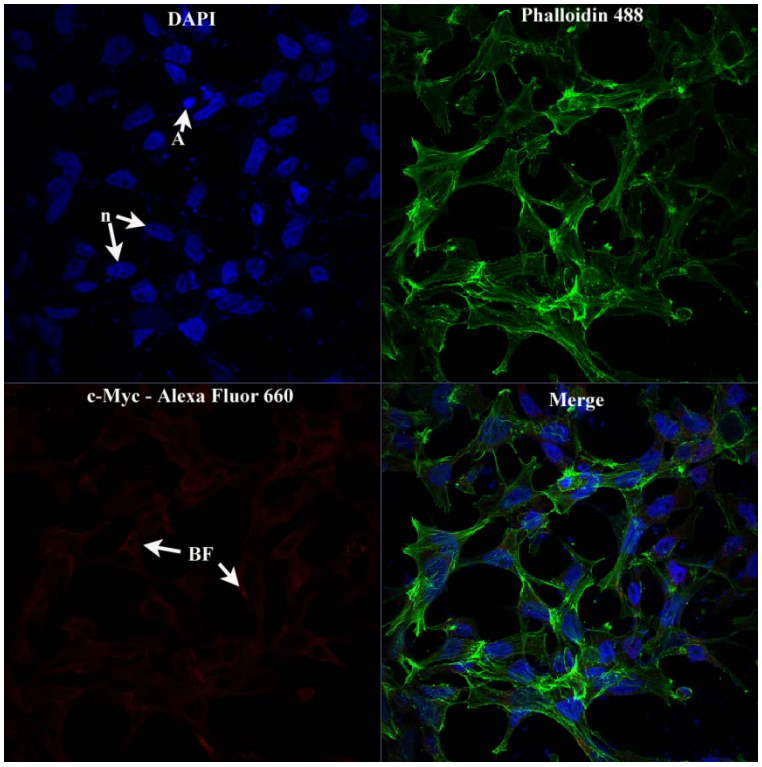


Figure 24: b.) Expression of c-Myc in CD133+ and CD133- fractions of the HT29 cell line; nuclei shown with (n) and cell undegoing apoptosis with (A). In comparison to the DLD1 cell line a more definite differentiation betweeen the CD133+ and the CD133- fractions can be made here. Furthermore, selected HT29 CD133+ cells emitted a more concentrated fluorescence. Fluorescence seen in negative fraction could be attributed to weak background fluorescence (BF) (Original Magnification 63X).

Table 15: Corrected Total Cell Fluorescence (CTCF) of HT29 CD133+ cells, stained with an anti-c-Myc antibody

	Integrated density	Area of selected cell	Background fluorescence	CTCF
	3358	1244	0.013	3341.828
	3488	799	0.013	3477.613
	3604	583	0.013	3596.421
Average CTCF				3471.954

Table 16: Corrected Total Cell Fluorescence (CTCF) of HT29 CD133- cells, stained with an anti-c-Myc antibody

	Integrated density	Area of selected cell	Background fluorescence	CTCF
	1578	601	0.009	1572.591
	1614	764	0.009	1607.124
	1521	546	0.009	1516.086
Average CTCF				1565.267

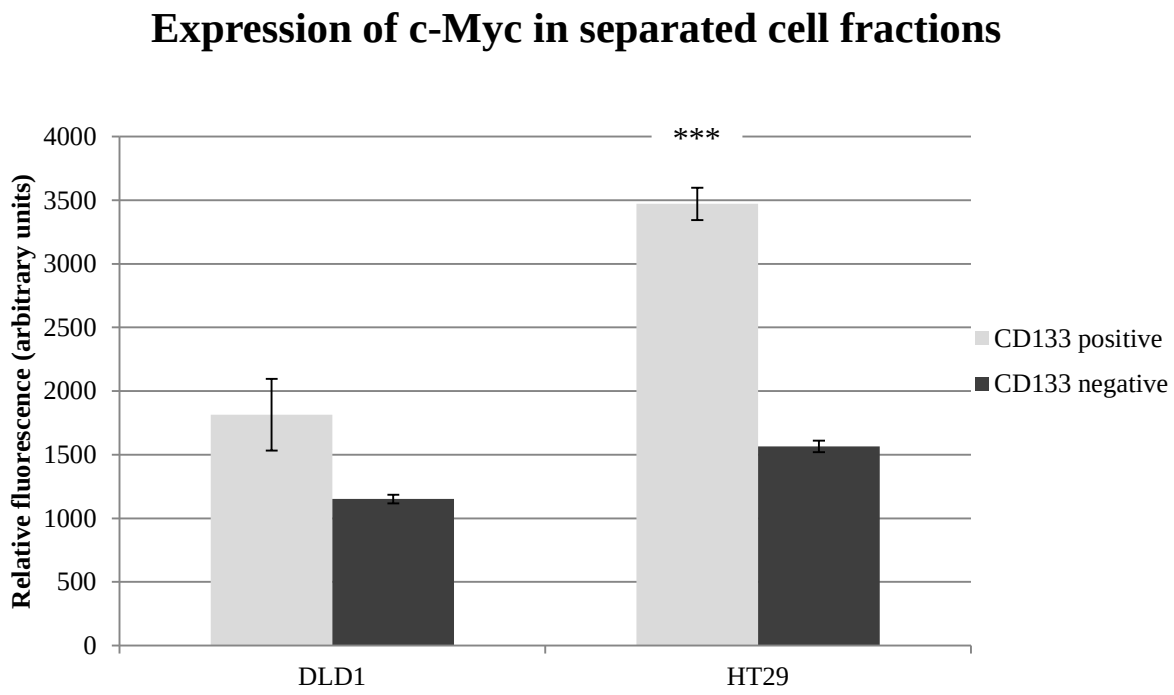
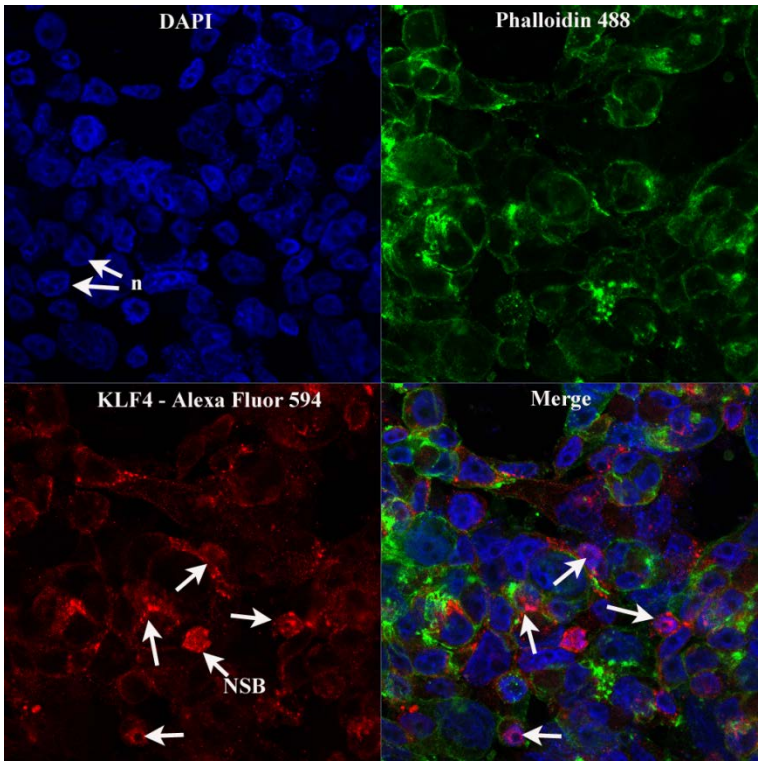


Figure 25: Summary of the c-Myc expression in the DLD1 and HT29 cell lines. A non-significant difference in relative fluorescence is noted in the DLD1 cell line (p= 0.051), whilst a highly significant difference in c-Myc expression is seen in the HT29 cell line (p= 0.0003***).

6.4.4 Immunofluorescence localization of KLF4 in CD133+ and CD133- cells

a.) DLD1

CD133+



CD133-

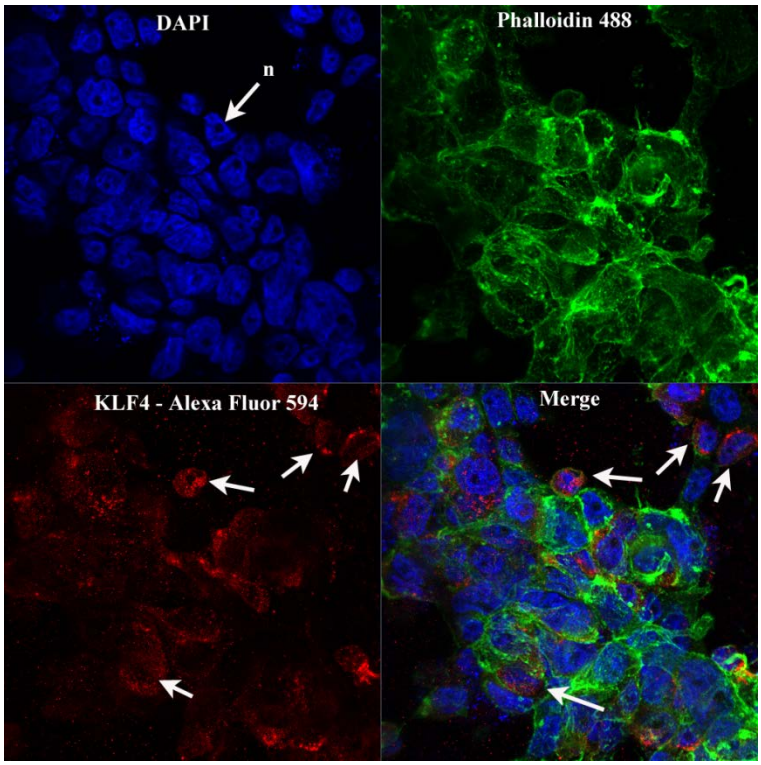


Figure 26: a.) Expression of KLF4 in CD133+ and CD133- fractions of DLD1 cell line; nuclei shown with (n). The zinc-finger transcription factor KLF4 is expressed by both DLD1 CD133+ as well as DLD1 CD133- cells. The intensity in the positive fraction is greater than in the negative fraction with a distinct punctuate perinuclear staining pattern seen in both. An area of non-specific binding is also visible (NSB). In addition, some fluorescence is observed in the control slide of the CD133- fraction (see Appendix B), suggesting the possibility of non-specific binding. This background fluorescence was subtracted upon calculation of the CTCF value (Original Magnification 63X).

Table 17: Corrected Total Cell Fluorescence (CTCF) of DLD1 CD133+ cells, stained with an anti-KLF4 antibody

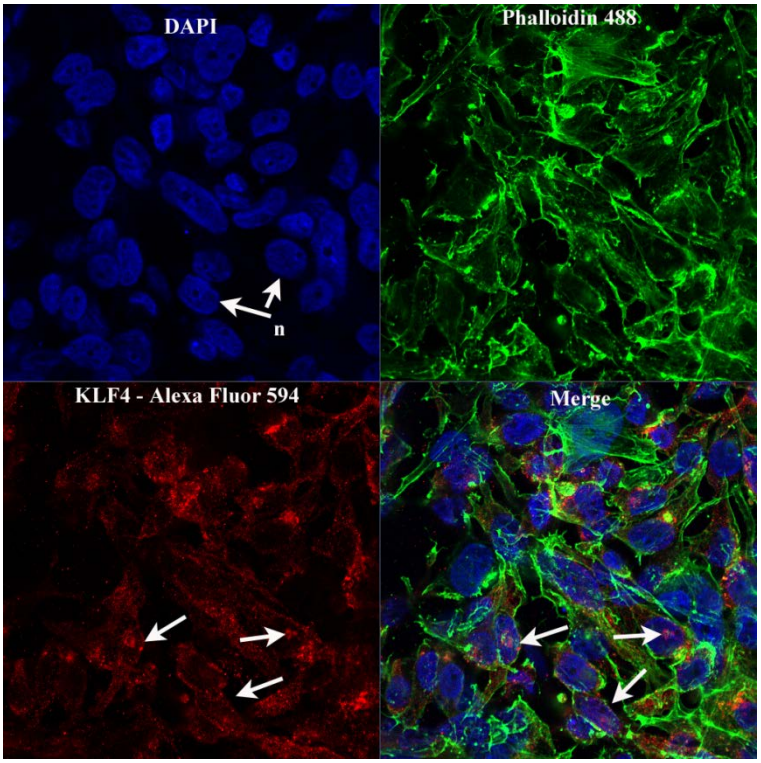
	Integrated density	Area of selected cell	Background fluorescence	CTCF
	7727	438	0.067	7697.654
	7054	378	0.067	7028.674
	6472	670	0.067	6427.11
Average CTCF				7051.146

Table 18: Corrected Total Cell Fluorescence (CTCF) of DLD1 CD133- cells, stained with an anti-KLF4 antibody

	Integrated density	Area of selected cell	Background fluorescence	CTCF
	4351	860	0.662	3781.68
	4458	702	0.662	3993.276
	4118	1018	0.662	3444.084
Average CTCF				3739.68

b.) HT29

CD133+



CD133-

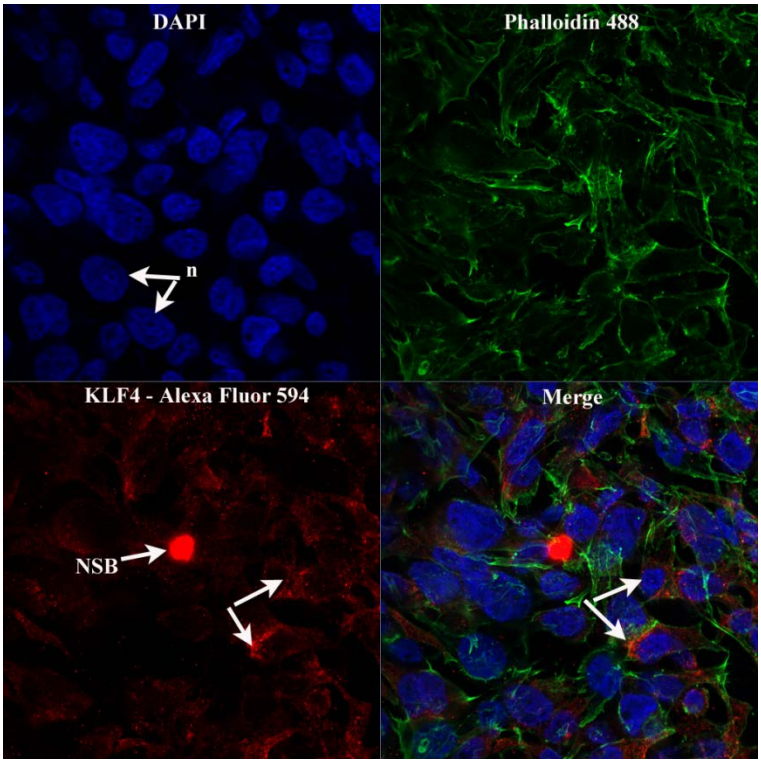


Figure 27: b.) Expression of KLF4 in CD133+ and CD133- fractions of HT29 cell line, nuclei shown with (n). Although the fluorescence intensity appears similar in both the CD133+ and CD133- fractions distinctly brighter fluorescence is visible in the CD133+ fraction, with only smaller areas of fluorescence visible in the negative fraction. Arrows indicate the nucleosomal association of KLF4 in the CD133+ fraction. Once again the staining forms a punctate pattern and is perinuclear and not nucleosomal. The bright spot seen in the CD133- fraction indicated with an arrow is non-specific binding (NSB) and was excluded in the integrated density measurements, to avoid an outlier that may skew the final CTCF value (Original Magnification 63X).

Table 19: Corrected Total Cell Fluorescence (CTCF) of HT29 CD133+ cells, stained with an anti-KLF4 antibody

	Integrated density	Area of selected cell	Background fluorescence	CTCF
	13648	1141	0.72	12826.48
	14613	915	0.72	13954.2
	13042	1237	0.72	12151.36
Average CTCF				12977.35

Table 20: Corrected Total Cell Fluorescence (CTCF) of HT29 CD133- cells, stained with an anti-KLF4 antibody

	Integrated density	Area of selected cell	Background fluorescence	CTCF
	1707	391	0.117	1661.253
	1676	557	0.117	1610.831
	1633	807	0.117	1538.581
Average CTCF				1603.555

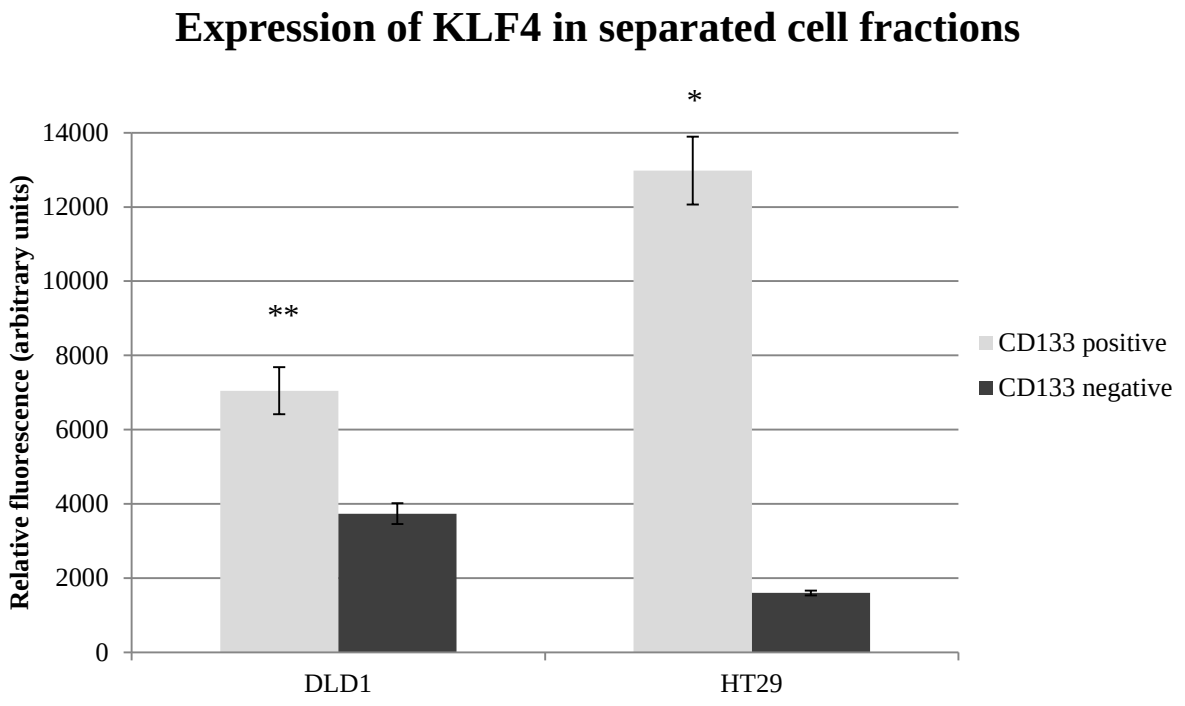
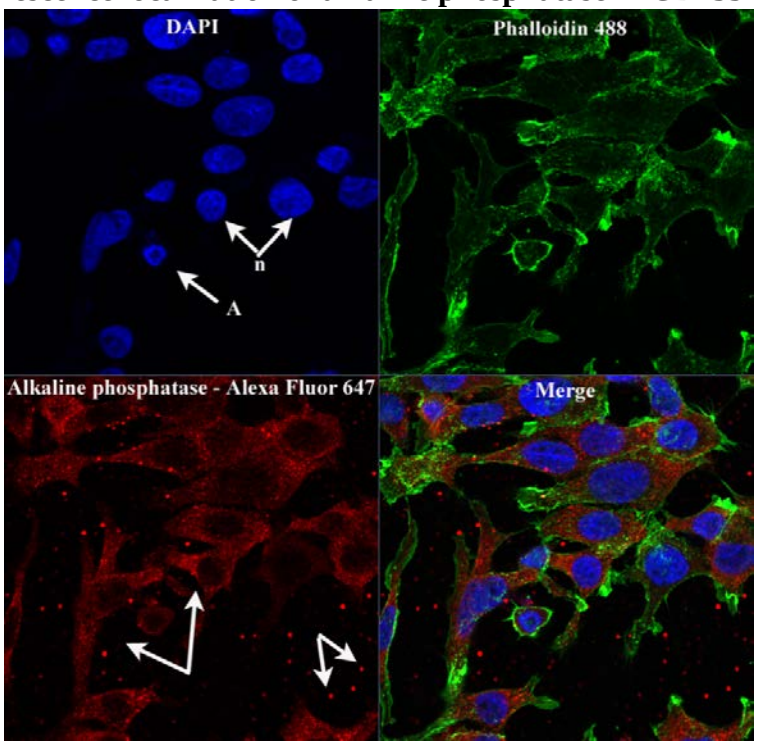


Figure 28: Bar graph summarizing KLF4 expression in DLD1 and HT29 cell lines. The expression of KLF4 is significantly increased in CD133+ fractions of both the DLD1 (p= 0.0031**) and HT29 (p= 0.0295*) cell lines. Following measurement of the integrated density and calculation of the CTCF, a greater difference in relative fluorescence associated with the HT29 cell line.

6.4.5 Immunofluorescence localization of alkaline phosphatase in CD133+ and CD133- cells

a.) DLD1

CD133+



CD133-

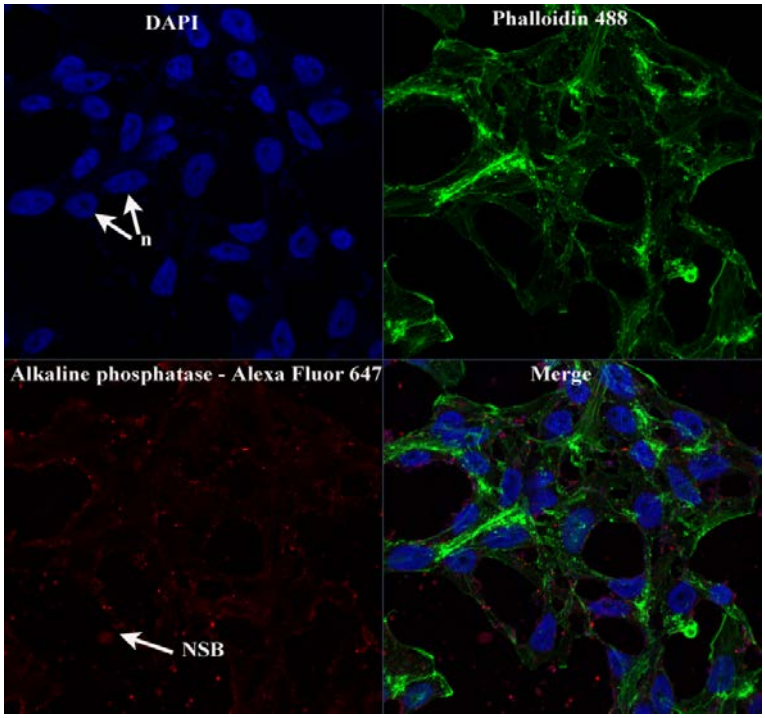


Figure 29: a.) Expression of alkaline phosphatase in CD133+ and CD133- fractions of the DLD1 cell line, nuclei shown with (n) and apoptosis (A). Localization is perinuclear with more intense areas possibly associated with the *trans* – Golgi network. The punctate staining may be cell surface related as alkaline phosphatase is secreted onto the cell surface as well as extracellularly. Flecks of fluorescence, shown with arrows, are also seen surrounding the CD133+ cells. A far lower level of expression is noted in the CD133- fraction and could perhaps represent a low level of cell membrane associated alkaline phosphatase (Original Magnification 63X).

Table 21: Corrected Total Cell Fluorescence (CTCF) of DLD1 CD133+ cells, stained with an anti-alkaline phosphatase antibody

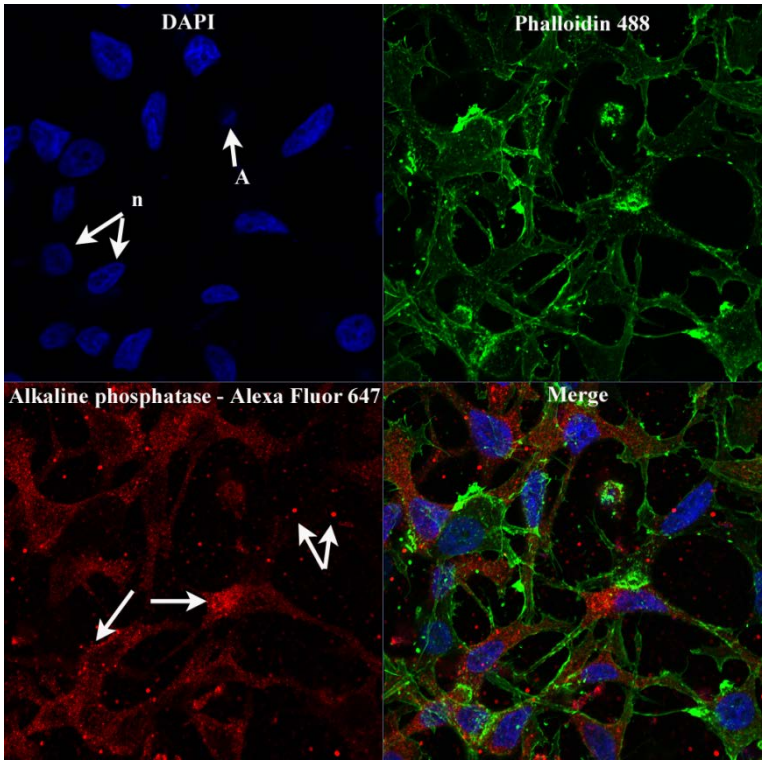
	Integrated density	Area of selected cell	Background fluorescence	CTCF
	16774	1480	0.207	16467.64
	16523	1557	0.207	16200.7
	17563	1765	0.207	17197.65
Average CTCF				16622

Table 22: Corrected Total Cell Fluorescence (CTCF) of DLD1 CD133- cells, stained with an anti-alkaline phosphatase antibody

	Integrated density	Area of selected cell	Background fluorescence	CTCF
	1119	499	0.134	1052.134
	1085	396	0.134	1031.936
	1018	749	0.134	917.634
Average CTCF				1000.568

b.) HT29

CD133+



CD133-

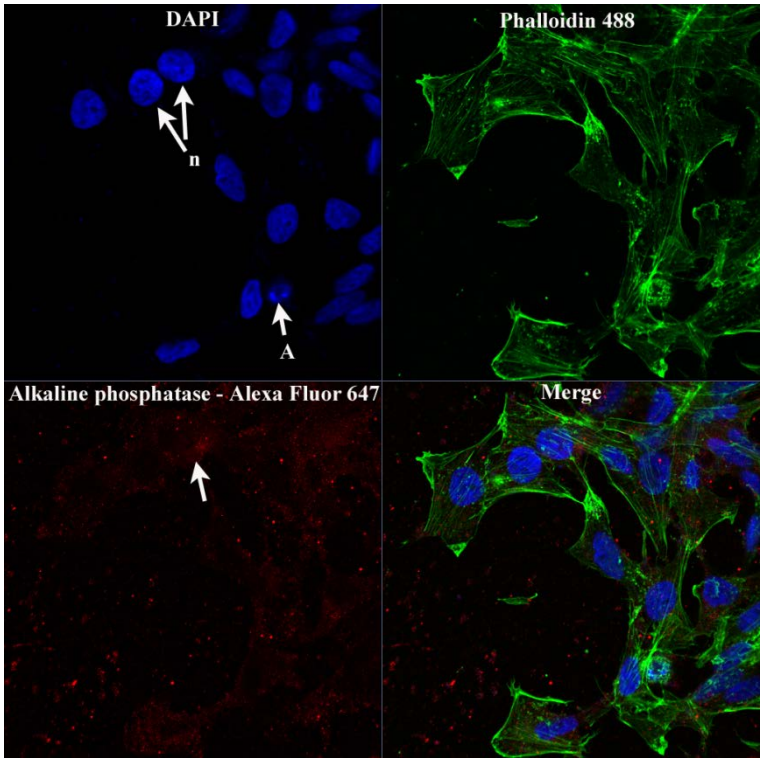


Figure 30: b.) Expression of alkaline phosphatase in CD133+ and CD133- fractions of HT29 cell line; nuclei shown with (n) and apoptosis (A). Increased fluorescence intensity is evident on the cell surface of the CD133+ fraction of the HT29 cell line. Punctate staining for alkaline phosphatase is present in extracellular spaces. A far lower level of expression is seen in the CD133- fraction. Despite extracellular detection of alkaline phosphatase than in the CD133- fraction, it is far less prominent than the CD133+ fraction (Original Magnification 63X).

Table 23: Corrected Total Cell Fluorescence (CTCF) of HT29 CD133+ cells, stained with an anti-alkaline phosphatase antibody

	Integrated density	Area of selected cell	Background fluorescence	CTCF
	20701	1497	0.327	20211.48
	20595	1866	0.327	19984.82
	19289	1476	0.327	18806.35
Average CTCF				19667.55

Table 24: Corrected Total Cell Fluorescence (CTCF) of HT29 CD133- cells, stained with an anti-alkaline phosphatase antibody

	Integrated density	Area of selected cell	Background fluorescence	CTCF
	1940	553	0.47	1680.09
	1976	790	0.47	1604.7
	1911	670	0.47	1596.1
Average CTCF				1626.963

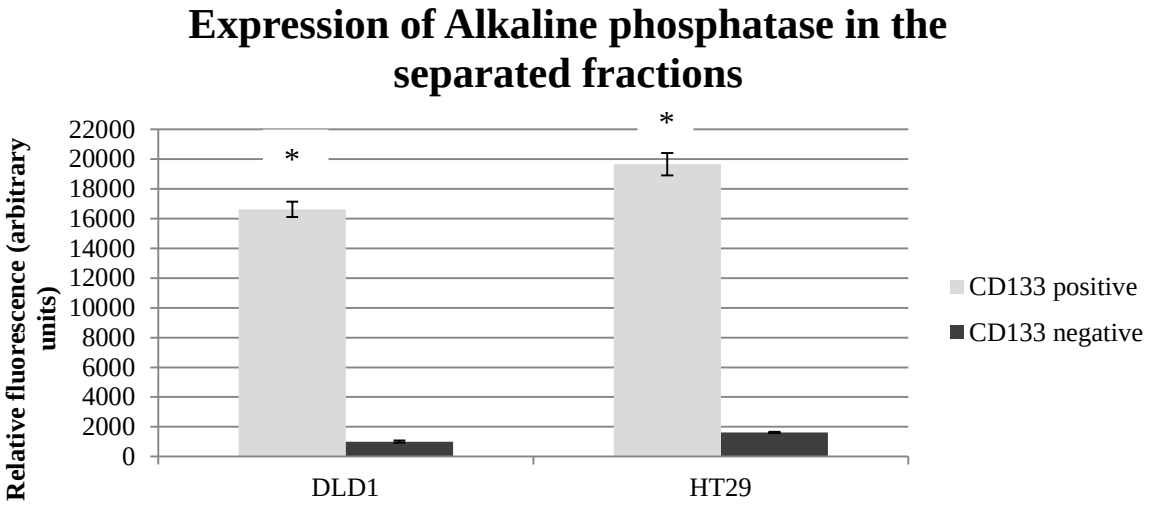


Figure 31: Bar graph representing alkaline phosphatase expression in DLD1 and HT29 cell lines. Alkaline phosphatase staining clearly differentiated between CD133 positive and CD133 negative fractions of DLD1 (p= 0.0354*) and HT29 cells (p= 0.0380*), respectively. There is a significant difference (p< 0.05) in relative fluorescence between the two cell populations of both cell lines.

Overall the expression of CSC markers c-Myc, KLF4 and alkaline phosphatase was found to be increased in both the DLD1 and HT29 CD133+ fractions (Figure 23- 31). In most cases this increase was calculated to be significantly higher than that of the CD133- fraction except for the expression of c-Myc in the DLD1 cell line.

6.5 CELL ADHESION ASSAYS

The adhesion to extracellular matrix proteins is vital for the invasion of neoplastic cells. The ability of CD133+ cells to adhere was compared to CD133- cells using cell adhesion assays (Figure 32). Thereafter the potential of the Shh small molecule inhibitors cyclopamine and SANT-2 or the control molecule tomatidine, to impede this binding was evaluated (Figure 33-36). Cell adhesion to Geltrex™ (containing components of the ECM) was determined following incubation with the small molecule inhibitors. Cells were transferred to a 96-well plate, either coated with Geltrex™ or uncoated, for 2 hours at 37°C. Attached cells were fixed, stained with crystal violet and absorbance was measured at 550 nm. The attachment of cells to the uncoated control plate represents the background binding. The absorbance of the stain present in the coated plates correlates directly with the percentage of Geltrex™-attached cells. Data are representative of experiments carried out in triplicate.

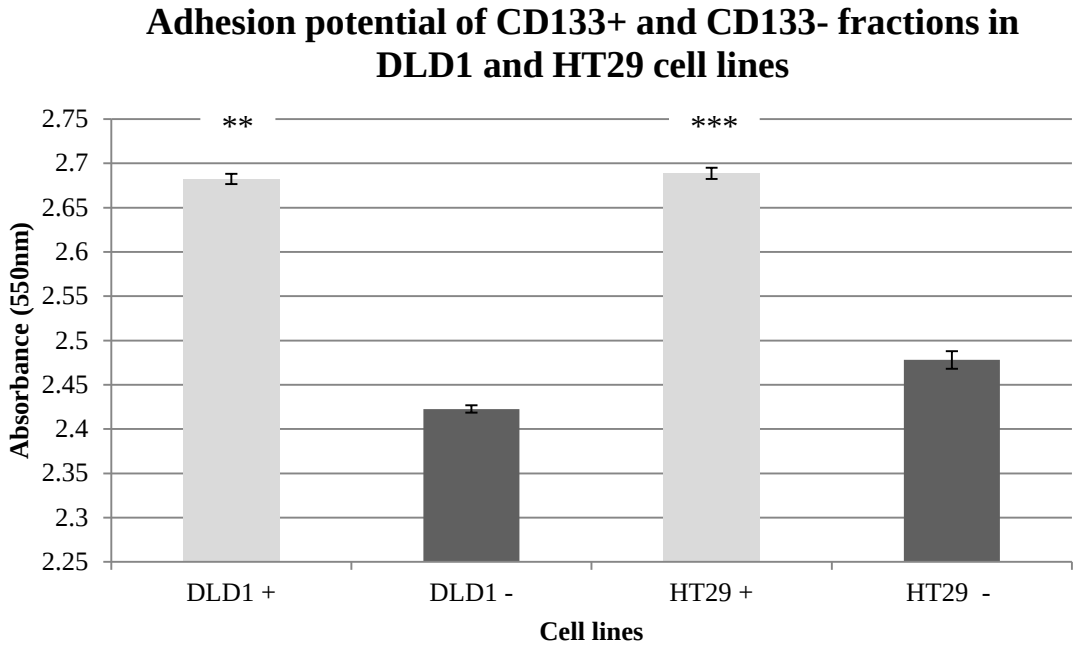


Figure 32: Bar graph representing cell adhesion to Geltrex™. A significantly increased adhesion potential was noted in both the $CD133^+$ fractions (light grey) of DLD1 (p= 0.0028**) and HT29 (p= 0.0006***) cell lines, in comparison to the negative fractions (dark grey). This indicates the enhanced ability of CSC's to adhere, a key step in the process of metastasis. Experiments were carried out in triplicate.

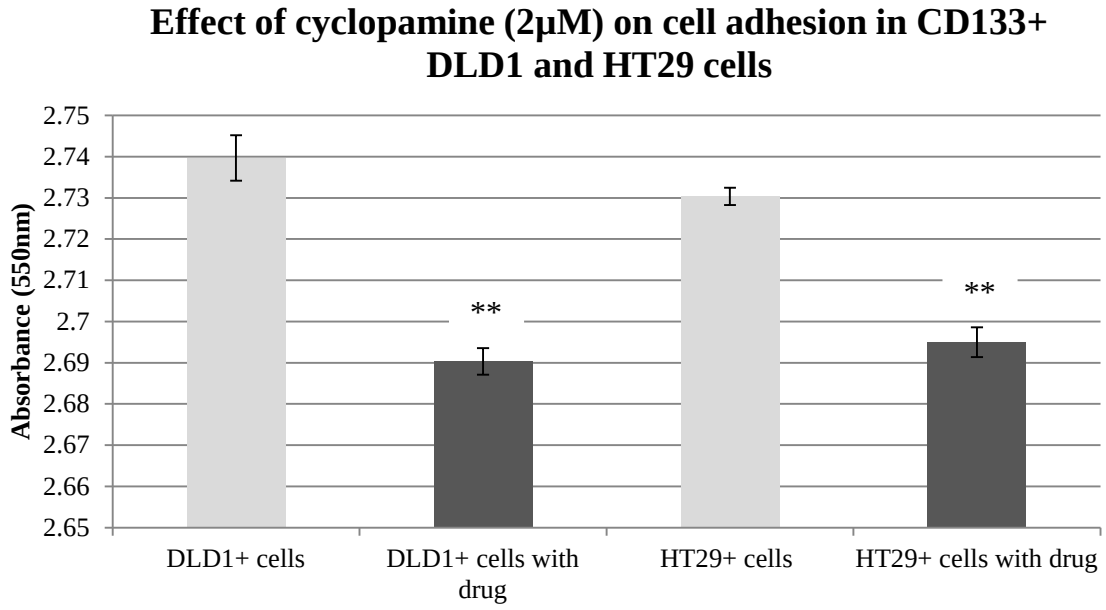


Figure 33: Bar graph representing the effects of cyclopamine on cell adhesion.Treatment with 2µM cyclopamine resulted in a marked reduction in the adhesion potential of both DLD1 CSC's (*p*= 0.0020**) and HT29 CSC's (*p*= 0.0025**) in comparison to untreated cells following a 2 hour incubation.

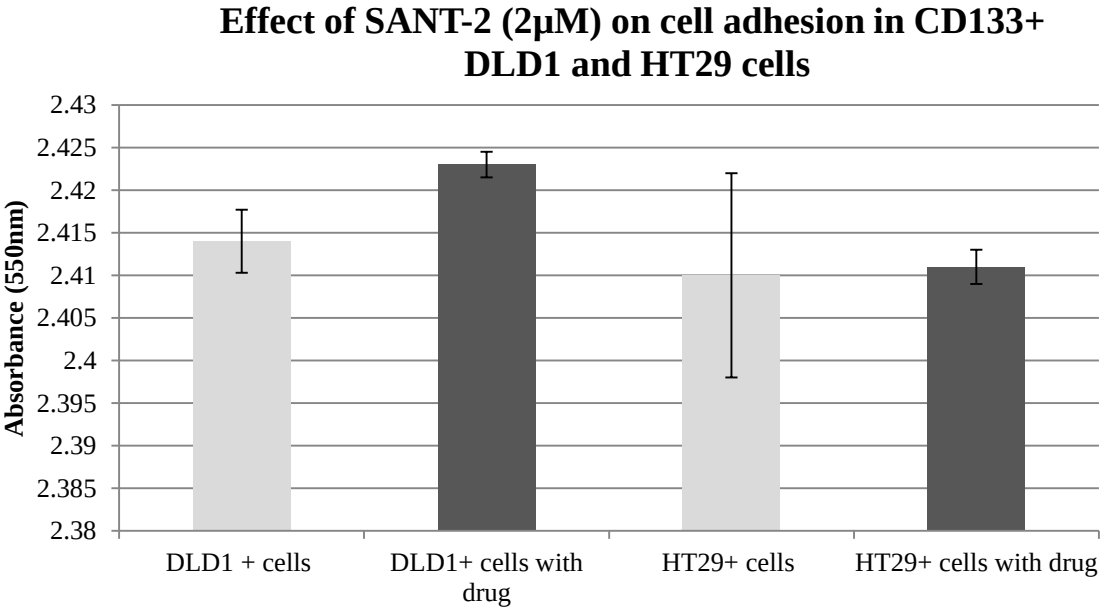


Figure 34: Bar graph representing the effects of SANT-2 on cell adhesion. No significant decrease in adhesion potential was seen after 2µM of SANT-2 treatment. In both cell lines an unusually increased level of adhesive ability was noted in comparison to the untreated cells. The results obtained do suggest that at a concentration of 2µM SANT-2 would be ineffective in impeding cell adhesion in both the DLD1 and HT29 cell lines.

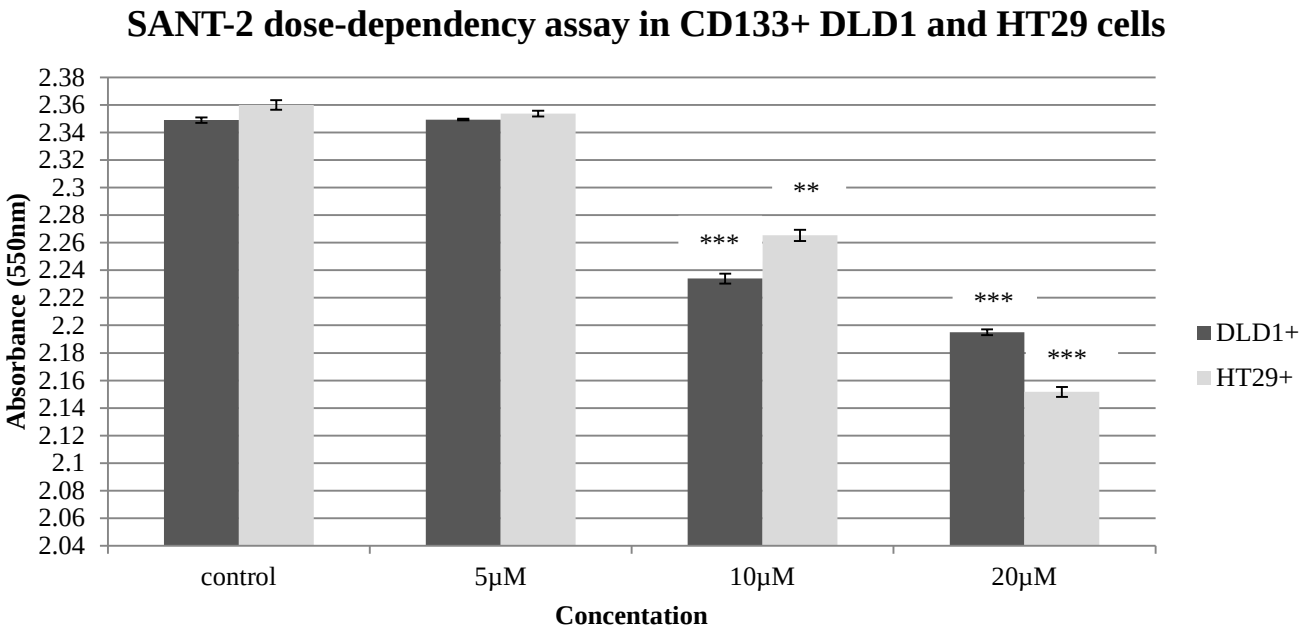


Figure 35: Bar graph representing the dose-dependent effects of SANT-2 on cell adhesion. A dose-dependency assay demonstrated that at higher concentrations SANT-2 had a more significant effect on cell adhesion of both DLD1 (dark grey) and HT29 (light grey) CSC's. A 5-fold increase in concentration resulted in a significantly decreased adhesion (DLD1 p= 0.0007***, HT29 p= 0.0020**) while a further reduction was seen with a 10-fold increase in concentration (in comparison to untreated controls) (DLD1 p= 0.0001***, HT29 p= 0.0001***). Subsequently in further experiments, the concentration of 20µM was then utilized in treating cells.

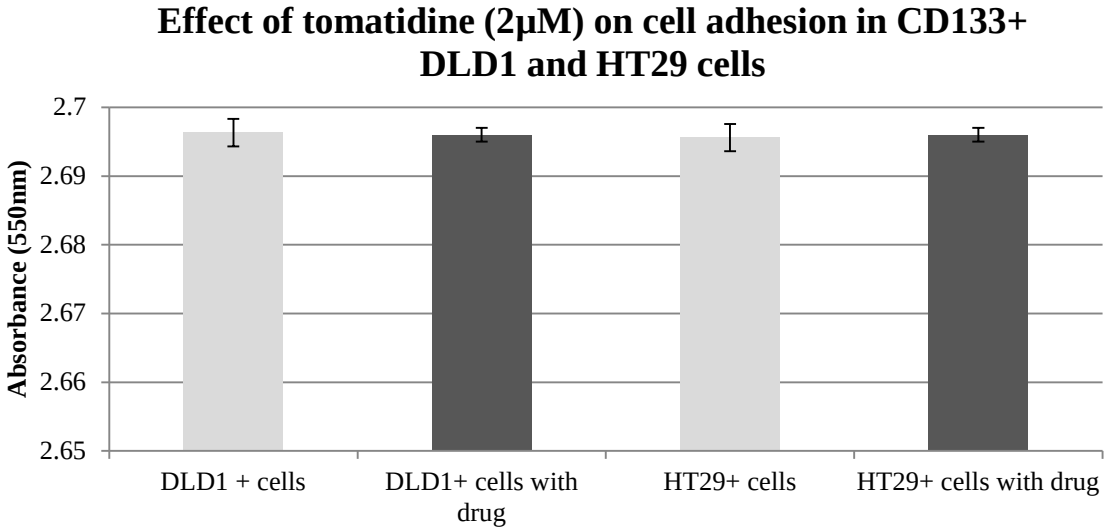


Figure 36: Bar graph representing the effects of the inert cyclopamine analogue, tomatidine on cell adhesion. No significant changes in adhesion potential are apparent following treatment with tomatidine at a concentration of 2µM. Neither the DLD1 (p= 0.2301) nor the HT29 (p= 0.2354) cell lines were affected by this analogue.

6.6 CELL INVASION ASSAYS

The experimental approach to determine the potential of cells to invade an extracellular matrix (ECM) is the chemo-invasion assay. It makes use of a polycarbonate filter to facilitate cell invasion through an extracellular matrix (Geltrex™) containing the protein laminin. The cells are stimulated to migrate through the Geltrex™ coated membrane by a chemoattractant, this usually being nutrients contained in culture medium. The invasion assays were performed using the aforementioned neoplastic cell lines to evaluate the ability of the Shh small molecule inhibitors to hinder cell invasion. Prior to commencing each assay, cells were pre-incubated with one of either cyclopamine (2µM), SANT-2 (20µM) or tomatidine (2µM). Cells that were able to actively penetrate the membrane and attach to the underside within the 20 hour incubation time were fixed and stained with Toluidine Blue. Once extracted from the cells the absorbance of the dye was measured at 620nm.; where increasing absorbancy was directly associated with increases in the number of invasive cells (Figure 37-39). The assays were performed in triplicate and the background absorbance excluded.

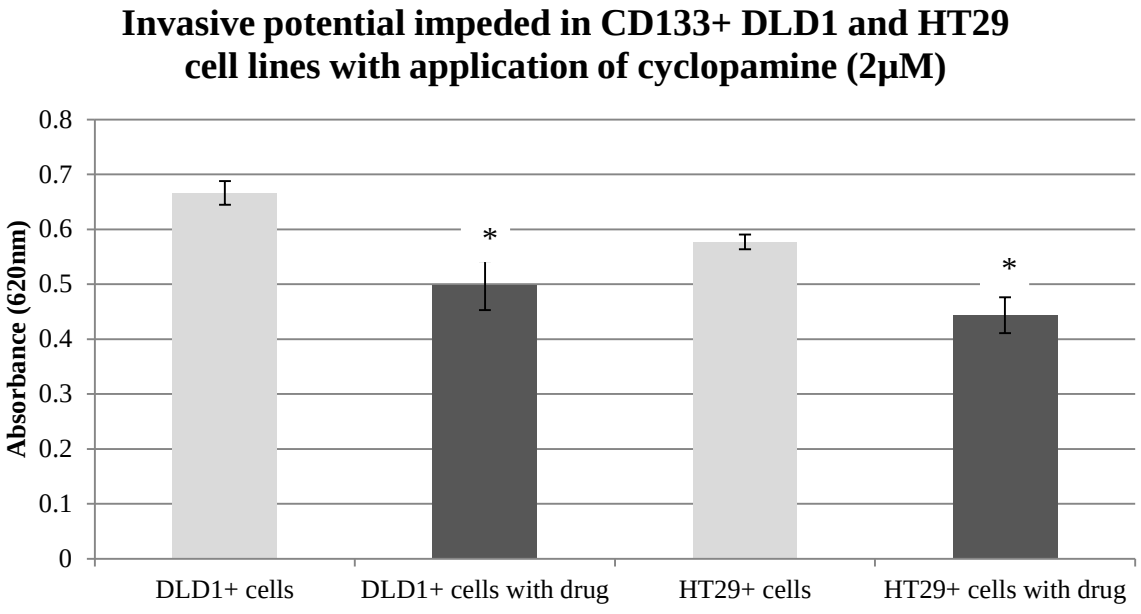


Figure 37: Bar graph representing the effect of cyclopamine on the invasive potential of CD133+ DLD1 and HT29 cells. With cyclopamine treatment (2µM), the invasive ability of both DLD1 (p= 0.0205*) and HT29 (p= 0.0122*) cell lines was significantly decreased. Both cell lines responded similarly to the drug.

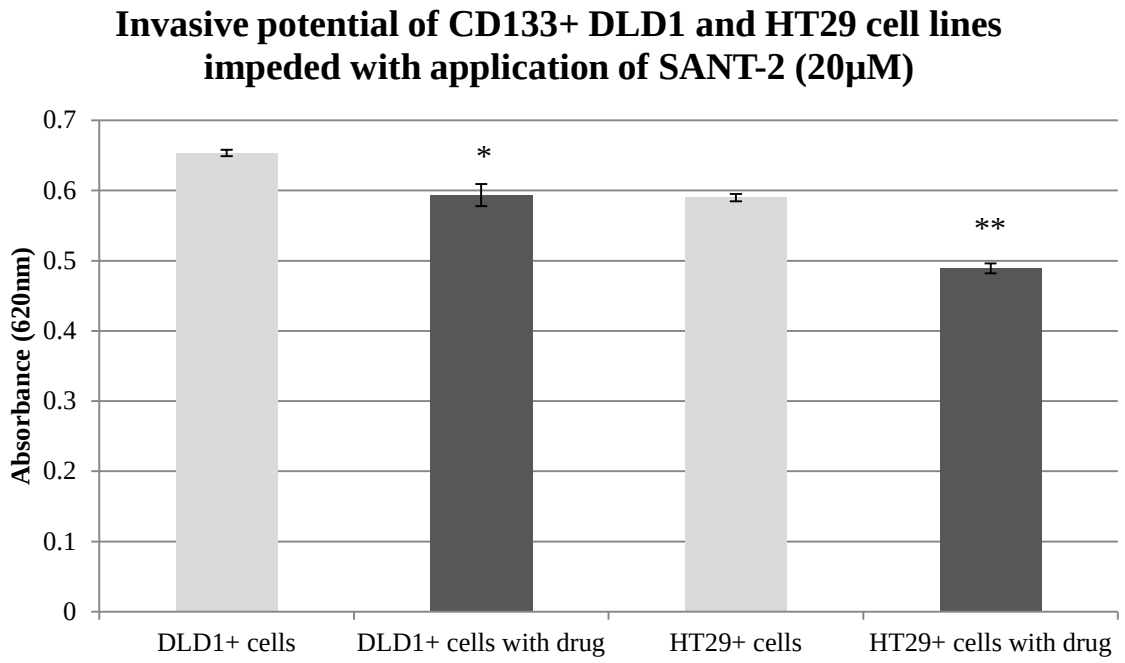


Figure 38: Bar graph representing the effect of SANT-2 on the invasive potential of CD133+ DLD1 and HT29 cells. The synthetic analogue molecule SANT-2 at a concentration of 20µM had a similar inhibitory effect to cyclopamine and was found to significantly impede the invasive capabilities of both DLD1 (p= 0.0117*) as well as HT29 (p= 0.0021**) CSC's, respectively.

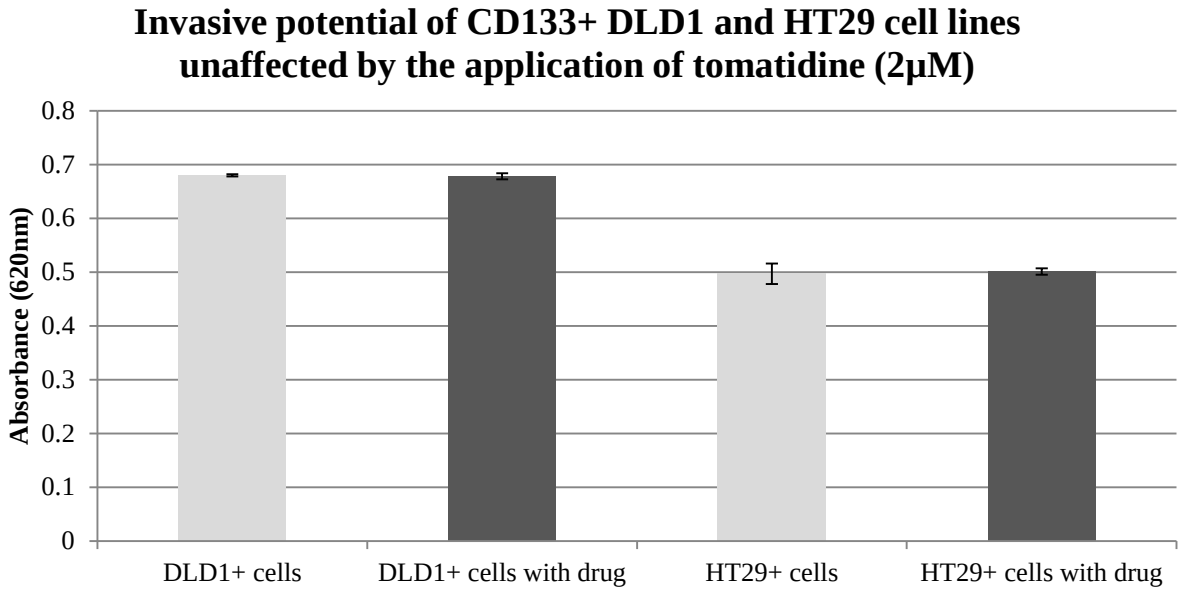


Figure 39: Bar graph representing the effects of the inert cyclopamine analogue, tomatidine on cell invasion.The control molecule tomatidine (2µM) had no significant effect on the invasive potential of DLD1 (p= 0.5286) and HT29 (p= 0.7460) CSC's, respectively. Interestingly, the overall invasive potential of HT29 CSC's proved to be lower than that of DLD1 CSC's.

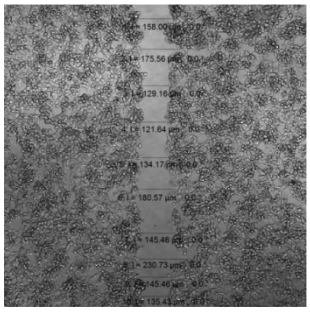
6.7 CELL MIGRATION/SCRATCH ASSAYS

Cell migration or scratch assays were performed to ascertain the potential effect that a Shh inhibitor could have on cell migration. This was done by creating a cell-free area in a confluent monolayer of cells and monitoring gap closure by means of differential interference contrast (DIC) microscopy, over a 24 hour period. An initial experiment was performed using a 500µl micropipette tip to form the scratch and the gap closure was assessed at time 0, 6 hours and 24 hours (See Appendix C). It was found that the gap was too wide to obtain accurate measurements, and furthermore the cells seemed to have some difficulty recovering from a wound to that extent. It was also observed that much growth/migration occurred between the start time and the first measurement time of 6 hours. Subsequently, a smaller diameter sterile 200µl micropipette tip was used to score through the confluent cell monolayer to generate a cell-free area for assessment of cell migration over a 24 hour period; and these findings are presented below. Based on the results of the cell adhesion assays for the purposes of cell migration, only the CD133+ cells were evaluated here, since CD133+ cells proved to have enhanced adhesion ability.

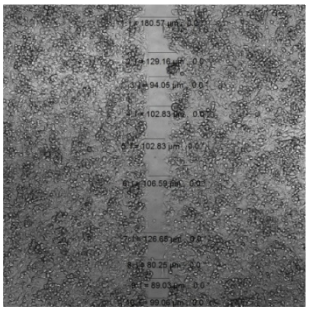
Cyclopamine treatment of migrating cells:

a.) DLD1 CD133+ cells, no treatment control

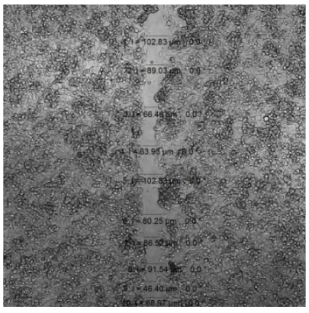
0 hours



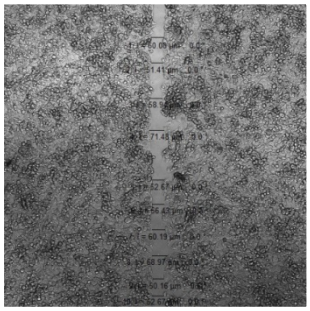
2 hours



4 hours



6 hours

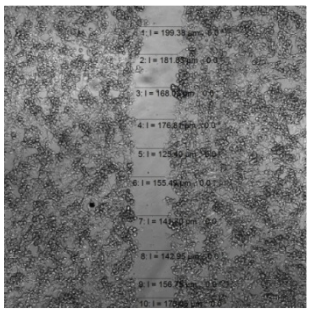


24 hours

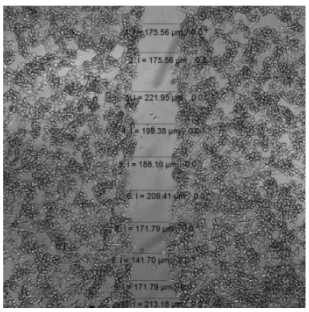


b.) DLD1 CD133+ cells, treated with cyclopamine

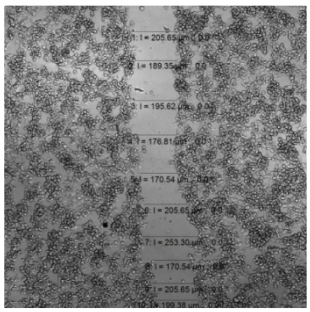
0 hours



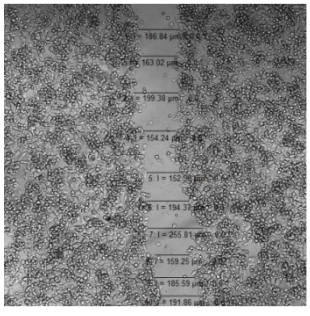
2 hours



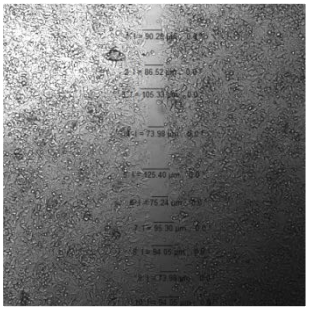
4 hours



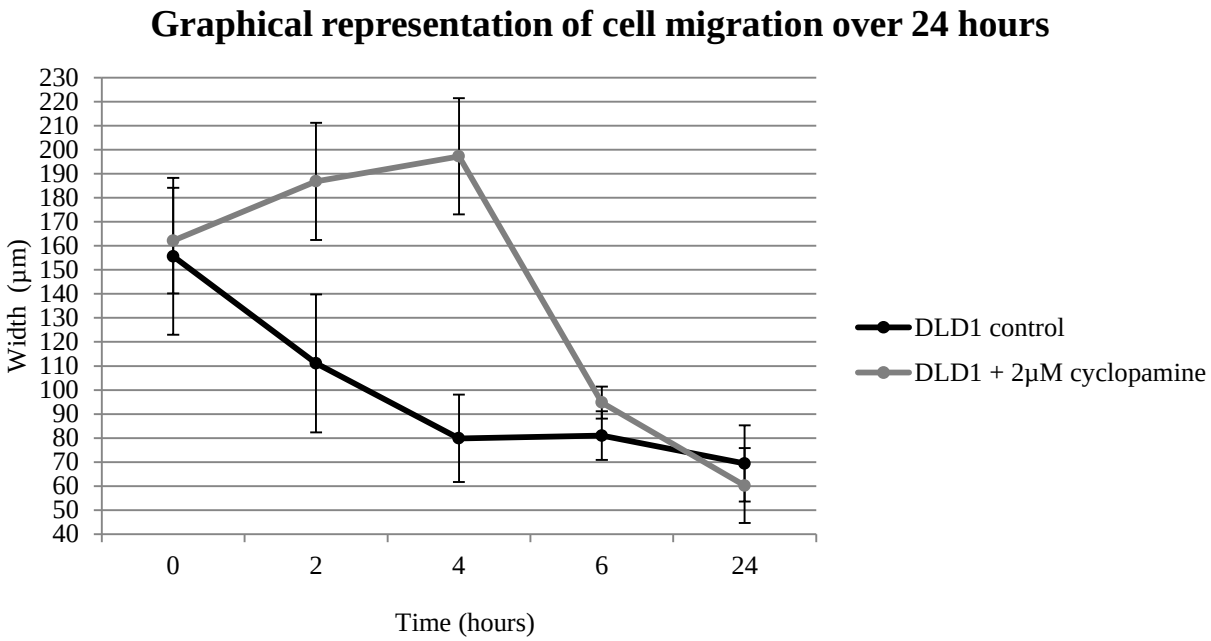
6 hours



24 hours



c.)



d.)

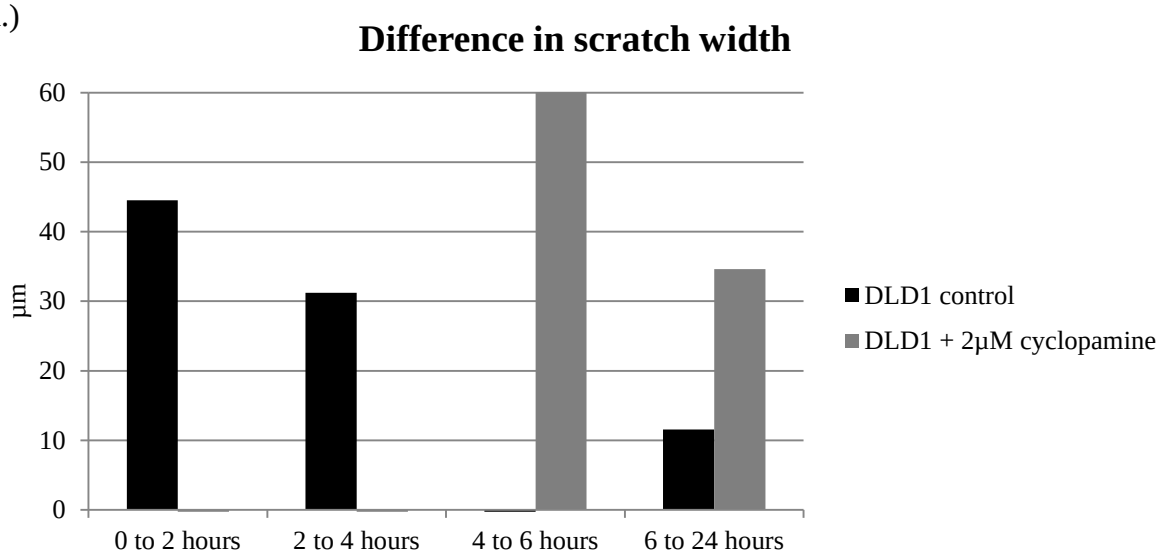
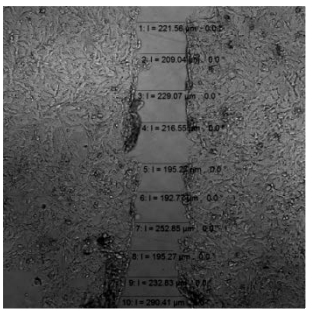


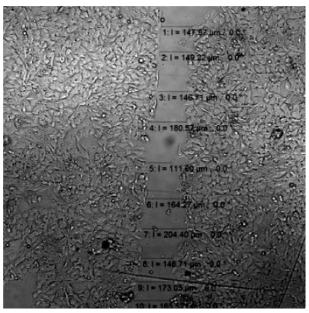
Figure 40: DIC images were captured every 2 hours for first 6 hours, with a final measurement at 24 hours. a.) DLD1 CD133+ cells show steady cell growth and gap closure over the 6 hour period and almost complete closure after 24 hours. b.) The addition of cyclopamine appears to slow gap closure within first 6 hours. c.) Change in scratch diameter illustrated graphically, with an increase in scratch width in first 6 hours due to cyclopamine treatment. Thereafter normal growth is seen and the width is similar to that of the control after 24 hours of incubation. d.) Bar graph representing cell migration (µM) over a 24 hour period. The difference in scratch diameter peaking in the period of 6 to 24 hours despite the application of cyclopamine. The control shows steady gap closure throughout the 6 hour period (Original Magnification 20X).

a.) HT29 CD133+ cells, no treatment control

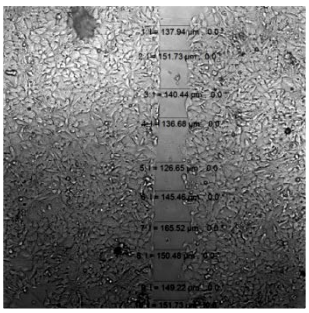
0 hours



2 hours



4 hours



6 hours



24 hours

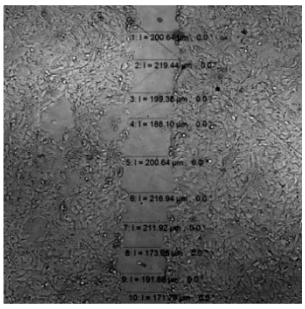


b.) HT29 CD133+ cells, treated with cyclopamine

0 hours



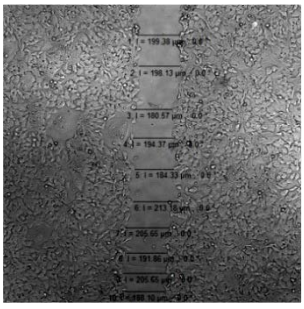
2 hours



4 hours



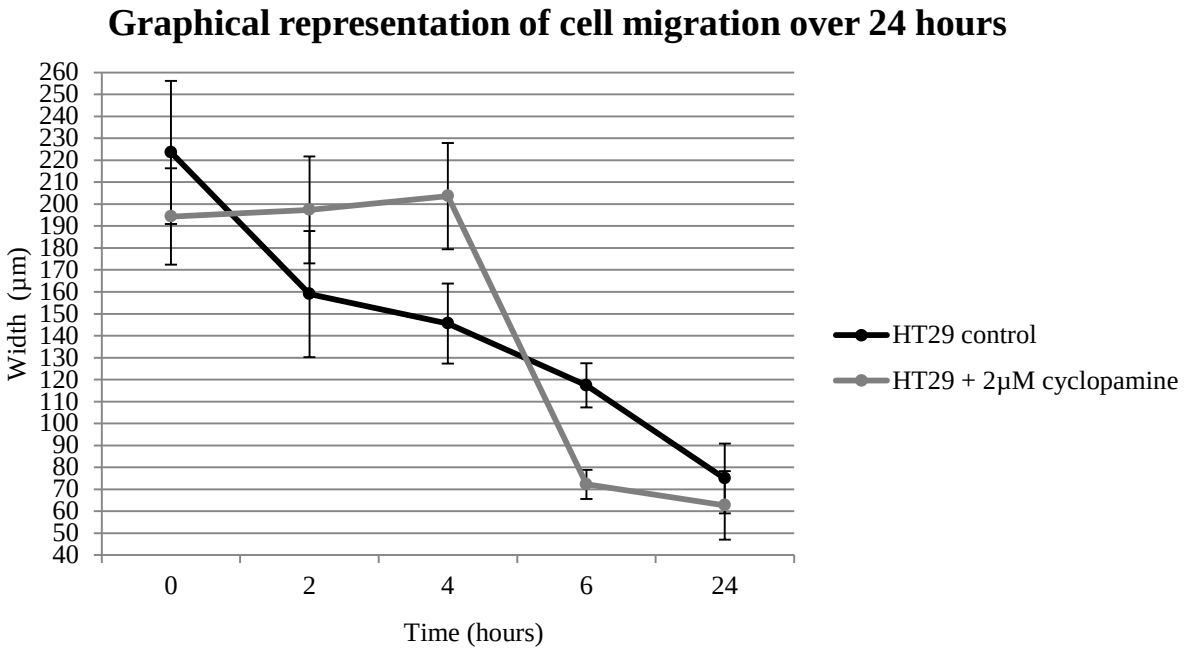
6 hours



24 hours



c.)



d.)

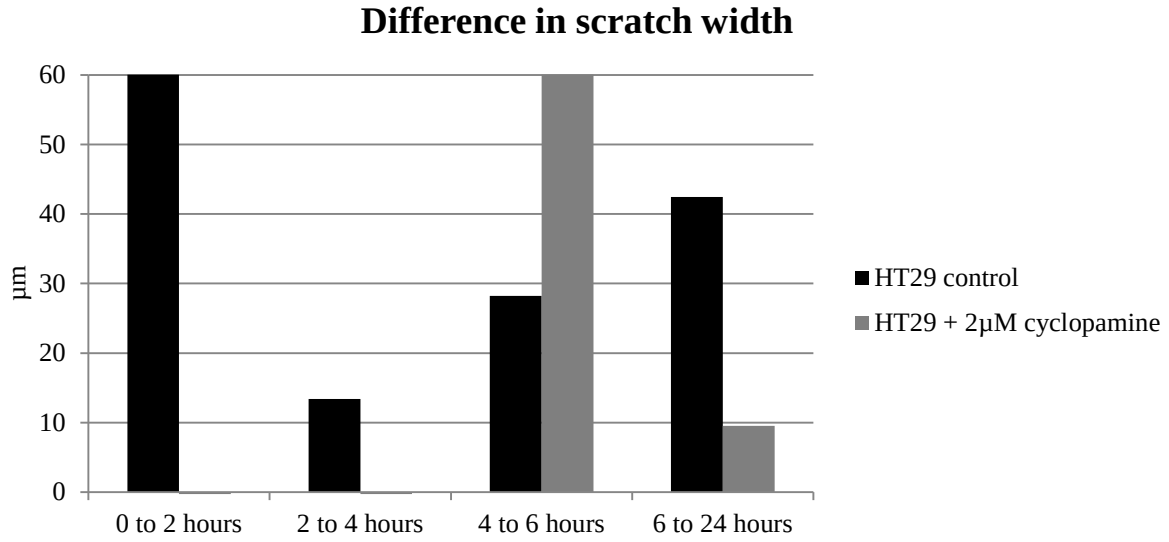
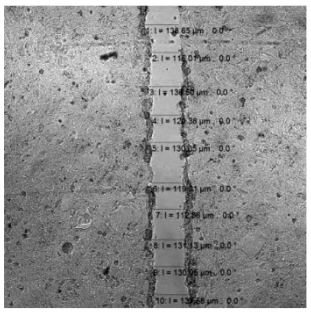


Figure 41: HT29 CSC's treated with cyclopamine indicated a similar reaction to the DLD1 cell line, a.) the control displayed consistent gap closure over the 24 hour period, b.) However, a definite hindrance in closure was seen with the addition of cyclopamine particularly during the first 6 hours. c.) The effect of the small molecule inhibitor is visible graphically where the scratch actually increased in width before closing at the 6 hour mark, the steady growth of the control is seen with the linear decrease in diameter. d.) bar graph illustrating the sudden growth/migration of the cells exposed to cyclopamine during the 4 to 6 hour period in contrast to the growth throughout the 24 hour incubation of the control (Original Magnification 20X).

SANT-2 treatment of migrating cells:

a.) DLD1 CD133+ cells; no treatment control

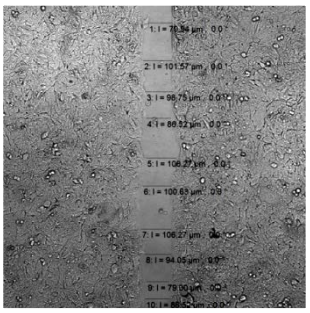
0 hours



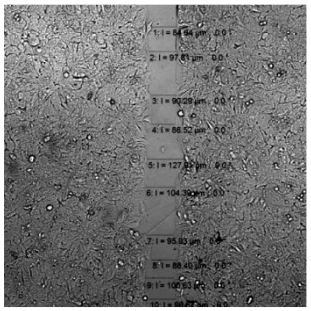
2 hours



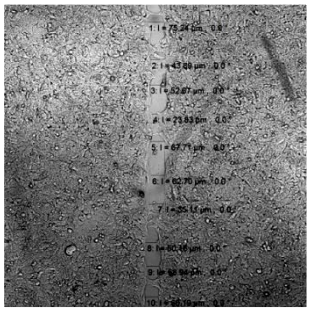
4 hours



6 hours

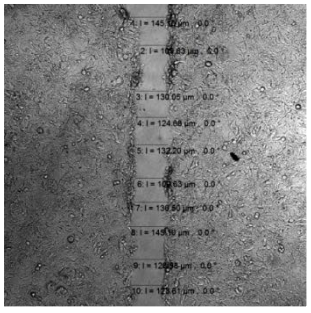


24 hours

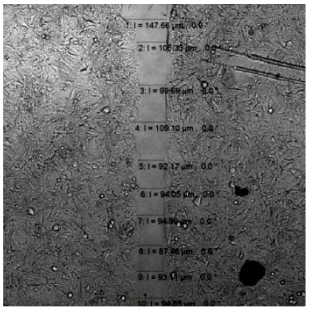


b.) DLD1 CD133+ cells, treated with SANT-2

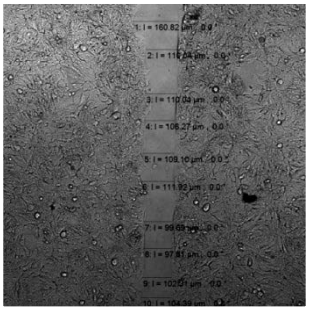
0 hours



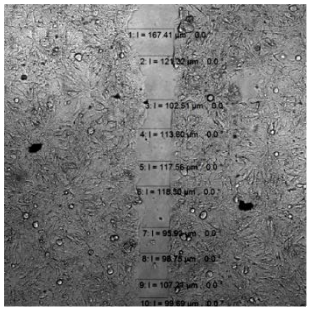
2 hours



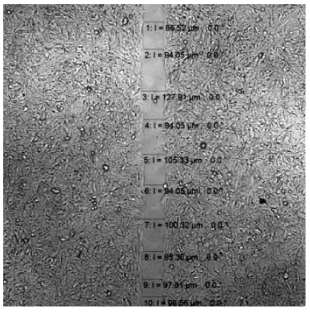
4 hours



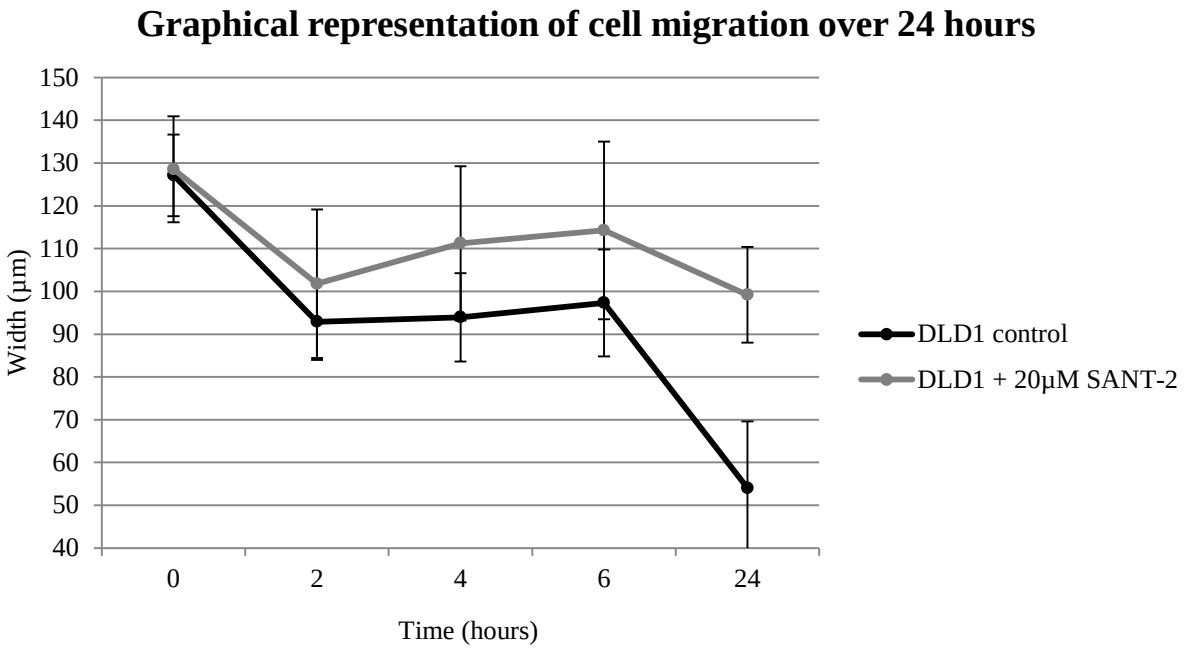
6 hours



24 hours



c.)



d.)

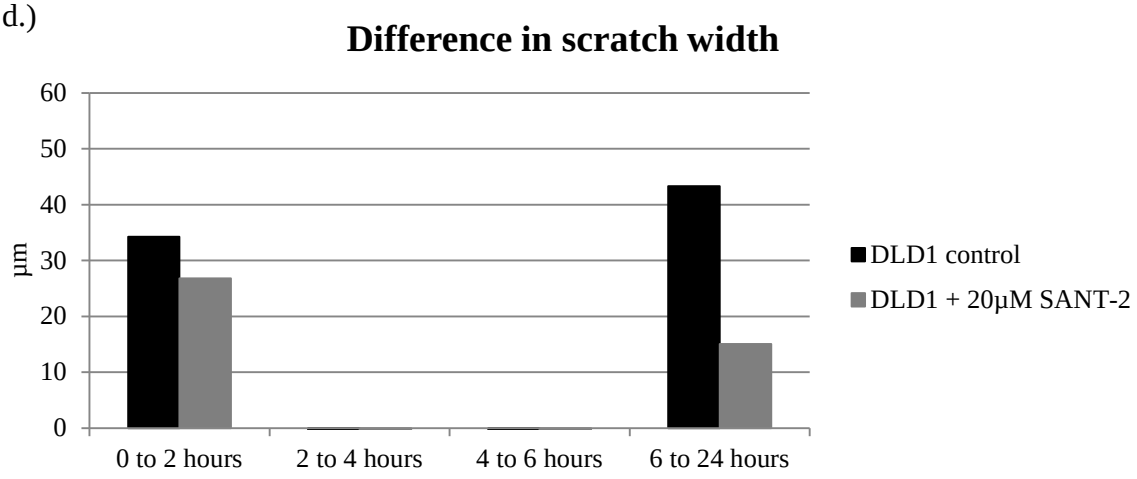
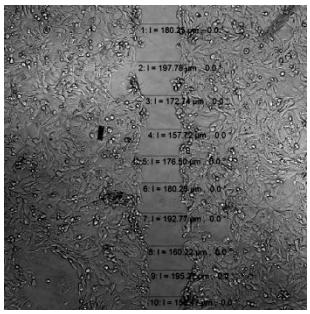


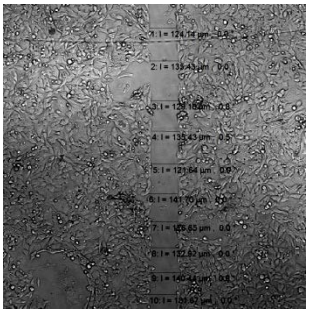
Figure 42: DLD1 CSC's responded differently to SANT-2 treatment as compared to cyclopamine. a.) The early observations showed an initial phase of cell migration and closure of the cell-free area from time 0 to 2 hours, followed by a seeming stabilization of migration and maintenance of a constant width. However, an almost complete closure of the gap was reached at the end of the 24 hour period. b.) When exposed to SANT-2 the width of the scratch did not appear to change much. c.) From the graph it can be noted that despite both scratch widths beginning at approximately the same point, their end width differs significantly. An initial growth is seen in both the DLD1 CSC's treated with SANT-2 as well as the control, with almost a plateau of growth visible with both once again. A final growth spurt results in the gap almost closing in the control; while conversely a gap still remains on the experimental slide. d.) Bar graph representing the early and late growth surges experienced by both the control and the DLD1 cells exposed to SANT-2 (Original Magnification 20X).

a.) HT29 CD133+ cells; no treatment control

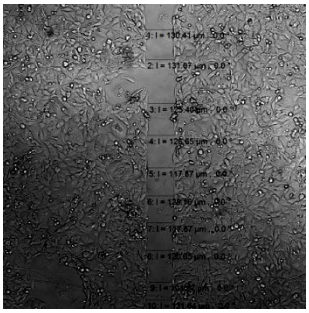
0 hours



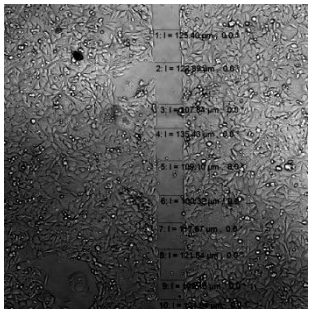
2 hours



4 hours



6 hours



24 hours



b.) HT29 CD133+ cells, treated with SANT-2

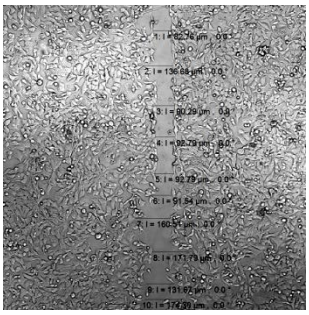
0 hours



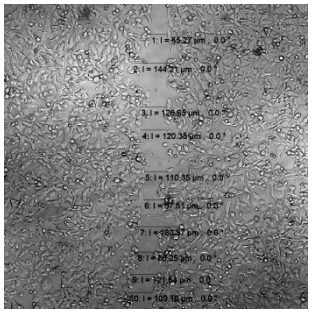
2 hours



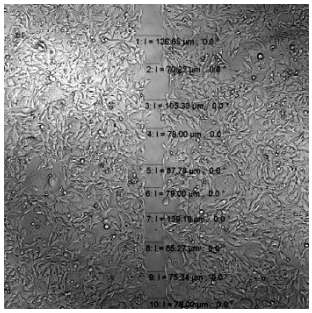
4 hours



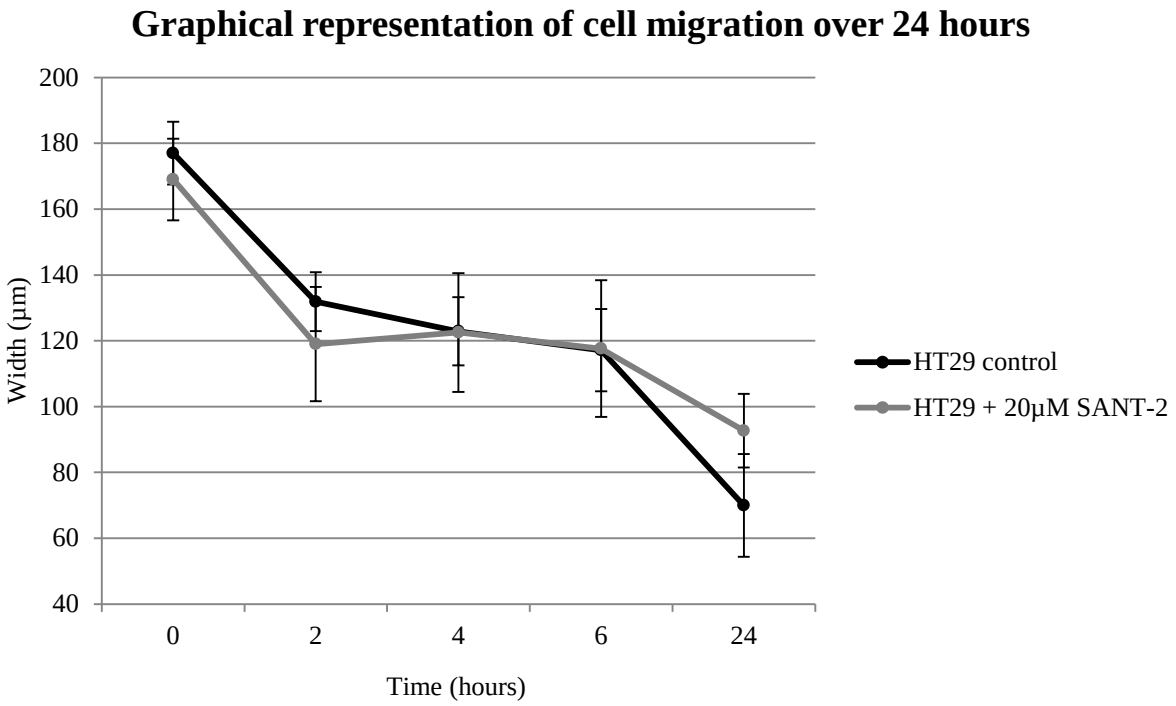
6 hours



24 hours



c.)



d.)

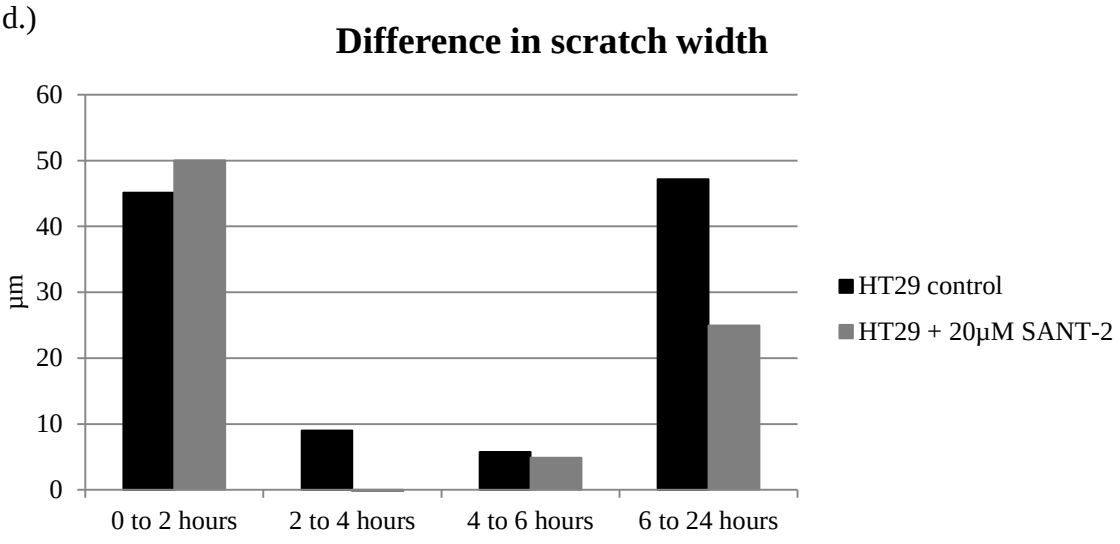
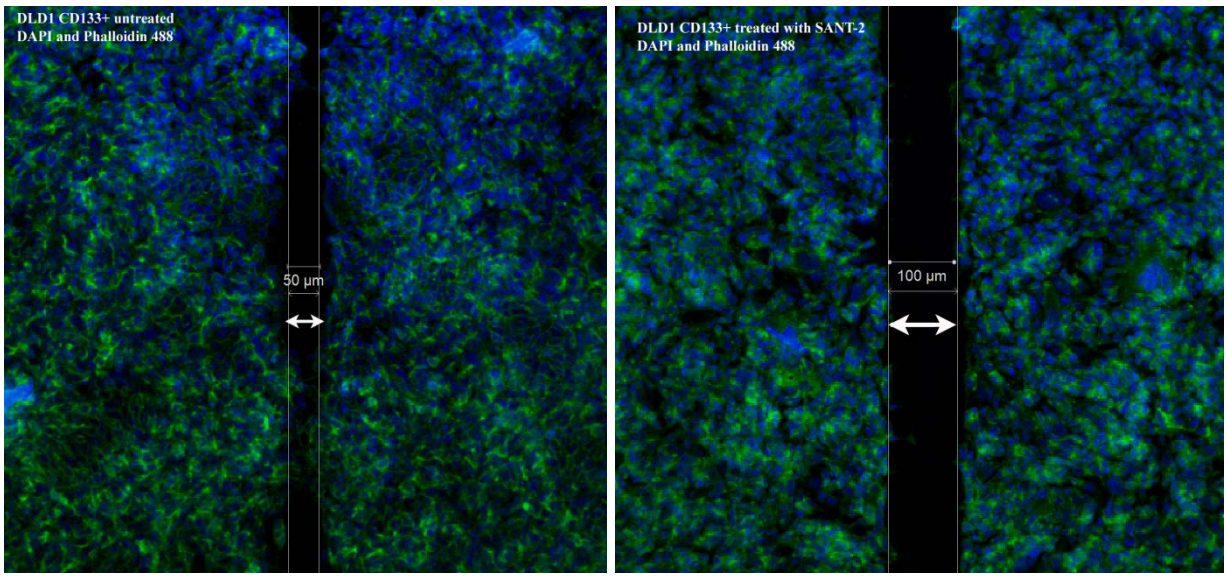


Figure 43: The HT29 cell line shows an almost identical pattern when treated with SANT-2, a.) The control scratch began closing within the first 2 hours, appeared to lag after which gap closure resumed until near closure. b.) The same trend occurred with the cells that were incubated with SANT-2; however the gap remained clearly apparent even after 24 hours. c.) The preliminary scratch width decrease in both the experimental slide as well as the control, the stabilization of closure during the 2 to 6 hour period and the final accelerated closure prior to reaching the end of the 24 hour incubation. Notably, the final width point remains distinctly higher in the HT29 CSC's with SANT-2 treatment. d.) Bar graph showing that most growth occurred during the first two hours of incubation and prior to the final 24 hour measurement (Original Magnification 20X).

DLD1 CD133+

Untreated

Treated with 20µM SANT-2



HT29 CD133+

Untreated

Treated with 20µM SANT-2

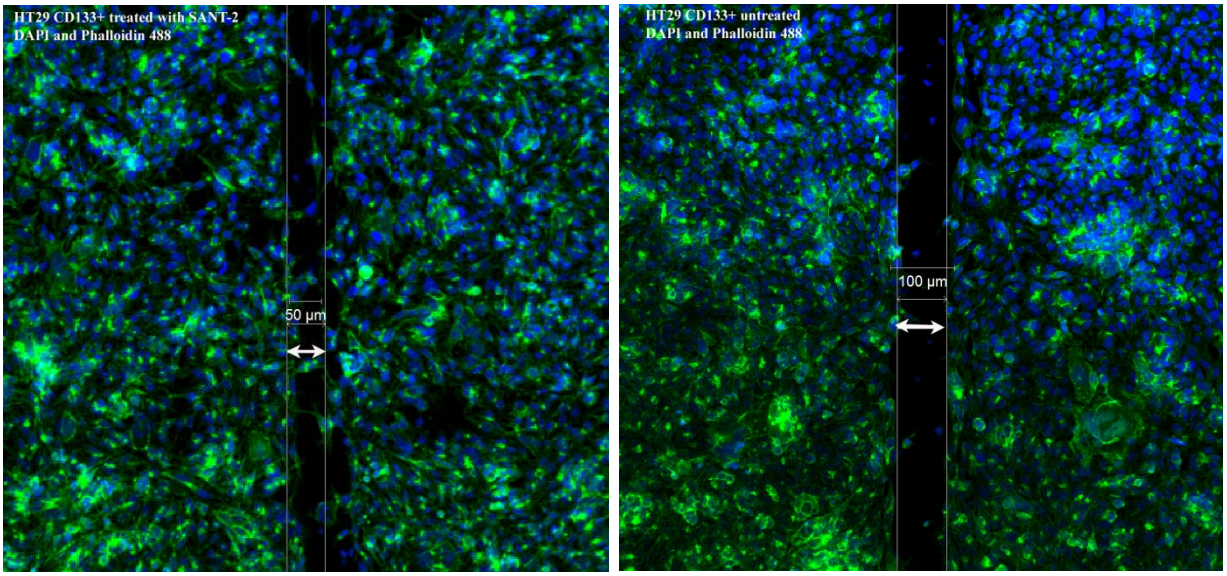
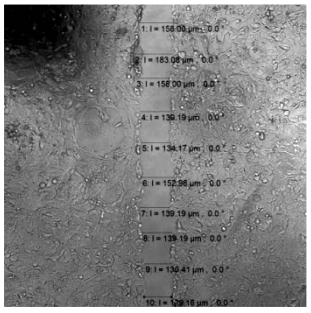


Figure 44: Fluorescence staining of CD133+ DLD1 and HT29 cells after treatment with SANT-2. Following F-actin staining with Phalloidin 488 (green) and nuclear staining with DAPI (blue) the difference in scratch width is clearly visible. Pharmacological treatment with SANT-2 clearly retarded cell migration into the cell free areas in both DLD1 and HT29 CSCs (Original Magnification 20X).

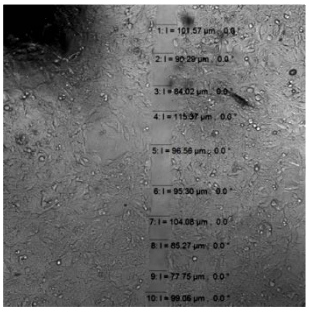
Tomatidine treatment of migrating cells:

a.) DLD1 CD133+ cells, no treatment control

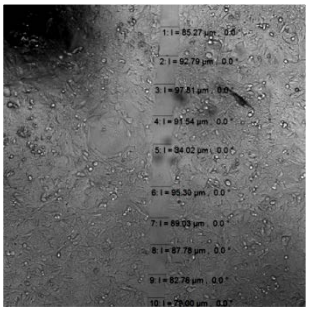
0 hours



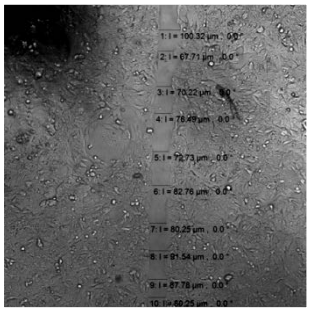
2 hours



4 hours



6 hours

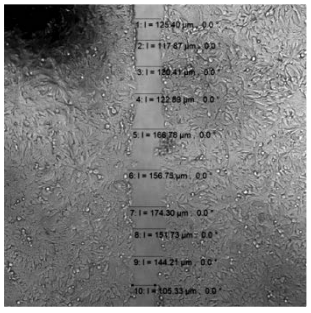


24 hours

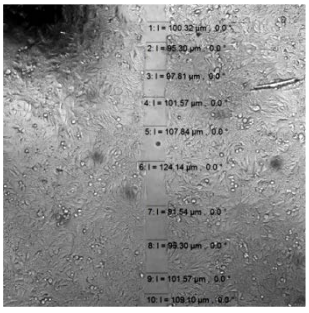


b.) DLD1 CD133+ cells, treated with tomatidine

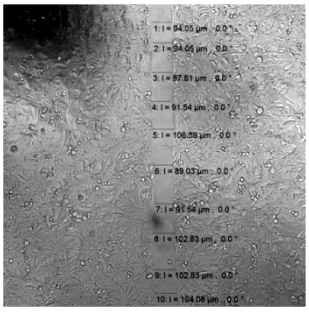
0 hours



2 hours



4 hours



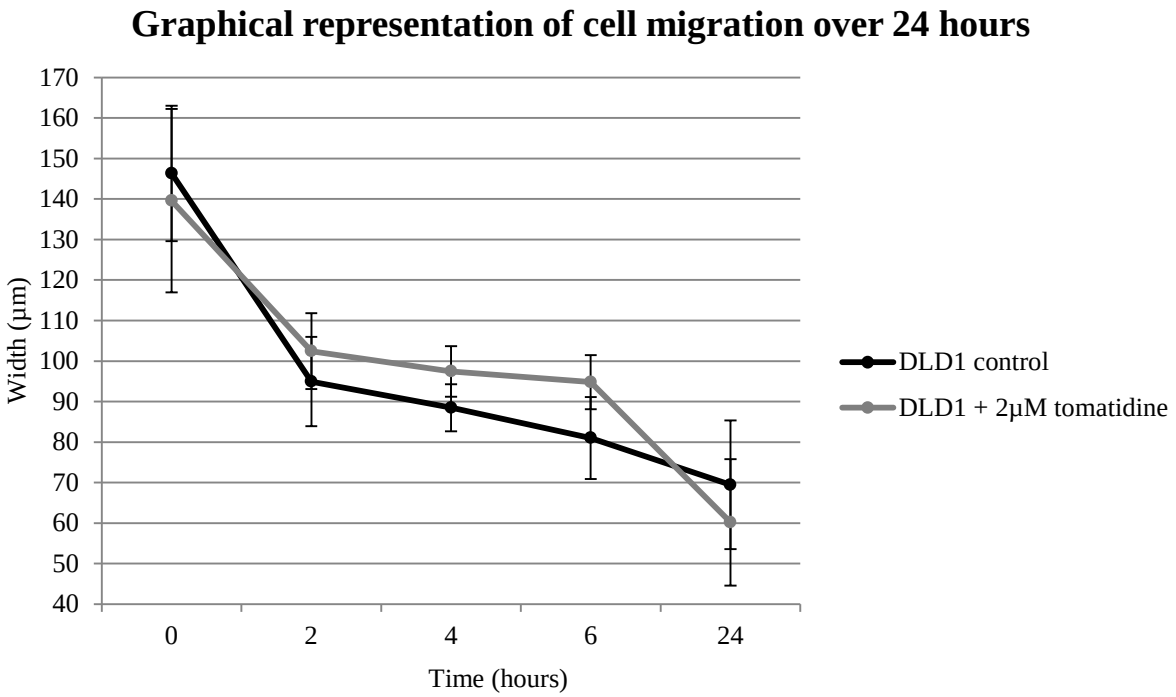
6 hours



24 hours



c.)



d.)

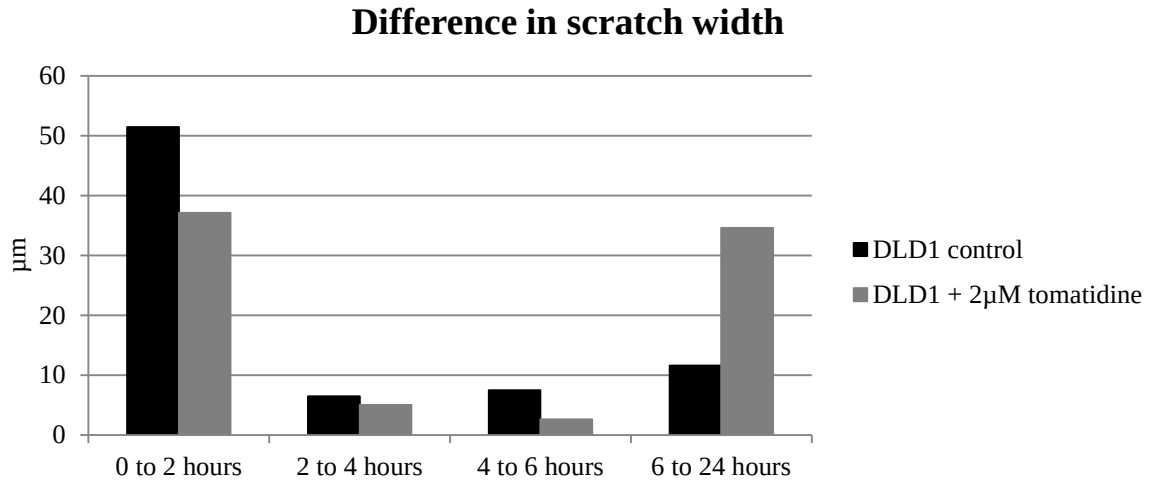
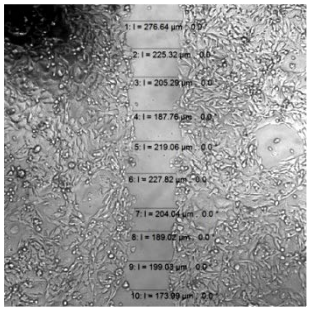


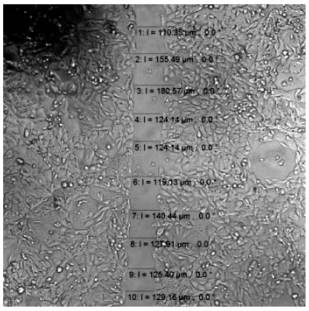
Figure 45: With the inclusion of the control molecule tomatidine DLD1 CSC's appeared to undergo unimpeded cell migration. a.) Closure of the gap in the no treatment control, as well as the slide treated with b.) tomatidine occurred steadily throughout the 24 hour incubation time. The final images captured illustrate an almost virtual gap closure in both. c.) Both the experimental and control slide had approximately the same start and end point scratch width, with linear growth indicated by the steady decrease in width. d.) Bar graph showing the difference in scratch diameter. It appears to be almost identical in both the experimental and control slides with a discrepancy only visible in the final incubation period, however despite this the end points remained rather similar (Original Magnification 20X).

a.) HT29 CD133+ cells, no treatment control

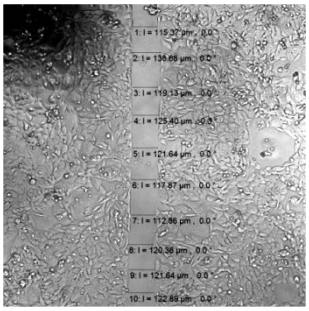
0 hours



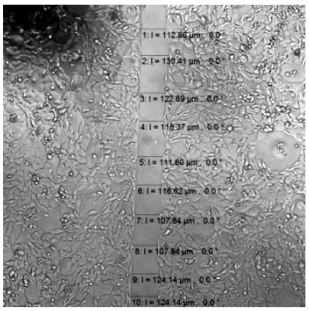
2 hours



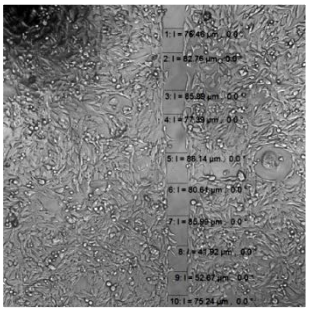
4 hours



6 hours

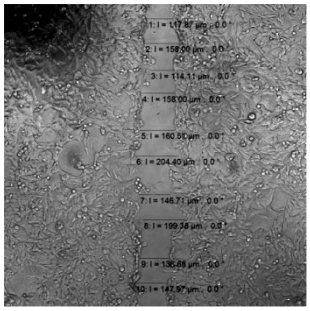


24 hours

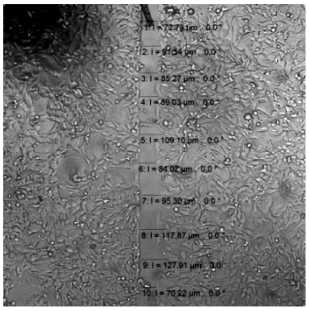


b.) HT29 CD133+ cells, treated with tomatidine

0 hours



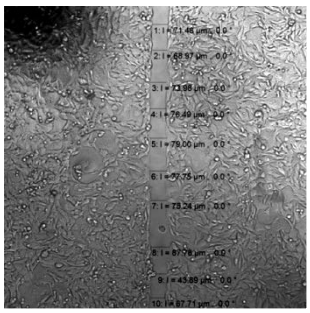
2 hours



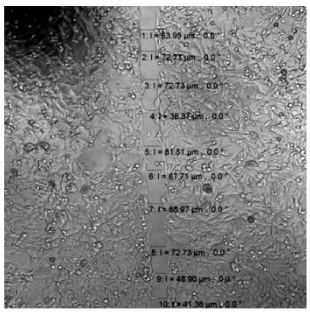
4 hours



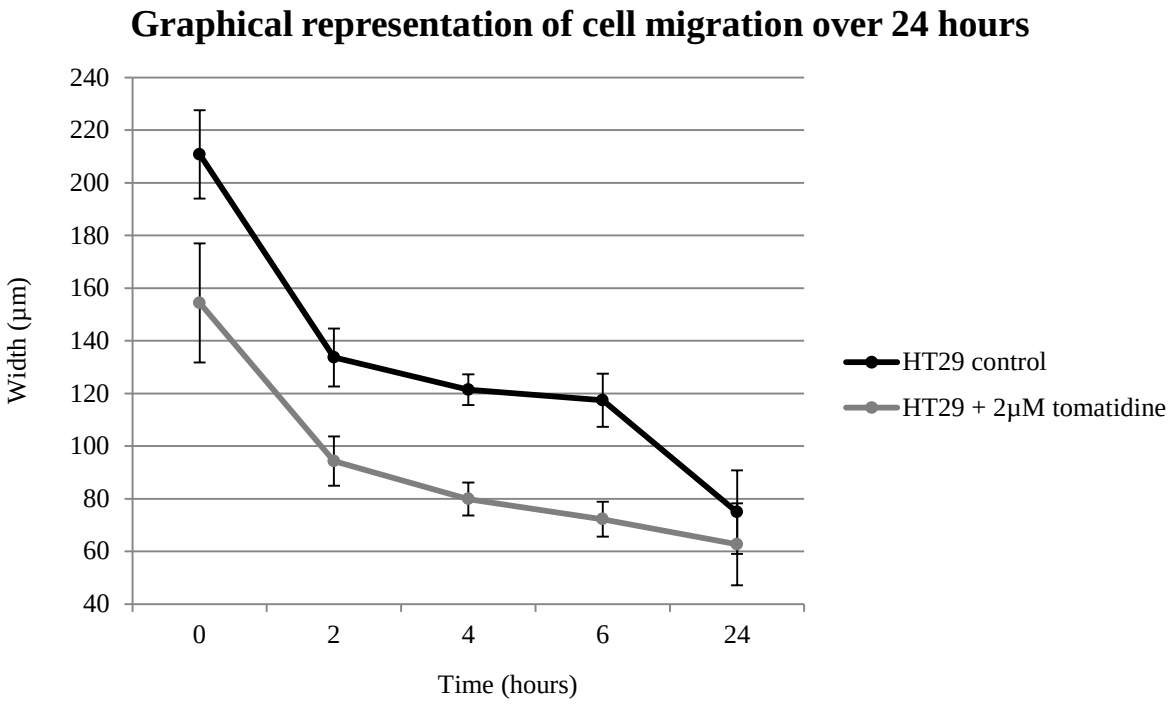
6 hours



24 hours



c.)



d.)

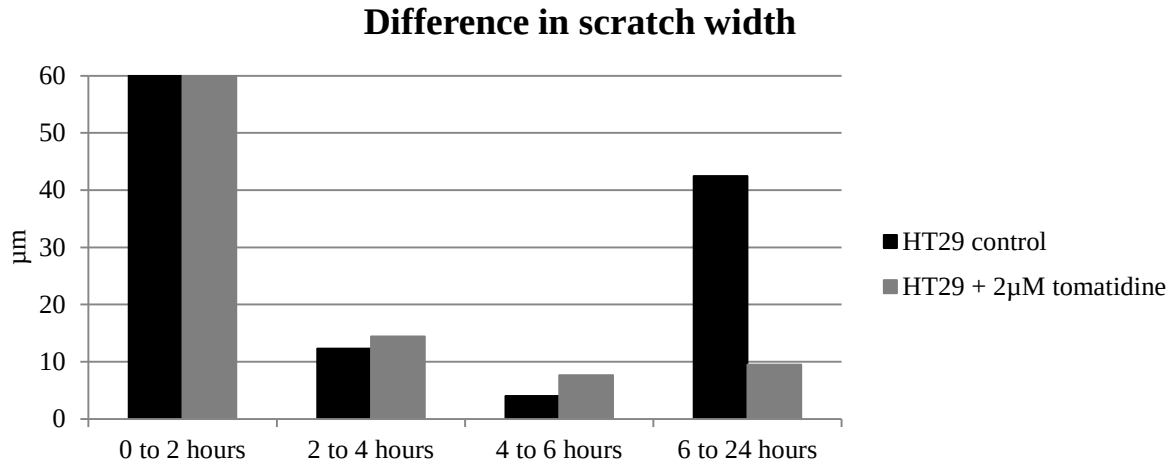


Figure 46: Following the same trend as the DLD1 cell line, the HT29 CSC's steady gap closure was visible in a.) the control and b.) cells incubated with tomatidine. While complete closure of the gap did not occur, many cells did however protrude into original cell free zone. c.) Despite the differing starting points the pattern seen by the control and tomatidine treated cells remains the same. Although a slight lag is observed in the 2 to 6 hour period there was a lack of overall impedance to migration. d.) The differences in scratch widths remain indistinguishable up until the last measurement where the control appeared to undergo a growth spurt resulting in the final scratch width being approximately the same regardless of the varying start widths (Original Magnification 20X).

The scratch/migration assays provided information on the ability of CD133+ CSC's to migrate and close a gap in order to form a confluent cell monolayer once again (Figure 40-46). Initial testing with drug was performed (see Appendix C) in order to determine an ideal scratch width, the most suitable duration for the assay as well as appropriate times of measurement. A 200µl micropipette tip was finally selected to create a narrow scratch, with the collection of more measurements in the first 6 hours of incubation so as to optimize the experiment for more precise measurement of gap closure rate. The difference in scratch width gives an indication of the extent of the effect the small molecule inhibitors had on the CSC's at the different time intervals. By assessing the differences in the progression of cell migration it can be seen that the most crucial time for drug activity is the first 6 hours of incubation. DLD1 cells expressing CD133 showed steady cell growth and gap closure over the 6 hour period and almost complete closure after 24 hours. With the addition of cyclopamine a hindrance in gap closure is noticed within the first 6 hours thereafter normal growth is seen and the width is similar to that of the control after 24 hours of incubation. HT29 CSC's responded similarly to cyclopamine as the DLD1 cell line suggesting that the drug has a negative effect on the ability to migrate within the first 6 hours. The effect of the small molecule inhibitor is visible graphically (see Figure 40-41) where the scratch actually increased in width before closing at the 6 hour mark, in contrast to the sustanined growth of the control throughout the 24 hour incubation period. DLD1 and HT29 CSC's displayed a somewhat different response to SANT-2 treatment; despite both scratch widths beginning at approximately the same point, their end width differs significantly particularly in the DLD1 cell line. This would infer that SANT-2 has an inhibitory effect on cell migration over the 24 hour incubation period. This is in contrast to cyclopaminie that was effective only up to 6 hours of treatment. Similar to the untreated control, tomatidine did not have any effect on cell migration, and the gaps being almost totally closed in both cell lines after 24 hours.

6.8 EXPRESSION OF SHH

DLD1 CD133+

Untreated

Treated with 2µM cyclopamine

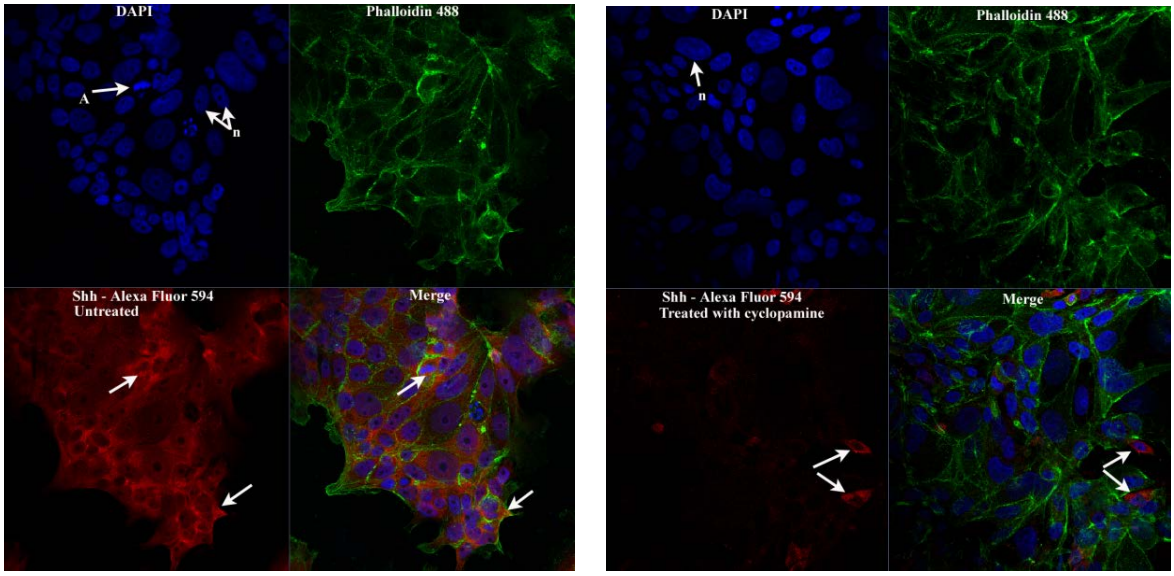


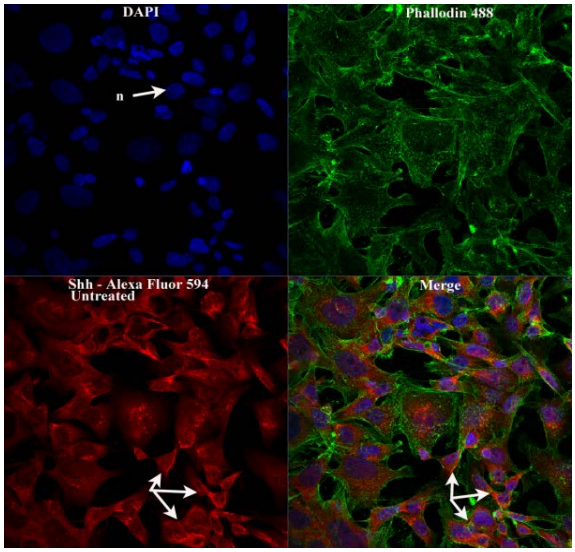
Figure 47: Expression of Shh in DLD1 CD133+ cells after treatment with cyclopamine, nuclei shown with (n) and apoptosis (A). Following incubation with 2µM cyclopamine it was found that the expression levels of cell surface Shh (red) had decreased indicated with arrows. This was visible by fluorescence microscopy after staining with a Shh specific primary antibody. The nuclei were stained with DAPI (blue) and F-actin filaments were stained with Phalloidin 488 (green). The relative CTCF values were calculated and displayed below (Original Magnification 63X).

Table 25: Corrected Total Cell Fluorescence (CTCF) of DLD1 CD133+ cells, stained with an anti-Shh antibody prior to treatment and following with treatment with 2µM cyclopamine

Untreated	**Integrated density**	**Area of selected cell**	**Background fluorescence**	**CTCF**
	73039	1401	0.061	72953.53
	72065	1805	0.061	71954.90
	79110	1979	0.061	78989.28
Average CTCF				74632.57
Treated				
	39111	1036	0.987	38088.46
	47091	1402	0.987	45797.23
	51675	1352	0.987	50340.58
Average CTCF				44742.09

HT29 CD133+

Untreated



Treated with 2µM cyclopamine

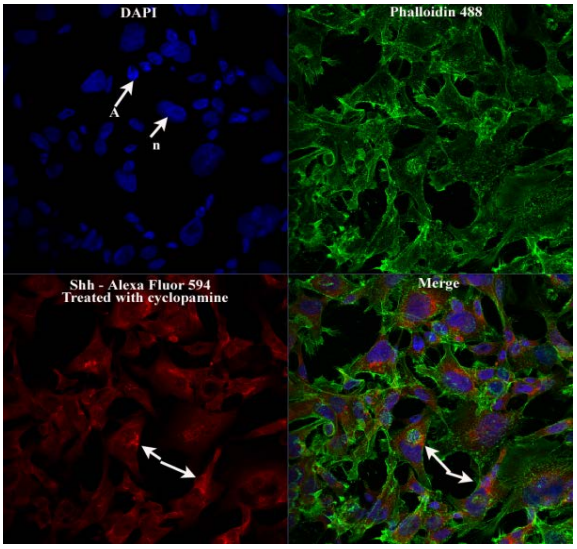


Figure 48: Expression of Shh in HT29 CD133+ cells after treatment with cyclopamine, nuclei shown with (n) and apoptosis (A).Cell surface Shh (red) had decreased, indicated with arrows, following treatment with cyclopamine.Some Shh is still expressed following treatment but to a lesser extent. The nuclei were stained with DAPI (blue) and F-actin filaments were stained with Phalloidin 488 (green) (Original Magnification 63X).

Table 26: Corrected Total Cell Fluorescence (CTCF) of HT29 CD133+ cells, stained with an anti-Shh antibody prior to treatment and following with treatment with 2µM cyclopamine

Untreated	**Integrated density**	**Area of selected cell**	**Background fluorescence**	**CTCF**
	135558	4530	0.008	135521.76
	133743	4654	0.008	133705.77
	142291	5097	0.008	142250.22
Average CTCF				137159.25
Treated				
	90720	2410	0.070	90551.3
	88588	2102	0.070	88440.86
	93988	2304	0.070	93826.72
Average CTCF				90939.62

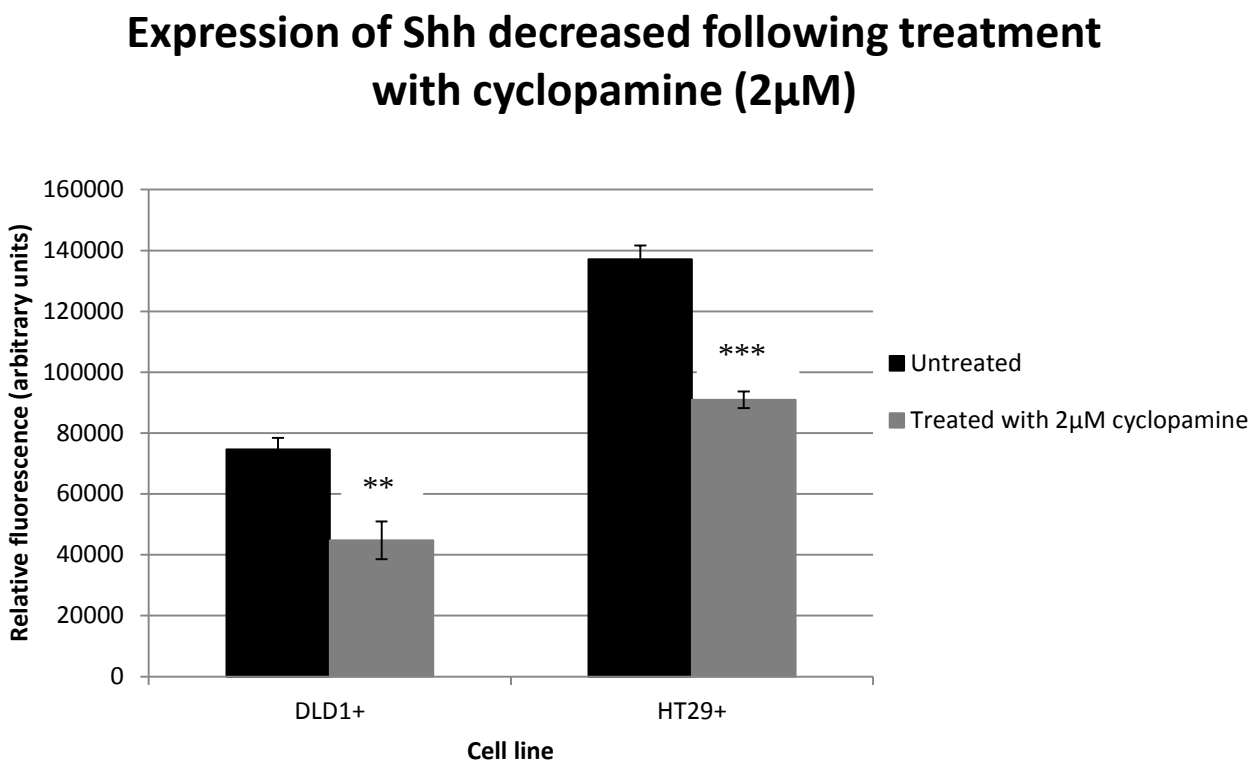


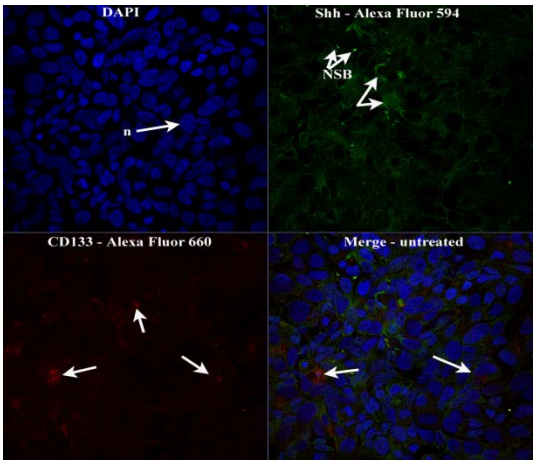
Figure 49: Shh expression in DLD1+ and HT29+ cells treated with cyclopamine. Both cell lines showed a decreased expression of Shh on their cell surface following treatment with the antagonist of the Hh signalling pathway.

Following treatment with 2µM cyclopamine both DLD1 and HT29 CD133+ cells showed a decreased expression of Shh with significant decreases of 29890.48 units (** p= 0.0021) and 46219.63 units (*** p= 0.0001) respectively (Figure 47-49). These decreases are visually apparent with the fluorescence intensity appearing far less intense after treatment with the drug.

6.9 EXPRESSION OF CD133 AND SHH

DLD1 CD133+

Untreated



Treated with 2µM cyclopamine

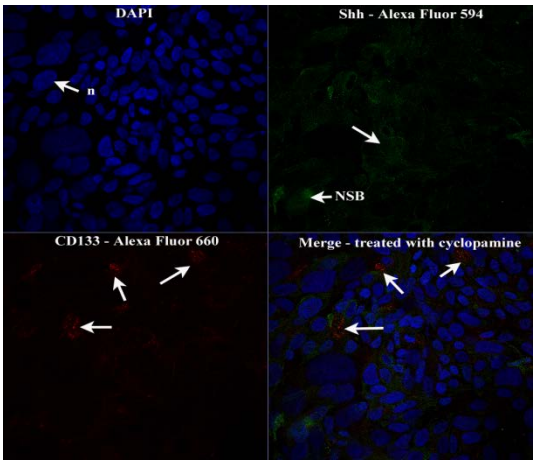


Figure 50: The expression levels of CD133 in conjunction with Shh expression was assessed subsequent to treatment with cyclopamine (2µM). Nuclei were stained with DAPI (blue), Shh (green), and CD133 (red). A decrease in Shh can be seen with a minimal change in cell surface CD133 expression (Original Magnification 63X).

Table 27: Corrected Total Cell Fluorescence (CTCF) of DLD1 CD133+ cells, stained with an **anti-Shh** antibody prior to treatment and following treatment with 2µM cyclopamine

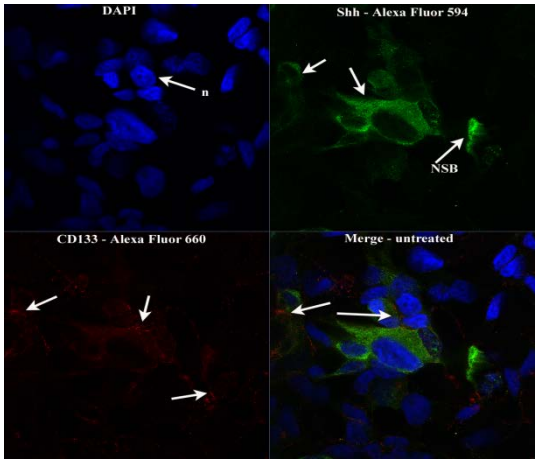
Untreated	**Integrated density**	**Area of selected cell**	**Background fluorescence**	**CTCF**
	53560	1542	1.092	51876.14
	55875	2286	1.092	53378.69
	46770	2054	1.092	44527.03
Average CTCF				49927.29
Treated				
	34510	1915	1.176	32257.96
	37784	2513	1.176	34828.71
	30516	2240	1.176	27881.76
Average CTCF				31656.14

Table 28: Corrected Total Cell Fluorescence (CTCF) of DLD1 CD133+ cells, stained with an **anti-CD133** antibody prior to treatment and following treatment with 2µM cyclopamine

Untreated	**Integrated density**	**Area of selected cell**	**Background fluorescence**	**CTCF**
	20792	1800	3.896	13779.2
	22186	1999	3.896	14397.9
	23303	1774	3.896	16391.5
Average CTCF				14856.2
Treated				
	20949	2280	2.481	15292.32
	20405	1952	2.481	15562.09
	19377	1626	2.481	15342.89
Average CTCF				15399.1

HT29 CD133+

Untreated



Treated with 2µM cyclopamine

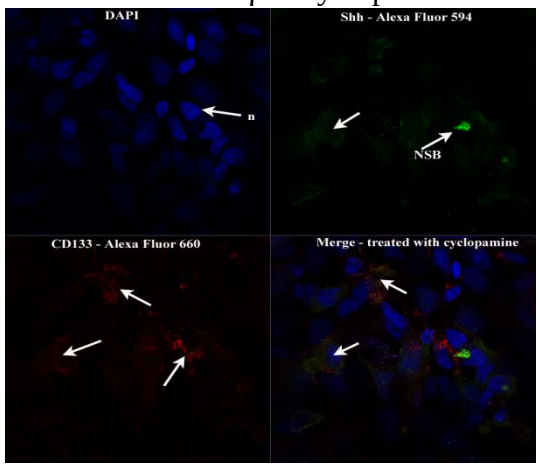


Figure 51: Expression of CD133 in conjunction with Shh following treatment with cyclopamine (2µM). Nuclei were stained with DAPI (blue), Shh (green), and CD133 (red). A decrease in Shh is clearly evident; however a change in cell surface CD133 expression is not apparent (Original Magnification 63X).

Table 29: Corrected Total Cell Fluorescence (CTCF) of HT29 CD133+ cells, stained with an **anti-Shh** antibody prior to treatment and following treatment with 2µM cyclopamine

Untreated	**Integrated density**	**Area of selected cell**	**Background fluorescence**	**CTCF**
	201572	11079	4.894	147351.4
	213184	12262	4.894	153173.8
	201681	11257	4.894	146589.2
Average CTCF				149038.1
Treated				
	32548	2915	1.376	28536.96
	34954	4331	1.376	28994.54
	33584	2360	1.376	30336.64
Average CTCF				29289.38

Table 30: Corrected Total Cell Fluorescence (CTCF) of HT29 CD133+ cells, stained with an **anti-CD133** antibody prior to treatment and following with treatment with 2µM cyclopamine

Untreated	**Integrated density**	**Area of selected cell**	**Background fluorescence**	**CTCF**
	73640	5569	1.810	63560.11
	71865	5396	1.810	62098.24
	70347	5124	1.810	61072.56
Average CTCF				62243.64
Treated				
	74283	7849	0.978	66606.68
	76223	7447	0.978	68939.83
	75456	6697	0.978	68906.33
Average CTCF				68150.95

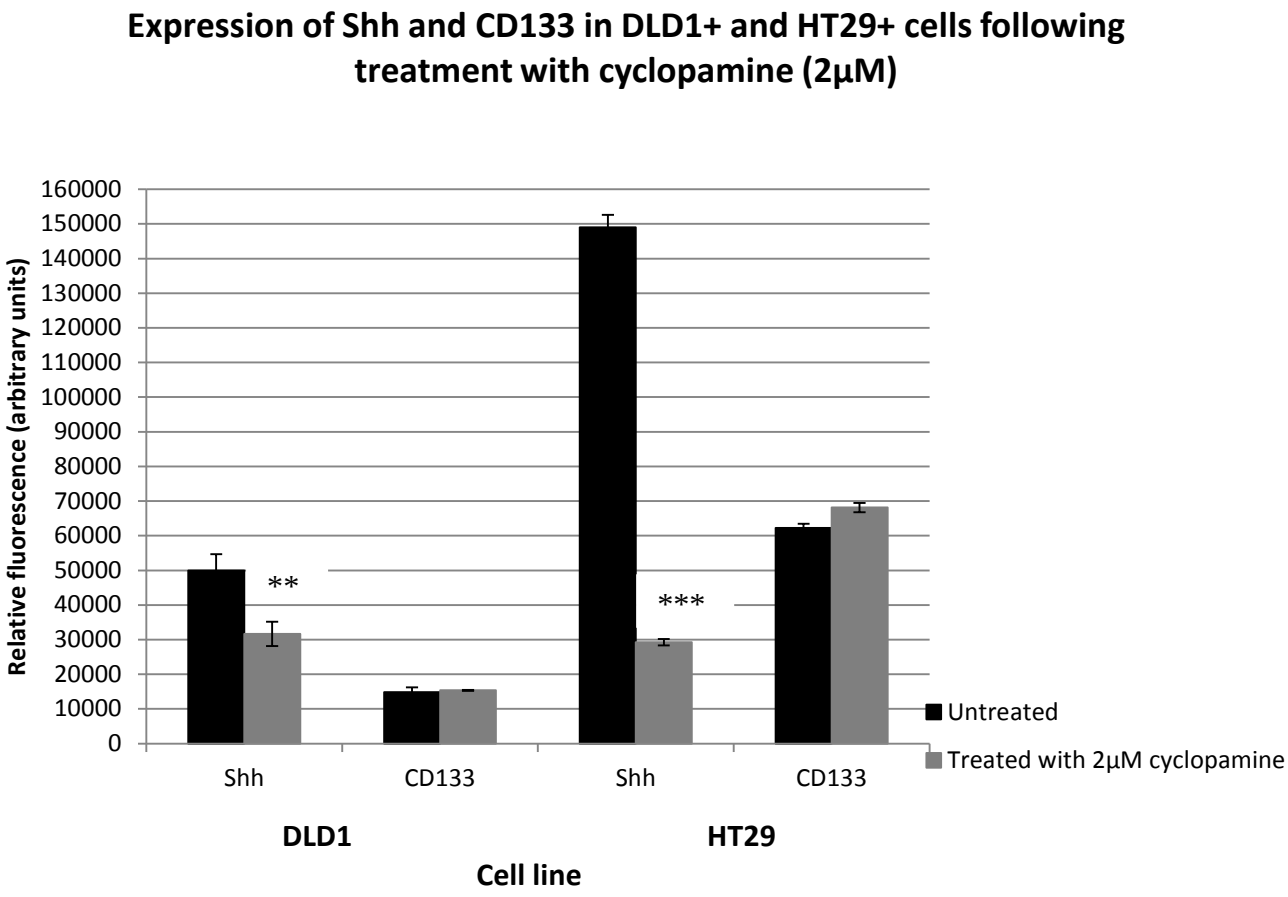


Figure 52: Expression of Shh as well as CD133 in DLD1+ and HT29+ cells after treatment with cyclopamine. Both DLD1 and HT29 cells had a decreased expression of Shh following treatment with cyclopamine, however with no significant change in CD133 expression.

In both the DLD1 (** p =0.0058) and HT29 (*** p=0.0001) CD133+ cells there was a significantly decreased expression of Shh following treatment with cyclopamine, with differences in the CTCF values of 18271.15 and 119748.72 respectively (Figure 50-52). A far greater decrease in expression was seen in the HT29 cell line. The expression of CD133 did not decrease in either the DLD1 or HT29 cell lines.

6.10 CORRELATION OF METASTATIC PROPERTIES

Correlation between decrease in <u>adhesion</u> and decrease in <u>invasion</u> with application of small molecule inhibitors:

A distinct property of metastatic cells is the efficiency of their adhesive interactions with other cells as well as components of the extracellular matrix[100]. Adhesion is a necessary step in the process of invasion and migration. Studies have shown that together, the adhesive and invasive potential of cancer cells have a high correlation (r=0.77)[98], inferring that a reduced ability to adhere should result in a decreased invasive potential and migratory ability. In this study, with the application of small molecule inhibitors of the Shh pathway impeding cell adhesion, invasion, and migration this theory was tested. The linear dependence between two variables was expressed using Pearson's (r) correlation coefficient. By using the difference in adhesion potential and the difference in invasion potential the following was calculated:

Cyclopamine	SANT-2	Tomatidine
r = 0.4299	r = 0.924	r = 0.2823

By calculating the Pearson's correlation co-efficient between the decrease in adhesion potential and the difference in invasion potential, it was found to be 0.4299, 0.924 and 0.2823 for cyclopamine, SANT-2 and tomatidine respectively. This indicates that the correlation is positive for all three compounds, indicating a positive association with treatment. The strongest positive relationship is reflected following SANT-2 treatment and the weakest is with the cyclopamine analogue, tomatidine. Therefore, we propose that in most instances a decreased adhesion potential correlates with a decreased invasive potential.

Correlation between decrease in <u>adhesion</u> and decrease in <u>migration</u> with application of small molecule inhibitors:

Cyclopamine	SANT-2	Tomatidine
r = -0.4287	r = 0.5021	r = -0.0352

These results indicate that a decreased adhesion potential due to the action of SANT-2 results in a decreased ability to migrate. However, a decreased adhesive potential due to application of cyclopamine does not necessarily result in a decreased ability to migrate. The negative value calculated implies that there is a negative correlation, meaning that adhesion may decrease while migration may increase. Similarly, this is the case with tomatidine, but there is only a slightly negative correlation in comparison to the strongly negative value of -0.4287 calculated for cyclopamine.

7. DISCUSSION

7.1 INTRODUCTION

Evidence for the existence of Cancer Stem Cells (CSC's) in solid tumours has accumulated in recent years[20,22]. It is believed that tumours are heterogeneous and upon dissociation and transplantation into an immune-compromised mouse model, human CSC's are able to reinitiate and form a similar heterogeneous tumour *in vivo.* While these cells display many characteristic features of mesenchymal stem cells in terms of their growth properties, they have however, also been found to be resilient to therapy[101], are extremely invasive and therefore highly metastatic. CSC's have been positively identified in, and isolated from various human solid cancers, including colon cancer[27,28]. Most colon cancers begin as local adenomas in the intestine and progress to invasive carcinomas. It has been suggested their recurrence and metastatic potential have been attributed to the presence of CSC's expressing cell surface CD133[102]. In the present study this cell surface protein has been used as a marker to successfully isolate and identify CSC's from a heterogeneous cancer cell population. An active Hedgehog-Gli pathway has been detected in both human colon carcinoma cells and in their stem cells[76]. During embryonic development this pathway is a key regulator and ensures that axis symmetry as well as the correct distribution of cell types is maintained[56]. In adult tissue although the Hh pathway is mainly inactive[57], it is thought to play a role in regulating adult stem cells which consequently maintain and regenerate old or damaged tissue; and notably expression also occurs in human adult gut epithelium[58]. Reactivation of the Hh pathway in adult tissues may be linked to the development of some cancers which occurs either by the genetic modification of the pathway components or excessive secretion of the Hh ligands. The mechanism by which the Shh pathway is reactivated involves the surface protein Ptch suppressing the activity of the cytoplasmic protein Smo, however, following the binding of the Hh ligand to Ptch, this suppression is then inhibited. This then allows for the activation of downstream targets through the Gli transcription factors (Figure 53). When a Hh ligand is absent it results in the phosphorylation and cleavage of Gli. However in the presence of a Hh ligand, Gli is not cleaved and the full length Gli translocates to the nucleus where it exhibits transcriptional activity and the up-regulation of key oncogenes. The involvement of this pathway specifically in metastasis by inducing Epithelial to Mesenchymal Transitions (EMT) makes it an obvious option for a targeted therapeutic. As mentioned, Sonic Hedgehog (Shh) inhibitors such as cyclopamine have been successful in the treatment of other cancer types including basal cell carcinoma, medulloblastoma and

rhabdomyosarcoma[59]. The pathway inhibition induced by this small molecule is as an antagonist of Smo preventing activation of Gli, its movement into the nucleus and thus precluding oncogene transcriptions.

Considering the need for targeted therapy against cancer stem cells and their occurrence in colon cancer, as well as the role of Shh in EMT and metastasis, we hypothesized that disrupting this pathway using small molecule inhibitors would be effective in impeding the invasive and adhesive potential of colorectal CSC's.

7.2 Isolation of CSC's

In this study CSC's were successfully isolated from 3 colorectal cancer cell lines representing early and middle-late stages of the disease. The SW480 cell line which is thought to be derived from an early tumour was found to contain very few CSC's upon several attempts at separation. These cells proved to be too few in number to proliferate and form a new population of stem cells in the specified media. It is for this reason that confirmation by flow cytometry was not possible and therefore these cells were not used in experiments thereafter. The low number of stem cells in early tumours concurs with the literature wherein more advanced (metastatic) cancers have been found to contain far higher quantities of stem cells in comparison to early stage tumours. In a cohort study fewer Dukes' stage A tumours (5%) were found to have expression of CD133 in comparison to Dukes' stage B and C tumours (25%)[103]. With the DLD1 and HT29 cell lines which are representative of middle-late stage colon cancer, sufficient quantities of stem cells were isolated and this allowed for the culturing of a relatively pure stem cell population of each line. The increased number of $CD133^+$ cells found in cancer cell lines most likely results from their oncogenic transformation[104].

Following the magnetic separation the stem cells were cultured in a defined media lacking FBS to maintain the cells in an undifferentiated state. The media did however contain several other defined growth factors that promoted cell proliferation, including insulin, FGF and EGF. The isolated cells initially grew typically as spheroids and thereafter were able to adhere to the cell culture plate to form a single monolayer. The ability to form spheroids is a distinct characteristic of CSC and studies have shown that primary cancer cells from adherent

cultures fail to form these structures when grown in a 3D culture system[105]. Other studies using colon cancer cells report that about 1 in 16 CD133 expressing cells have an increased ability to form spheroids, whereas approximately only 1 in 250 CD133- cells have this same ability, inferring that it is more likely that spheroid formation will occur in a cell population that express cell surface CD133[102].

After several days of growth the isolated cells reached a sufficient level of confluence for flow cytometry analysis. Using the CD133 receptor as a definitive marker the DLD1 CSC's had a purity level of 73%; and similarly, the HT29 cell line displayed a 70% purity level. This level of purity is above what was found in literature where after magnetic separation of glioblastoma-derived CSC's a purity level of 53% was determined using flow cytometry[106].

7.3 CSC GROWTH PROFILES

As mentioned previously, the isolated CSC's initially grew as typical spheroids, a property indicative of "stemness". Next, their expression of CD133 was then confirmed by flow cytometry, and taken together, it could therefore be deduced that a CSC population had been isolated from a general non-CSC population and a comparison could be then made in terms of their proliferation rate and growth patterns. The use of a real-time cell analyser was employed to carefully elucidate the differences in the growth patterns between "normal" colon cancer cells and colon CSC's. As little is known about the behavior of colon CSC's, this assay provided some insights into the proliferation patterns of these cells.

Prior to determining a characteristic real-time growth curve, the optimal seeding density of each cell type was determined in a titration assay. This is important since an excess of cells will result in rapid overgrowth, whilst a nominal cell number may negatively affect cell growth. From the preliminary study, the optimal number of cells needed to form a suitable growth curve was found to be 50 000 cells/ml for the CSC's and 25 000 cells/ml for the non-CSC's. These concentrations were then employed in subsequent experiments.

Following the determination of optimal cell seeding densities, real time cell impedance assays were carried out. The real-time proliferation curves generated showed distinct differences between DLD1 and HT29 cell lines. This was somewhat expected as all cell lines

have a distinct signature pattern and deviations from this would indicate stimulation, suppressed growth or even apoptosis. Notably, we report here a defined difference in the growth pattern of the CSC's (CD133+) as compared to their non-CSC (CD133-) counterparts. The non-CSC's grew more rapidly, reaching confluence in approximately 48 hours, while the CSC's required at least 72 hours. This differing growth pattern was reflected in the cells derived from both cell lines. These results are in accordance with the literature, where it is reported that stem cells generally have a slower proliferation rate in comparison to normal cells[99].

The cancer stem cell model suggests that these cells display similar characteristic features to normal stem cells, including entering the cell cycle infrequently. This is one of the biggest challenges therapeutically, since current therapies are designed to abolish rapidly cycling cells, rather than slow cycling CSC's, making the CSC's highly resistant[107]. The proliferation assay clearly displayed the slow cycling of CSC's expressing CD133 in comparison to non-CSC's.

7.4 STEM CELL MARKER EXPRESSION

After observing the morphological and proliferation properties of the isolated CSC's the expression of a number of key stem cell markers were evaluated in the CSC's and non-CSC's, using confocal microscopy. Apart from CD133, these included c-Myc, KLF4 and alkaline phosphatase, and their relevance is discussed below.

7.4.1 CD133

This marker was assessed both on the cell surface and cytoplasmically. Firstly CD133 was detected in non-permeabilised cells on the cell surface and subsequently within the cytoplasm of detergent permeabilised cells. In all instances, the CD133+ cells expressed more cell surface and cytoplasmic CD133 than the CD133- cells. From this analysis, it would seem that the CSC's express CD133 on their cell surface, whilst non-CSC's only express it intracellularly.

The CD133+ and CD133- permeabilized cells of both cell lines displayed cytoplasmic expression of CD133. Since CD133 is a secreted protein, following translation it would be processed through the endoplasmic reticulum, where it would probably undergo glycosylation, a step required for protein secretion onto the cell surface. The observed perinuclear association of CD133 may reflect its association with the trans-Golgi network, which is closely associated with the nucleus. Furthermore, the lack of cell surface CD133 in CD133- cells (non-permeabilized) from both cell lines may relate to a functional absence of secreted CD133.

To better elucidate the cellular localization of CD133, Z-stack analyses were performed to reflect CD133 expression in relation to the nuclei and cell membrane. These confirmed the confocal observations of cell surface CD133 on non-permeabilized CD133+ DLD1 and HT29 cells. Moreover, the nuclear association of CD133 was corroborated in permeabilized cells by co-localization of DAPI and Alexa Fluor 532 staining, producing a pink coloration.

It should however be noted here that some of the cells, (approximately 10%) in the negative fraction did express CD133. This may relate to the negative fraction being a heterogenous population of cells, containing a few cells that were able to dedifferentiate into CSC's. It is

also possible that the magnetic separation may not have been absolutely effective, allowing a few positive cells to be washed into the negative fraction.

The purity of the cell sample in the present study could have possibly been improved by performing an additional separation or passing it through the isolation column several more times. Such an approach has proven effective in other studies where CD133 was also used as a CSC marker. It was found that the CSC's accounted for a mere 2.5% of the original population by expressing the marker CD133 and these CSC's were isolated as using the same magnetic separation kit employed in this study[28].

From these results it can clearly be seen that a successful magnetic separation took place since selection was made based on the CD133 receptor. These microscopy images were captured after several weeks of growth in the selective CSC media. From this one can deduce that the cell surface expressed CD133 would be a fair indication of stemness of cancer cells.

7.4.2 c-Myc

The regulator gene c-Myc codes for a transcription factor that plays a key role in cell cycle progression, regulation of cell growth, differentiation and apoptosis[48]. Mutations in the gene may arise and in many cases results in the formation of cancer. The two cell lines chosen for this study, DLD1 and HT29, both express the *myc* oncogene (see Appendix A). Not only is this gene activated upon mitotic signals such as Shh, it is also a factor implicated in the production of human induced pluripotent stem cells[108]. c-Myc was selected in this study as a stem cell marker and its expression was evaluated using fluorescent microscopy.

7.4.3 KLF4

This marker which forms part of the KLF family of transcription factors plays a role in regulating various cellular processes including differentiation, proliferation and apoptosis. Furthermore it has been found to be a tumour suppressor in colorectal cancer[109]. Expression of this gene has also proven to be an accurate indicator of "stemness" in embryonic and mesenchymal stem cells[50]. Its capacity as being a factor for the generation of human induced pluripotent stem cells has also been demonstrated. It forms part of the group of genes which includes Oct3/4, SOX2, c-Myc, nanog, LIN28 and Glis1 all of which have been identified as

crucial transcriptional regulators involved in the induction process of human pluripotent stem cells[50]. For these reasons it was selected as a marker in this study to further characterize the isolated CSC's.

This was done by observing the levels of c-Myc and KLF4 expressed on the cell surface of CD133+ cells. It was found that the level of both markers was increased, (not significantly for c-Myc levels in DLD1 cells) in DLD1 and HT29 CD133+ cell lines in comparison to the CD133- counterparts. Selected CD133+ cells expressed c-Myc strongly but overall the expression of c-Myc was elevated in both the CD133+ fractions of the DLD1 and HT29 cell lines. This was to be expected since both markers are indicators for the presence of CSC's.

7.4.4 Alkaline phosphatase

Alkaline phosphatase has long been known as a stem cell marker whereby its presence in high levels provides an indication of pluripotency[51]. In humans four isoenzymes have been identified namely; intestinal alkaline phosphatase, placental alkaline phosphatase, germ cell alkaline phosphatase (expressed in primordial cells), and tissue non-specific alkaline phosphatase. Intestinal, placental and germ cell alkaline phosphatase are expressed by embryonic cells as well as carcinoma cells[110].

Like CD133 alkaline phosphatase is membrane bound and can therefore be identified on the cell surface of potential CSC's, however in some instances the enzyme is also secreted extracellularly. Of all the stem cell markers evaluated in this study, the most distinct difference was observed in alkaline phosphatase levels. The high expression of alkaline phosphatase in the CD133+ fractions of DLD1 and HT29 cells was found to be significantly higher in comparison to the CD133- fractions and further confirms the "stemness" of the CD133+ cells. Moreover, the expression of alkaline phosphatase indicates that the cells are pluripotent and undifferentiated. Overall, the over-expression of CD133 and other stem cell markers was visually apparent in the stem cell fractions of both cell lines, providing convincing evidence of the existence of a stem cell population. A definite isolation of CSC's had to be made in order to continue with further experiments in this study as a mixed population would not provide accurate results nor insight into the effects of CSC-targeted drugs.

7.5 THERAPEUTIC DEVELOPMENT

With the recent discovery and development of the cancer stem cell theory, researching possible therapeutics aimed at blocking the activation of this pathway could prove to be most valuable since CSC's seemingly display the same properties as their normal human stem cell counterparts and are regulated by the same signalling molecules[95]. Inhibiting the Shh pathway would result in minimal side effects due to its limited activation in adults. Furthermore a targeted therapeutic would avoid collateral damage to other normal tissue. Various drugs have been developed and affect different components of the Shh pathway including the Hh ligand itself, the surface proteins Ptch and Smo, as well as the Gli transcription factors.

The target of the compound cyclopamine is Smo and the semi-synthetic derivative of it Saridegib (IPI-926), is currently available for the treatment of haematologic malignancies. Cyclopamine is appealing as a cancer therapeutic since it is a natural compound and rather well established, however, synthesis of it in large enough quantities has proven to be challenging. A further drawback is its relatively low affinity for Smo[111,112]. Although Saridegib has an extended half-life, it is only effective in the treatment of a subset of Hh dependent tumours. A Phase II trial using Saridegib in conjunction with gemcitabine for the treatment of pancreatic cancer was recently stopped due to the drug showing limited efficacy[113]. Other analogues of cyclopamine including KAAD-Cyclopamine and HhAntag-691 have shown an increased efficiency in comparison to cyclopamine but are still under investigation and have not been proven safe for clinical trials yet [59,114]. In order for cyclopamine and these other analogues that target Smo to be effective in the treatment of cancer certain criteria must be met. In particular, the cancer type must be dependent on the activation of the Hh ligand or induced by mutations in the receptors Ptch and Smo. Once the aforementioned criteria have been met, it is essential to develop a mechanistic understanding of Smo and its interaction with these compounds. This research made use of Smo inhibitors in the form of the small molecules cyclopamine and the analogue SANT-2 which are believed to be potent antagonists of the Hh pathway.

7.6 Assessment of physiological properties of CSC's

As mentioned previously, cancer cells display distinct characteristics in comparison to normal cells which allow them to thrive and grow uncontrollably (Figure 53). A key hallmark, which is a particular focus of this study, is the ability to invade surrounding tissue and metastasize. The ability of tumorigenic cells to travel to distant sites and form secondary tumours are the cause of 90% of cancer-related deaths in humans[115].

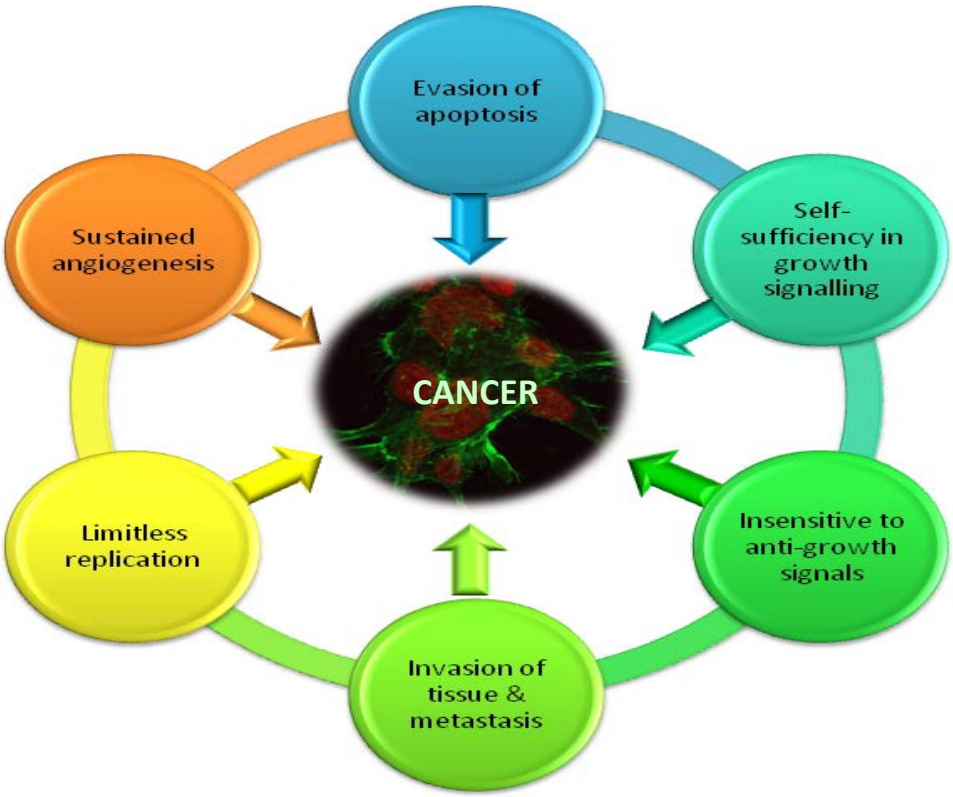


Figure 53: Aquired capabilities of cancer; developed through mutations, activation of oncogenes or silencing tumour suppressor genes (adapted from Figure 1[96]).

It is believed that CSC's have an enhanced ability to invade surrounding tissue and are highly metastatic[116]. Furthermore cells isolated from an invasive pancreatic tumour were found to express CD133, classified as CSC's, and determined the metastatic phenotype of the individual tumour[104]. In this study CSC's isolated from the two colorectal cancer cell lines DLD1 and HT29 were subjected to various assays analysing their ability to adhere (a vital step in metastasis, see Figure 54), to invade, and migrate *in vitro* and key findings are described below.

7.6.1 Cell adhesion

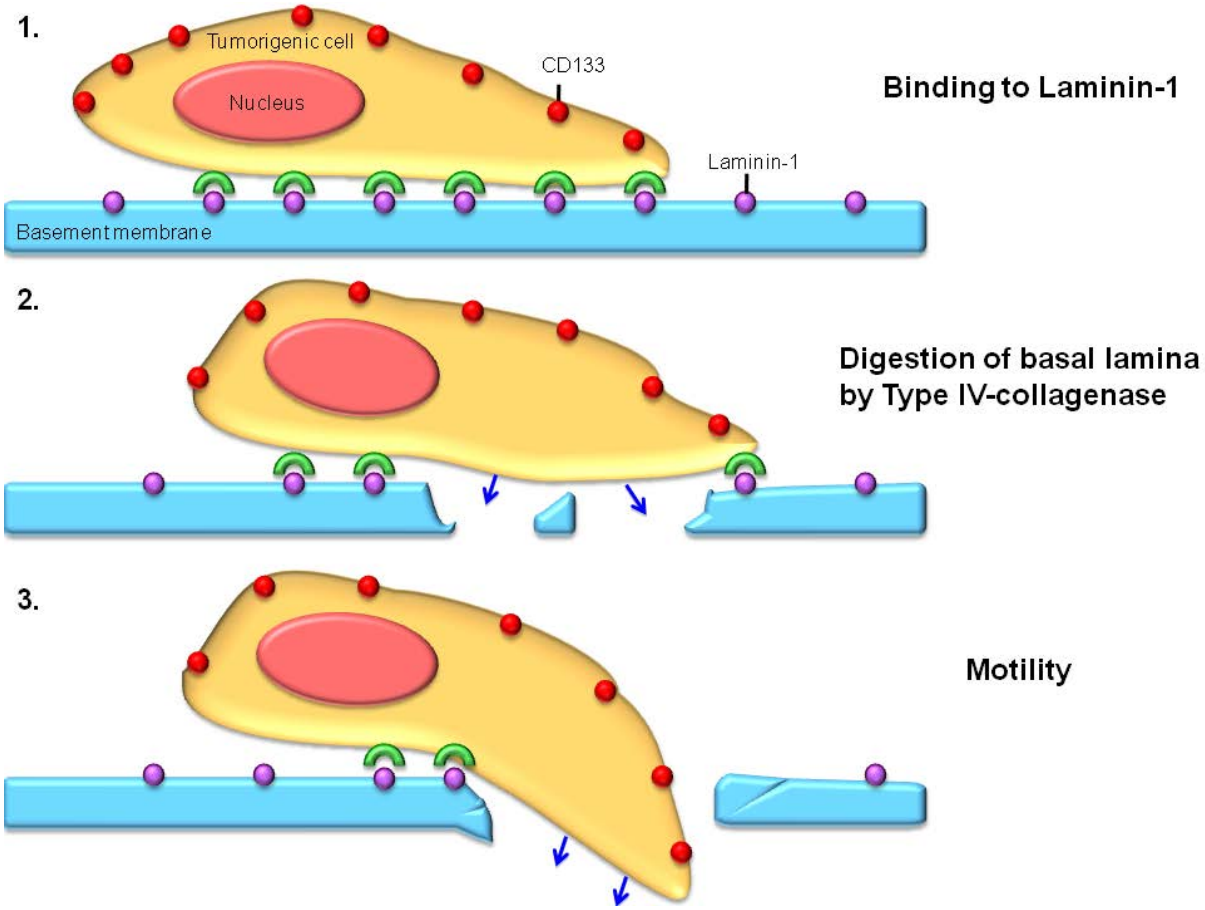


Figure 54: Schematic diagram illustrating initial cell adhesion, invasion, and Type IV-collagenase ECM degradation allowing for cell migration. 1.) Attachment of CD133 expressing tumorigenic cell to Laminin-1 on the basement membrane. 2.) Digestion of the basal lamina by Type IV-collagenase secretion induced upon attachment, 3.) Degradation of the basement membrane allows for tumorigenic cell motility into the blood stream (modified from graphical abstract, A. Omar, et al 2012[98]).

The positively identified isolated CSC's were subjected to various forms of testing with the inclusion of the small molecule inhibitors. Their ability to adhere to Geltrex™ (components of a Laminin ECM) was evaluated as this was an important step towards the elucidation of CSC behaviour and their capacity to metastasize. Observing the effects that cyclopamine would have on the adhesive and invasive potential of CSC's was vital since the Shh pathway has been found to play a major role in metastasis. The first parameter to be assessed was cell adhesion to a laminin based extracellular matrix. The activation of the cell adhesion pathway is an important step in the mesenchymal transition, as well as in the upregulation of metastasis-associated genes such as *SNAIL*[95]. By quantifying the ability of CSC to adhere with the use of an adhesion assay, and juxtaposing these results with those of non-CSC's it was possible to see that although non-CSC are capable of successfully adhering to a

Geltrex™ coated surface, CSC's are even more proficient at this supporting notion that CSC's have an enhanced adhesion potential[117]. A significantly increased adhesion potential was noted in the CD133+ fractions of both the HT29 and DLD1 cell lines in comparison to their negative fractions. This reveals that the CSC's have an enhanced ability to adhere, a key step in the process of metastasis. Small molecule inhibitors were employed to assess the role of the Shh pathway in the adhesive ability displayed by the CSC's. Upon the application of 2μM cyclopamine a marked reduction in the adhesion potential was observed in both HT29 CSC's and DLD1 CSC's in comparison to untreated cells. These results are in agreement with previous studies performed within the Oncology Laboratory and unpublished data indicated that at a concentration 2μM metastatic behaviour was inhibited and concentrations above this induced apoptosis. The effect noted, that is blockage of the Shh pathway, with this concentration of cyclopamine is expected and has been observed in *in vivo* studies using mice[118]. When SANT-2 was applied at this same concentration no reduction in adhesion potential was found. Subsequently, when a dose dependency assay was performed, SANT-2 was found to be effective only in impeding adhesion at a concentration of 10μM or higher. It appears that cyclopamine had a greater inhibitory effect on the DLD1 cell line while SANT-2 was more effective in hindering adhesion in the HT29 cell line. The reason for this while unknown, it was however noted that slightly elevated levels of CD133 were detected in the DLD1 cell line in comparison to HT29 cells and this could possibly be related. This would suggest that therapeutics targeting CD133 would be highly effective in the treatment of CSC's. The cyclopamine analogue tomatidine had no effect in adhesion assays.

7.6.2 Cell invasion

In order to further understand the effect cyclopamine and the other small molecules would have on the process of metastasis, *in vitro* invasion assays were performed. Following adhesion to cell membranes *in vivo,* neoplastic cells require the ability to invade surrounding tissue or enter the blood or lymphatic system. Once attached to a target basement membrane, this is enzymatically digested by Type IV-collagenase, allowing entry into the circulatory system, migration and finally a metastatic (secondary) tumour is then established by attachment of migrating cells to the blood vessel once again[119]. Therefore, as invasion assays mimic this process, they provide an indication of the ability of cells to pass through an extracellular matrix (Laminin-1) coated membrane similar, to that of the basal lamina. CSC's from both the DLD1 and HT29 cell lines migrated through the matrix coated membrane

attaching to the underside. However, the inclusion of cyclopamine (2μM) or SANT-2 in the assay, significantly hindered cell invasion resulting in far fewer numbers of cells traversing through the membrane. SANT-2 (20μM) treatment effected the most significant reduction in invasive potential in the HT29 derived stem cells. The cyclopamine (control) analogue, tomatidine, as expected had no significant effect on cell invasion. These findings concur with the adhesion assays, since cell adhesion is a pre-requisite step for invasion to occur. In this regard, a positive correlation between adhesion and invasion has been reported in previous studies using breast, lung, cervix, prostate and colon cancer cell lines[98]. Moreover, on further analysis, we report here a positive correlation between the effects of cyclopamine and SANT-2 on limiting both cell adhesion and invasion (note a positive Pearson's correlation co-efficient of 0.43 and 0.924 was calculated for cyclopamine and SANT-2 respectively, see results section 6.10). It follows that in most instances a decreased ability of cells to adhere to matrix molecules correlates with a diminished invasive potential. This would have implications in therapeutic efficacy since drugs targeting the adhesion of neoplastic cells could result in them having a decreased ability to invade surrounding tissue and migrate.

7.6.3 Cell migration

As mentioned, following attachment and invasion across the basement membrane neoplastic cells then need to invade surrounding tissue, adhere again, and proliferate to form a secondary tumour. This process involves the ability of cells to migrate and undergo EMT. For successful motility to occur cellular signalling networks are activated and in turn induce morphological changes[120], whereby cells lose their epithelial characteristics and assume mesenchymal-like features such as their expression of E-cadherin. These signalling networks encompass various molecules and receptors that may respond to stimuli, or may be affected by inhibitors; and can be assessed *in vitro* using cell migration or scratch assays[120]. In a study using colorectal CSC's it was found that the biomarker CD44v6 was over-expressed and played a pivotal role in migration and the formation of metastatic tumours. The expression of CD44v6 was stimulated by cytokines and thereby the Wnt/β-catenin pathway was activated. Furthermore, inhibition of this expression resulted in a decreased migration and metastatic growth, and CD44v6 was shown to be both a functional biomarker as well as therapeutic target[121].

In assessing the inhibition of the Hedgehog pathway in the present study, cyclopamine effected a limited inhibition of cell migration inclusive of up to 6 hours in both DLD1 and HT29 cells, after which migration appeared to reflect that of the controls. Interestingly, the cyclopamine caused an initial widening of the gap (in the first 4 hours), perhaps caused by the induction of apoptosis. This finding concurs with studies done using cyclopamine whereby cell proliferation was arrested and possibly apoptosis induced[73,81]. In contrast, SANT- 2 was highly effective in retarding cell migration over the full 24 hour period of treatment.

From these results one can deduce that both cyclopamine and SANT-2 were able to disrupt pathways involved in the migration of colon CSC's and their ability to populate a cell free zone, however the negative effect of cyclopamine appeared to be neutralized after 6 hours perhaps due to a shorter half-life (cyclopamine half-life 1.1 +/- 0.1 h). Another possibility could be that the drug becomes ineffective as Smo may undergo mutations that allow for the activation of the Shh pathway by acquired resistance (Figure 55). There are reports of mutations occurring in Smo, rendering Smo inhibition ineffective. In this regard, Smo mutation has been noted with use of the Smo inhibitor GDC-0449 whereby initial tumour regression was seen in the patient, followed by recurrence of metastatic tumours due to mutations in Smo resulting in drug resistance[122]. Pathway-specific resistance that may develop during Smo antagonist treatment could occur at the site of Smo, whereby the drug is unable to interact with Smo and therefore Hh activation results in tumour progression[123]. The potential of Hh pathway inhibitors is evident in this same study as the patients' tumours were unresponsive to conventional therapeutic agents[124]. Other studies have shown that cyclopamine acts to stimulate an accumulation of Smo within the cell's primary cilium and upon drug removal, continuous activation of the pathway could result[93]. This could explain the lack of inhibitory effect of cyclopamine reported here, following 6 hours of treatment in the migration/scratch assay.

A correlation between a hindered adhesion of CD133+ CSC's and a decreased migration was calculated as being -0.429 and 0.502 for cyclopamine and SANT-2 respectively (see Results section 6.10). This would suggest that SANT-2 is effective in impeding cell adhesion and thereby a decreased migratory ability results; however with the application of cyclopamine it may decrease adhesion but not necessarily migration, hence the negative correlation.

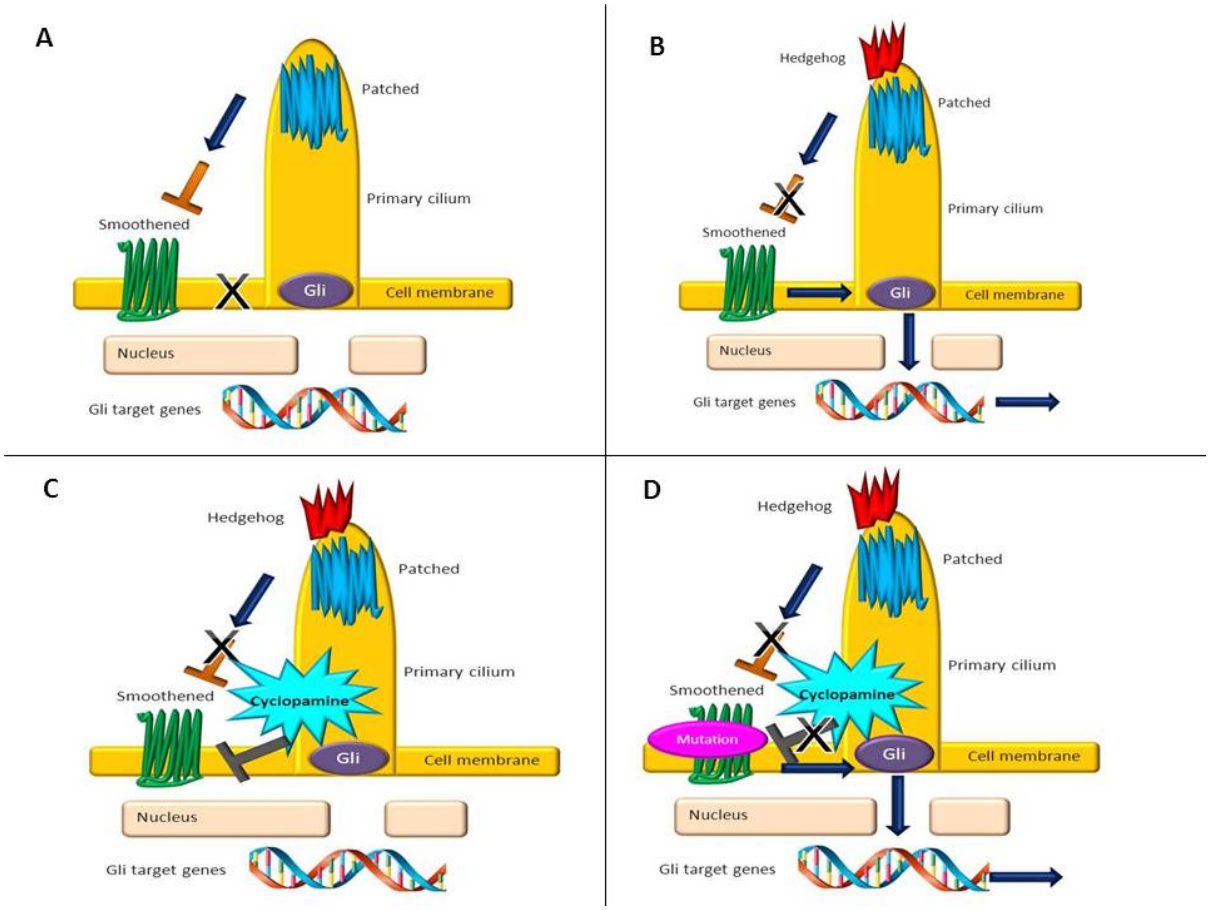


Figure 55: Shh pathway inhibition and mutations. (A) Diagram illustrating an inactive Hh pathway whereby Ptch inhibits Smo. (B) The mechanism by which the Shh pathway is reactivated: following the binding of the Hh ligand to Ptch, this suppression is then inhibited allowing for the activation of downstream targets through the Gli transcription factors. (C) With the addition of the Smo antagonist cyclopamine Hh activation is suppressed and tumour progression is retarded. (D) Smo point mutations can occur and nullify the effect of Smo antagonists, Hh activation continues and tumour growth results due to the expression of Gli target genes (own figure).

7.6.4 Inhibition of Shh; relationship to CD133 expression

Finally the potential effect of Shh inhibition was queried in relation to the expression of the cancer stem cell marker CD133. This is of some importance with a view to targeting CSC's. Notably here, with cyclopamine treatment, the cell surface expression of Shh significantly decreased in comparison to the untreated control. However, there was no apparent reduction in the expression of cell membrane associated CD133, suggesting that this particular stem cell marker is not necessarily influenced by the Hh pathway. From this, it would seem that cyclopamine possibly has no effect on the ability of CSC's to express CD133.

7.7 FUTURE DIRECTIONS

This research aimed at evaluating a targeted therapeutic against the Shh pathway in colorectal CSC's. Although Shh inhibition had no direct effect on CD133 expression, the neoplastic properties of the CD133+ CSC's were inhibited. This could suggest that another stem cell pathway or a related signalling pathway was affected by cyclopamine and SANT-2 treatment. Under normal circumstances this pathway is essential in embryonic development. After birth however the pathway remains active at sites of continuous renewal for example in the gut epithelium and when repair of tissue is required[95]. An organ where this would be of concern would be the brain and since cyclopamine and other small molecules are able to cross the blood-brain barrier the consequences of the drug hampering the Shh pathway in neural tissue could be detrimental since regular stem cell renewal is vital. In studies where the growth of medullablastomas and gliomas was stunted in mice following treatment with cyclopamine, no notable side effects were documented; however minor cognitive defects could not be analyzed in mice[114]. The possibility that cyclopamine reduces the number of normal stem cells is rather likely and this side effect could become apparent when regeneration is required. However, localized and limited treatment with the drug could leave quiescent stem cells unaffected and allow for them to once more demonstrate their ability to self-renew and induce tissue regeneration. Other challenges with the application/use of the drug could include the increased intestinal epithelial proliferation that occurs in neonates and the possible side effect of tumour formation resulting from this[125]. This as well as the problems that could occur during injury, such as the inability to repair damaged tissue (particularly in the colon), are issues that must be given careful consideration and further experimentation is required in order to rule these out as harmful side effects.

7.8 OUTLOOK

The therapeutic potential of cyclopamine and its analogues for the treatment of colon CSC's is clearly evident but a better understanding of the genes expressed would certainly provide direction regarding drug limitations and how best to enhance the potential anti-metastatic effects. In this regard, it would be of particular interest to investigate the Shh pathway with respect to EMT, since as reported in the present study, properties of cell adhesion, migration and invasion were specifically implicated with the colon CSC population. A sensitive assay would be gene expression in an array format, to detect the up-regulation and down-regulation of pathway specific genes. This would need to be done together with protein expression studies, since changes in mRNA transcript levels don't necessarily equate to increased pathway activity. Together, these tools would permit for a finer evaluation of the small molecule inhibitors and their role/s in the Shh pathway. Recent studies have shown that cyclopamine successfully down-regulated the expression of pluripotent markers, EMT markers and Shh downstream markers in the colon cancer cell line HCT-116[126]. The Shh pathway could also be inhibited using anti-Hh antibodies which block the binding of the Hh ligand and therefore do not involve the impedance of Smo. Although a promising tool for the treatment of many cancer types, Smo antagonists are not always effective since the activation of the Hh pathway in certain cancers occurs downstream of Smo. The only way to successfully prevent disease progression in all Hh pathway dependent tumours would be to develop therapeutics that focus on the impairment of the downstream Gli transcription factors. Cases where pathway activation occurs downstream of Smo and cyclopamine would no longer be an effective therapeutic agent, other strategies such as SuFu mimetics and GliRNAi could be employed instead since their effects are downstream of Smo [95]. These strategies would result in an antagonistic effect on the Hh pathway and block Gli translocation.

8. REFERENCES

1 Ballinger, A. B. & Anggiansah, C. Colorectal cancer. *British Medical Journal* **335**, 715-718, doi:10.1136/bmj.39321.527384.BE (2007).

2 Mqoqi N, K. P., Sitas F, Jula M. Johannesburg: National Cancer Registry of South Africa, National Health Laboratory Service. *Cancer in South Africa, 1998 - 1999* (2004).

3 Parkin, D. M., Bray, F., Ferlay, J. & Jemal, A. Cancer in Africa 2012. *Cancer epidemiology, biomarkers & prevention : a publication of the American Association for Cancer Research, cosponsored by the American Society of Preventive Oncology* **23**, 953-966, doi:10.1158/1055-9965.EPI-14-0281 (2014).

4 Han-Shiang, C. Curative resection of colorectal adenocarcinoma: multivariate analysis of 5-year follow-up. *World journal of surgery* **23**, 1301-1306 (1999).

5 Asaad, S. M., Jubelirer, S. J. & Welch, C. A. Prognostic indicators for stage II (Dukes' stage B) adenocarcinoma of the colon. *West Virginia Medical Journal* **101**, 210-213 (2005).

6 Alici, S., Aykan, N. F., Sakar, B., Bulutlar, G., Kaytan, E. & Topuz, E. Colorectal cancer in young patients: characteristics and outcome. *Tohoku Journal of Experimental Medicine* **199**, 85-93 (2003).

7 Cunningham, D., Atkin, W., Lenz, H. J., Lynch, H. T., Minsky, B., Nordlinger, B. & Starling, N. Colorectal cancer. *Lancet* **375**, 1030-1047, doi:10.1016/S0140-6736(10)60353-4 (2010).

8 Watson, A. J. & Collins, P. D. Colon cancer: a civilization disorder. *Digestive Diseases* **29**, 222-228, doi:10.1159/000323926 (2011).

9 Akkoca, A. N., Yanik, S., Ozdemir, Z. T., Cihan, F. G., Sayar, S., Cincin, T. G., Cam, A. & Ozer, C. TNM and Modified Dukes staging along with the demographic characteristics of patients with colorectal carcinoma. *International Journal of Clinical and Experimental Medicine* **7**, 2828-2835 (2014).

10 Land, H., Parada, L. F. & Weinberg, R. A. Cellular oncogenes and multistep carcinogenesis. *Science* **222**, 771-778 (1983).

11 Barbacid, M. ras genes. *AnnualReview of Biochemistry* **56**, 779-827, doi:10.1146/annurev.bi.56.070187.004023 (1987).

12 Bodmer, W. F., Bailey, C. J., Bodmer, J., Bussey, H. J., Ellis, A., Gorman, P., Lucibello, F. C., Murday, V. A., Rider, S. H., Scambler, P. & et al. Localization of the gene for familial adenomatous polyposis on chromosome 5. *Nature* **328**, 614-616, doi:10.1038/328614a0 (1987).

13 Muleris, M., Salmon, R. J., Zafrani, B., Girodet, J. & Dutrillaux, B. Consistent deficiencies of chromosome 18 and of the short arm of chromosome 17 in eleven cases of human large bowel cancer: a possible recessive determinism. *Annales de Genetique* **28**, 206-213 (1985).

14 Fearon, E. R., Hamilton, S. R. & Vogelstein, B. Clonal analysis of human colorectal tumors. *Science* **238**, 193-197 (1987).

15 Vogelstein, B., Fearon, E. R., Hamilton, S. R., Kern, S. E., Preisinger, A. C., Leppert, M., Nakamura, Y., White, R., Smits, A. M. & Bos, J. L. Genetic alterations during colorectal-tumor development. *The New England Journal of Medicine* **319**, 525-532, doi:10.1056/NEJM198809013190901 (1988).

16 Morson, B. President's address. The polyp-cancer sequence in the large bowel. *Proceedings of the Royal Society of Medicine* **67**, 451-457 (1974).

17 Christine A, L. D., Elizabeth M. Epithelial neoplasms of the colorectum. *Gastrointestinal and Liver Pathology*, 367-394 (2005).

18 Guinn, B. A. & Mulherkar, R. International progress in cancer gene therapy. *Cancer Gene Therapy* **15**, 765-775, doi:10.1038/cgt.2008.66 (2008).
19 Shay, J. W. Meeting report: the role of telomeres and telomerase in cancer. *Cancer Research* **65**, 3513-3517, doi:10.1158/0008-5472.CAN-05-0728 (2005).
20 Dalerba, P., Dylla, S. J., Park, I. K., Liu, R., Wang, X., Cho, R. W., Hoey, T., Gurney, A., Huang, E. H., Simeone, D. M., Shelton, A. A., Parmiani, G., Castelli, C. & Clarke, M. F. Phenotypic characterization of human colorectal cancer stem cells. *Proceedings of the National Academy of Sciences of the United States of America* **104**, 10158-10163, doi:10.1073/pnas.0703478104 (2007).
21 Reya, T., Morrison, S. J., Clarke, M. F. & Weissman, I. L. Stem cells, cancer, and cancer stem cells. *Nature* **414**, 105-111, doi:10.1038/35102167 (2001).
22 Dalerba, P., Cho, R. W. & Clarke, M. F. Cancer stem cells: models and concepts. *Annual Review of Medicine* **58**, 267-284, doi:10.1146/annurev.med.58.062105.204854 (2007).
23 Jordan, C. T., Guzman, M. L. & Noble, M. Cancer stem cells. *The New England Journal of Medicine* **355**, 1253-1261, doi:10.1056/NEJMra061808 (2006).
24 Al-Hajj, M., Wicha, M. S., Benito-Hernandez, A., Morrison, S. J. & Clarke, M. F. Prospective identification of tumorigenic breast cancer cells. *Proceedings of the National Academy of Sciences of the United States of America* **100**, 3983-3988, doi:10.1073/pnas.0530291100 (2003).
25 Singh, S. K., Hawkins, C., Clarke, I. D., Squire, J. A., Bayani, J., Hide, T., Henkelman, R. M., Cusimano, M. D. & Dirks, P. B. Identification of human brain tumour initiating cells. *Nature* **432**, 396-401, doi:10.1038/nature03128 (2004).
26 Galli, R., Binda, E., Orfanelli, U., Cipelletti, B., Gritti, A., De Vitis, S., Fiocco, R., Foroni, C., Dimeco, F. & Vescovi, A. Isolation and characterization of tumorigenic, stem-like neural precursors from human glioblastoma. *Cancer Research* **64**, 7011-7021, doi:10.1158/0008-5472.CAN-04-1364 (2004).
27 O'Brien, C. A., Pollett, A., Gallinger, S. & Dick, J. E. A human colon cancer cell capable of initiating tumour growth in immunodeficient mice. *Nature* **445**, 106-110, doi:10.1038/nature05372 (2007).
28 Ricci-Vitiani, L., Lombardi, D. G., Pilozzi, E., Biffoni, M., Todaro, M., Peschle, C. & De Maria, R. Identification and expansion of human colon-cancer-initiating cells. *Nature* **445**, 111-115, doi:10.1038/nature05384 (2007).
29 Prince, M. E., Sivanandan, R., Kaczorowski, A., Wolf, G. T., Kaplan, M. J., Dalerba, P., Weissman, I. L., Clarke, M. F. & Ailles, L. E. Identification of a subpopulation of cells with cancer stem cell properties in head and neck squamous cell carcinoma. *Proceedings of the National Academy of Sciences of the United States of America* **104**, 973-978, doi:10.1073/pnas.0610117104 (2007).
30 Gou, S., Liu, T., Wang, C., Yin, T., Li, K., Yang, M. & Zhou, J. Establishment of clonal colony-forming assay for propagation of pancreatic cancer cells with stem cell properties. *Pancreas* **34**, 429-435, doi:10.1097/MPA.0b013e318033f9f4 (2007).
31 Gisina, A. M., Lupatov, A. Y., Karalkin, P. A., Mainovskaya, O. A., Petrov, L. O., Sidorov, D. V., Frank, G. A. & Yarygin, K. N. Subpopulation of colorectal adenocarcinoma cells co-expressing CD133 and cancer stem cells markers of other tumors. *Bulletin of Experimental Biology and Medicine* **152**, 739-742 (2012).
32 Baccelli, I. & Trumpp, A. The evolving concept of cancer and metastasis stem cells. *The Journal of Cell Biology* **198**, 281-293, doi:10.1083/jcb.201202014 (2012).
33 Islam, F., Gopalan, V., Smith, R. A. & Lam, A. K. Translational potential of cancer stem cells: A review of the detection of cancer stem cells and their roles in cancer

recurrence and cancer treatment. *Experimental Cell Research* **335**, 135-147, doi:10.1016/j.yexcr.2015.04.018 (2015).
34 Visvader, J. E. & Lindeman, G. J. Cancer stem cells: current status and evolving complexities. *Cell Stem Cell* **10**, 717-728, doi:10.1016/j.stem.2012.05.007 (2012).
35 Iinuma, H., Watanabe, T., Mimori, K., Adachi, M., Hayashi, N., Tamura, J., Matsuda, K., Fukushima, R., Okinaga, K., Sasako, M. & Mori, M. Clinical significance of circulating tumor cells, including cancer stem-like cells, in peripheral blood for recurrence and prognosis in patients with Dukes' stage B and C colorectal cancer. *Journal of Clinical Oncology: Official Journal of the American Society of Clinical Oncology* **29**, 1547-1555, doi:10.1200/JCO.2010.30.5151 (2011).
36 Corbeil, D., Roper, K., Hellwig, A., Tavian, M., Miraglia, S., Watt, S. M., Simmons, P. J., Peault, B., Buck, D. W. & Huttner, W. B. The human AC133 hematopoietic stem cell antigen is also expressed in epithelial cells and targeted to plasma membrane protrusions. *The Journal of BiologicalChemistry* **275**, 5512-5520 (2000).
37 Horn, P. A., Tesch, H., Staib, P., Kube, D., Diehl, V. & Voliotis, D. Expression of AC133, a novel hematopoietic precursor antigen, on acute myeloid leukemia cells. *Blood* **93**, 1435-1437 (1999).
38 Sanai, N., Alvarez-Buylla, A. & Berger, M. S. Neural stem cells and the origin of gliomas. *The New England Journal of Medicine* **353**, 811-822, doi:10.1056/NEJMra043666 (2005).
39 Singh, S. K., Clarke, I. D., Terasaki, M., Bonn, V. E., Hawkins, C., Squire, J. & Dirks, P. B. Identification of a cancer stem cell in human brain tumors. *Cancer Research* **63**, 5821-5828 (2003).
40 Shmelkov, S. V., St Clair, R., Lyden, D. & Rafii, S. AC133/CD133/Prominin-1. *The International Journal of Biochemistry and Cell Biology* **37**, 715-719, doi:10.1016/j.biocel.2004.08.010 (2005).
41 Mizrak, D., Brittan, M. & Alison, M. R. CD133: molecule of the moment. *The Journal of Pathology* **214**, 3-9, doi:10.1002/path.2283 (2008).
42 Marzesco, A. M. Prominin-1-containing membrane vesicles: origins, formation, and utility. *Advances in Experimental Medicine and Biology* **777**, 41-54, doi:10.1007/978-1-4614-5894-4_3 (2013).
43 Roper, K., Corbeil, D. & Huttner, W. B. Retention of prominin in microvilli reveals distinct cholesterol-based lipid micro-domains in the apical plasma membrane. *Nature Cell Biology* **2**, 582-592, doi:10.1038/35023524 (2000).
44 Mizrak, D., Brittan, M. & Alison, M. CD133: molecule of the moment. *The Journal of Pathology* **214**, 3-9, doi:10.1002/path.2283 (2008).
45 Corbeil, D., Roper, K., Fargeas, C. A., Joester, A. & Huttner, W. B. Prominin: a story of cholesterol, plasma membrane protrusions and human pathology. *Traffic* **2**, 82-91 (2001).
46 Irollo, E. & Pirozzi, G. CD133: to be or not to be, is this the real question? *American Journal of Translational Research* **5**, 563-581 (2013).
47 Shmelkov, S. V., Butler, J. M., Hooper, A. T., Hormigo, A., Kushner, J., Milde, T., St Clair, R., Baljevic, M., White, I., Jin, D. K., Chadburn, A., Murphy, A. J., Valenzuela, D. M., Gale, N. W., Thurston, G., Yancopoulos, G. D., D'Angelica, M., Kemeny, N., Lyden, D. & Rafii, S. CD133 expression is not restricted to stem cells, and both CD133+ and CD133- metastatic colon cancer cells initiate tumors. *The Journal of Clinical Investigation* **118**, 2111-2120, doi:10.1172/JCI34401 (2008).
48 Denis, N., Kitzis, A., Kruh, J., Dautry, F. & Corcos, D. Stimulation of methotrexate resistance and dihydrofolate reductase gene amplification by c-myc. *Oncogene* **6**, 1453-1457 (1991).

49 Kumar, S. M., Liu, S., Lu, H., Zhang, H., Zhang, P. J., Gimotty, P. A., Guerra, M., Guo, W. & Xu, X. Acquired cancer stem cell phenotypes through Oct4-mediated dedifferentiation. *Oncogene*, doi:10.1038/onc.2011.656 (2012).
50 Takahashi, K., Tanabe, K., Ohnuki, M., Narita, M., Ichisaka, T., Tomoda, K. & Yamanaka, S. Induction of pluripotent stem cells from adult human fibroblasts by defined factors. *Cell* **131**, 861-872, doi:10.1016/j.cell.2007.11.019 (2007).
51 *Appendix E: Stem Cell Markers.* , Date accessed: 10/06/2015 <http://stemcells.nih.gov/info/scireport/pages/appendixe.aspx> (2009).
52 Reubinoff, B. E., Pera, M. F., Fong, C. Y., Trounson, A. & Bongso, A. Embryonic stem cell lines from human blastocysts: somatic differentiation in vitro. *Nature Biotechnology* **18**, 399-404, doi:10.1038/74447 (2000).
53 Fang, D., Nguyen, T. K., Leishear, K., Finko, R., Kulp, A. N., Hotz, S., Van Belle, P. A., Xu, X., Elder, D. E. & Herlyn, M. A tumorigenic subpopulation with stem cell properties in melanomas. *Cancer Research* **65**, 9328-9337, doi:10.1158/0008-5472.CAN-05-1343 (2005).
54 Bapat, S. A., Mali, A. M., Koppikar, C. B. & Kurrey, N. K. Stem and progenitor-like cells contribute to the aggressive behavior of human epithelial ovarian cancer. *Cancer Research* **65**, 3025-3029, doi:10.1158/0008-5472.CAN-04-3931 (2005).
55 Rubin, L. L. & de Sauvage, F. J. Targeting the Hedgehog pathway in cancer. *Nature Reviews. Drug Discovery* **5**, 1026-1033, doi:10.1038/nrd2086 (2006).
56 Ingham, P. W., Nakano, Y. & Seger, C. Mechanisms and functions of Hedgehog signalling across the metazoa. *Nature Reviews. Genetics* **12**, 393-406, doi:10.1038/nrg2984 (2011).
57 Scales, S. J. & de Sauvage, F. J. Mechanisms of Hedgehog pathway activation in cancer and implications for therapy. *Trends in Pharmacological Sciences* **30**, 303-312, doi:10.1016/j.tips.2009.03.007 (2009).
58 Nielsen, C. M., Williams, J., van den Brink, G. R., Lauwers, G. Y. & Roberts, D. J. Hh pathway expression in human gut tissues and in inflammatory gut diseases. *Laboratory Investigation* **84**, 1631-1642, doi:10.1038/labinvest.3700197 (2004).
59 Taipale, J., Chen, J. K., Cooper, M. K., Wang, B., Mann, R. K., Milenkovic, L., Scott, M. P. & Beachy, P. A. Effects of oncogenic mutations in Smoothened and Patched can be reversed by cyclopamine. *Nature* **406**, 1005-1009, doi:10.1038/35023008 (2000).
60 Goodrich, L. V. & Scott, M. P. Hedgehog and patched in neural development and disease. *Neuron* **21**, 1243-1257 (1998).
61 Ingham, P. W. Transducing Hedgehog: the story so far. *The EMBO Journal* **17**, 3505-3511, doi:10.1093/emboj/17.13.3505 (1998).
62 Bai, R., Zhao, H., Zhang, X. & Du, S. Characterization of sonic hedgehog inhibition in gastric carcinoma cells. *Oncology Letters* **7**, 1381-1384, doi:10.3892/ol.2014.1964 (2014).
63 Gialmanidis, I. P., Bravou, V., Amanetopoulou, S. G., Varakis, J., Kourea, H. & Papadaki, H. Overexpression of hedgehog pathway molecules and FOXM1 in non-small cell lung carcinomas. *Lung Cancer* **66**, 64-74, doi:10.1016/j.lungcan.2009.01.007 (2009).
64 Watkins, D. N., Berman, D. M., Burkholder, S. G., Wang, B., Beachy, P. A. & Baylin, S. B. Hedgehog signalling within airway epithelial progenitors and in small-cell lung cancer. *Nature* **422**, 313-317, doi:10.1038/nature01493 (2003).
65 Liao, X., Siu, M. K., Au, C. W., Wong, E. S., Chan, H. Y., Ip, P. P., Ngan, H. Y. & Cheung, A. N. Aberrant activation of hedgehog signaling pathway in ovarian cancers:

effect on prognosis, cell invasion and differentiation. *Carcinogenesis* **30**, 131-140, doi:10.1093/carcin/bgn230 (2009).
66 Karhadkar, S. S., Bova, G. S., Abdallah, N., Dhara, S., Gardner, D., Maitra, A., Isaacs, J. T., Berman, D. M. & Beachy, P. A. Hedgehog signalling in prostate regeneration, neoplasia and metastasis. *Nature* **431**, 707-712, doi:10.1038/nature02962 (2004).
67 ten Haaf, A., Bektas, N., von Serenyi, S., Losen, I., Arweiler, E. C., Hartmann, A., Knuchel, R. & Dahl, E. Expression of the glioma-associated oncogene homolog (GLI) 1 in human breast cancer is associated with unfavourable overall survival. *BMC Cancer* **9**, 298, doi:10.1186/1471-2407-9-298 (2009).
68 Feng, Y. Z., Shiozawa, T., Miyamoto, T., Kashima, H., Kurai, M., Suzuki, A., Ying-Song, J. & Konishi, I. Overexpression of hedgehog signaling molecules and its involvement in the proliferation of endometrial carcinoma cells. *Clinical Cancer Research* **13**, 1389-1398, doi:10.1158/1078-0432.CCR-06-1407 (2007).
69 Daya-Grosjean, L. & Couve-Privat, S. Sonic hedgehog signaling in basal cell carcinomas. *Cancer Letters* **225**, 181-192, doi:10.1016/j.canlet.2004.10.003 (2005).
70 Berman, D. M., Karhadkar, S. S., Maitra, A., Montes De Oca, R., Gerstenblith, M. R., Briggs, K., Parker, A. R., Shimada, Y., Eshleman, J. R., Watkins, D. N. & Beachy, P. A. Widespread requirement for Hedgehog ligand stimulation in growth of digestive tract tumours. *Nature* **425**, 846-851, doi:10.1038/nature01972 (2003).
71 Mori, Y., Okumura, T., Tsunoda, S., Sakai, Y. & Shimada, Y. Gli-1 expression is associated with lymph node metastasis and tumor progression in esophageal squamous cell carcinoma. *Oncology* **70**, 378-389, doi:10.1159/000098111 (2006).
72 Qualtrough, D., Buda, A., Gaffield, W., Williams, A. C. & Paraskeva, C. Hedgehog signalling in colorectal tumour cells: induction of apoptosis with cyclopamine treatment. *International Journal of Cancer* **110**, 831-837, doi:10.1002/ijc.20227 (2004).
73 Thayer, S. P., di Magliano, M. P., Heiser, P. W., Nielsen, C. M., Roberts, D. J., Lauwers, G. Y., Qi, Y. P., Gysin, S., Fernandez-del Castillo, C., Yajnik, V., Antoniu, B., McMahon, M., Warshaw, A. L. & Hebrok, M. Hedgehog is an early and late mediator of pancreatic cancer tumorigenesis. *Nature* **425**, 851-856, doi:10.1038/nature02009 (2003).
74 Yoshikawa, K., Shimada, M., Miyamoto, H., Higashijima, J., Miyatani, T., Nishioka, M., Kurita, N., Iwata, T. & Uehara, H. Sonic hedgehog relates to colorectal carcinogenesis. *Journal of Gastroenterology* **44**, 1113-1117, doi:10.1007/s00535-009-0110-2 (2009).
75 Douard, R., Moutereau, S., Pernet, P., Chimingqi, M., Allory, Y., Manivet, P., Conti, M., Vaubourdolle, M., Cugnenc, P. H. & Loric, S. Sonic Hedgehog-dependent proliferation in a series of patients with colorectal cancer. *Surgery* **139**, 665-670, doi:10.1016/j.surg.2005.10.012 (2006).
76 Varnat, F., Duquet, A., Malerba, M., Zbinden, M., Mas, C., Gervaz, P. & Ruiz i Altaba, A. Human colon cancer epithelial cells harbour active HEDGEHOG-GLI signalling that is essential for tumour growth, recurrence, metastasis and stem cell survival and expansion. *EMBO Molecular Medicine* **1**, 338-351, doi:10.1002/emmm.200900039 (2009).
77 Katoh, Y. & Katoh, M. Hedgehog signaling, epithelial-to-mesenchymal transition and miRNA (review). *Internation Jounal of Molecular Medicine* **22**, 271-275 (2008).
78 K. A. Higgins, K. S. W. a. A. P. Characterizing the clinical relevance of epithelial mesenchymal transition (EMT) in human tumors. *Journal of Clinical Oncology (Meeting Abstracts)* **28** (2010).

79 Cooper, M. K., Porter, J. A., Young, K. E. & Beachy, P. A. Teratogen-mediated inhibition of target tissue response to Shh signaling. *Science* **280**, 1603-1607 (1998).
80 Incardona, J. P., Gaffield, W., Kapur, R. P. & Roelink, H. The teratogenic Veratrum alkaloid cyclopamine inhibits sonic hedgehog signal transduction. *Development* **125**, 3553-3562 (1998).
81 Wan, J., Zhou, J., Zhao, H., Wang, M., Wei, Z., Gao, H., Wang, Y. & Cui, H. Sonic hedgehog pathway contributes to gastric cancer cell growth and proliferation. *BioResearch open access* **3**, 53-59, doi:10.1089/biores.2014.0001 (2014).
82 Chen, J. K., Taipale, J., Cooper, M. K. & Beachy, P. A. Inhibition of Hedgehog signaling by direct binding of cyclopamine to Smoothened. *Genes & Development* **16**, 2743-2748, doi:10.1101/gad.1025302 (2002).
83 Sekulic, A., Migden, M. R., Oro, A. E., Dirix, L., Lewis, K. D., Hainsworth, J. D., Solomon, J. A., Yoo, S., Arron, S. T., Friedlander, P. A., Marmur, E., Rudin, C. M., Chang, A. L., Low, J. A., Mackey, H. M., Yauch, R. L., Graham, R. A., Reddy, J. C. & Hauschild, A. Efficacy and safety of vismodegib in advanced basal-cell carcinoma. *The New England Journal of Medicine* **366**, 2171-2179, doi:10.1056/NEJMoa1113713 (2012).
84 Chang, A. L. & Oro, A. E. Initial assessment of tumor regrowth after vismodegib in advanced Basal cell carcinoma. *Archives of Dermatology* **148**, 1324-1325, doi:10.1001/archdermatol.2012.2354 (2012).
85 LoRusso, P. M., Rudin, C. M., Reddy, J. C., Tibes, R., Weiss, G. J., Borad, M. J., Hann, C. L., Brahmer, J. R., Chang, I., Darbonne, W. C., Graham, R. A., Zerivitz, K. L., Low, J. A. & Von Hoff, D. D. Phase I trial of hedgehog pathway inhibitor vismodegib (GDC-0449) in patients with refractory, locally advanced or metastatic solid tumors. *Clinical Cancer Research* **17**, 2502-2511, doi:10.1158/1078-0432.CCR-10-2745 (2011).
86 Singh, B. N., Fu, J., Srivastava, R. K. & Shankar, S. Hedgehog signaling antagonist GDC-0449 (Vismodegib) inhibits pancreatic cancer stem cell characteristics: molecular mechanisms. *Public Library of Science One* **6**, e27306, doi:10.1371/journal.pone.0027306 (2011).
87 Sekulic, A., Migden, M. R., Oro, A. E., Dirix, L., Lewis, K. D., Hainsworth, J. D., Solomon, J. A., Yoo, S., Arron, S. T., Friedlander, P. A., Marmur, E., Rudin, C. M., Chang, A. L., Low, J. A., Mackey, H. M., Yauch, R. L., Graham, R. A., Reddy, J. C. & Hauschild, A. Efficacy and safety of vismodegib in advanced basal-cell carcinoma. *The New England Journal of Medicine* **366**, 2171-2179, doi:10.1056/NEJMoa1113713 (2012).
88 Stanton, B. Z., Peng, L. F., Maloof, N., Nakai, K., Wang, X., Duffner, J. L., Taveras, K. M., Hyman, J. M., Lee, S. W., Koehler, A. N., Chen, J. K., Fox, J. L., Mandinova, A. & Schreiber, S. L. A small molecule that binds Hedgehog and blocks its signaling in human cells. *Nature Chemical Biology* **5**, 154-156, doi:10.1038/nchembio.142 (2009).
89 Firestone, A. J., Weinger, J. S., Maldonado, M., Barlan, K., Langston, L. D., O'Donnell, M., Gelfand, V. I., Kapoor, T. M. & Chen, J. K. Small-molecule inhibitors of the AAA+ ATPase motor cytoplasmic dynein. *Nature* **484**, 125-129, doi:10.1038/nature10936 (2012).
90 Lauth, M., Bergstrom, A., Shimokawa, T. & Toftgard, R. Inhibition of GLI-mediated transcription and tumor cell growth by small-molecule antagonists. *Proceedings of the National Academy of Sciences of the United States of America* **104**, 8455-8460, doi:10.1073/pnas.0609699104 (2007).

91 Berman, D. M., Karhadkar, S. S., Hallahan, A. R., Pritchard, J. I., Eberhart, C. G., Watkins, D. N., Chen, J. K., Cooper, M. K., Taipale, J., Olson, J. M. & Beachy, P. A. Medulloblastoma growth inhibition by hedgehog pathway blockade. *Science* **297**, 1559-1561, doi:10.1126/science.1073733 (2002).
92 Adewumi, O., Aflatoonian, B., Ahrlund-Richter, L., Amit, M., Andrews, P. W., Beighton, G., Bello, P. A., Benvenisty, N., Berry, L. S., Bevan, S., Blum, B., Brooking, J., Chen, K. G., Choo, A. B., Churchill, G. A., Corbel, M., Damjanov, I., Draper, J. S., Dvorak, P., Emanuelsson, K., Fleck, R. A., Ford, A., Gertow, K., Gertsenstein, M., Gokhale, P. J., Hamilton, R. S., Hampl, A., Healy, L. E., Hovatta, O., Hyllner, J., Imreh, M. P., Itskovitz-Eldor, J., Jackson, J., Johnson, J. L., Jones, M., Kee, K., King, B. L., Knowles, B. B., Lako, M., Lebrin, F., Mallon, B. S., Manning, D., Mayshar, Y., McKay, R. D., Michalska, A. E., Mikkola, M., Mileikovsky, M., Minger, S. L., Moore, H. D., Mummery, C. L., Nagy, A., Nakatsuji, N., O'Brien, C. M., Oh, S. K., Olsson, C., Otonkoski, T., Park, K. Y., Passier, R., Patel, H., Patel, M., Pedersen, R., Pera, M. F., Piekarczyk, M. S., Pera, R. A., Reubinoff, B. E., Robins, A. J., Rossant, J., Rugg-Gunn, P., Schulz, T. C., Semb, H., Sherrer, E. S., Siemen, H., Stacey, G. N., Stojkovic, M., Suemori, H., Szatkiewicz, J., Turetsky, T., Tuuri, T., van den Brink, S., Vintersten, K., Vuoristo, S., Ward, D., Weaver, T. A., Young, L. A. & Zhang, W. Characterization of human embryonic stem cell lines by the International Stem Cell Initiative. *Nature Biotechnology* **25**, 803-816, doi:10.1038/nbt1318 (2007).
93 Wang, Y., Zhou, Z., Walsh, C. T. & McMahon, A. P. Selective translocation of intracellular Smoothened to the primary cilium in response to Hedgehog pathway modulation. *Proceedings of the National Academy of Sciences of the United States of America* **106**, 2623-2628, doi:10.1073/pnas.0812110106 (2009).
94 Chen, J. K., Taipale, J., Young, K. E., Maiti, T. & Beachy, P. A. Small molecule modulation of Smoothened activity. *Proceedings of the National Academy of Sciences of the United States of America* **99**, 14071-14076, doi:10.1073/pnas.182542899 (2002).
95 Kolterud, Å. T., R. Strategies for Hedgehog inhibition and its potential role in cancer treatment. *Drug Discovery Today Therapeutic Strategies* **4**, 229-235 (2007).
96 Hanahan, D. & Weinberg, R. A. The hallmarks of cancer. *Cell* **100**, 57-70 (2000).
97 Lobo, N. A., Shimono, Y., Qian, D. & Clarke, M. F. The biology of cancer stem cells. *Annual Review of Cell and Developmental Biology* **23**, 675-699, doi:10.1146/annurev.cellbio.22.010305.104154 (2007).
98 Omar, A., Reusch, U., Knackmuss, S., Little, M. & Weiss, S. F. Anti-LRP/LR-specific antibody IgG1-iS18 significantly reduces adhesion and invasion of metastatic lung, cervix, colon and prostate cancer cells. *Journal of Molecular Biology* **419**, 102-109, doi:10.1016/j.jmb.2012.02.035 (2012).
99 Li, L. & Neaves, W. B. Normal stem cells and cancer stem cells: the niche matters. *Cancer Research* **66**, 4553-4557, doi:10.1158/0008-5472.CAN-05-3986 (2006).
100 Behrens, J. The role of cell adhesion molecules in cancer invasion and metastasis. *Breast Cancer Research and Treatment* **24**, 175-184 (1993).
101 Takebe, N., Miele, L., Harris, P. J., Jeong, W., Bando, H., Kahn, M., Yang, S. X. & Ivy, S. P. Targeting Notch, Hedgehog, and Wnt pathways in cancer stem cells: clinical update. *Nature Reviews Clinical Oncology* **12**, 445-464, doi:10.1038/nrclinonc.2015.61 (2015).
102 Vermeulen, L., Todaro, M., de Sousa Mello, F., Sprick, M. R., Kemper, K., Perez Alea, M., Richel, D. J., Stassi, G. & Medema, J. P. Single-cell cloning of colon cancer stem cells reveals a multi-lineage differentiation capacity. *Proceedings of the*

National Academy of Sciences of the United States of America **105**, 13427-13432, doi:10.1073/pnas.0805706105 (2008).

103 Choi, D., Lee, H. W., Hur, K. Y., Kim, J. J., Park, G. S., Jang, S. H., Song, Y. S., Jang, K. S. & Paik, S. S. Cancer stem cell markers CD133 and CD24 correlate with invasiveness and differentiation in colorectal adenocarcinoma. *World Journal of Gastroenterology* **15**, 2258-2264 (2009).

104 Hermann, P. C., Huber, S. L., Herrler, T., Aicher, A., Ellwart, J. W., Guba, M., Bruns, C. J. & Heeschen, C. Distinct populations of cancer stem cells determine tumor growth and metastatic activity in human pancreatic cancer. *Cell Stem Cell* **1**, 313-323, doi:10.1016/j.stem.2007.06.002 (2007).

105 Todaro, M., Alea, M. P., Di Stefano, A. B., Cammareri, P., Vermeulen, L., Iovino, F., Tripodo, C., Russo, A., Gulotta, G., Medema, J. P. & Stassi, G. Colon cancer stem cells dictate tumor growth and resist cell death by production of interleukin-4. *Cell Stem Cell* **1**, 389-402, doi:10.1016/j.stem.2007.08.001 (2007).

106 Beier, D., Hau, P., Proescholdt, M., Lohmeier, A., Wischhusen, J., Oefner, P. J., Aigner, L., Brawanski, A., Bogdahn, U. & Beier, C. P. CD133(+) and CD133(-) glioblastoma-derived cancer stem cells show differential growth characteristics and molecular profiles. *Cancer Research* **67**, 4010-4015, doi:10.1158/0008-5472.CAN-06-4180 (2007).

107 Clarke, M. F., Dick, J. E., Dirks, P. B., Eaves, C. J., Jamieson, C. H., Jones, D. L., Visvader, J., Weissman, I. L. & Wahl, G. M. Cancer stem cells--perspectives on current status and future directions: AACR Workshop on cancer stem cells. *Cancer Research* **66**, 9339-9344, doi:10.1158/0008-5472.CAN-06-3126 (2006).

108 Takahashi, K. & Yamanaka, S. Induction of pluripotent stem cells from mouse embryonic and adult fibroblast cultures by defined factors. *Cell* **126**, 663-676, doi:10.1016/j.cell.2006.07.024 (2006).

109 El-Karim, E. A., Hagos, E. G., Ghaleb, A. M., Yu, B. & Yang, V. W. Kruppel-like factor 4 regulates genetic stability in mouse embryonic fibroblasts. *Molecular Cancer* **12**, 89, doi:10.1186/1476-4598-12-89 (2013).

110 Stefkova, K., Prochazkova, J. & Pachernik, J. Alkaline phosphatase in stem cells. *Stem Cells International* **2015**, 628368, doi:10.1155/2015/628368 (2015).

111 Sanchez, P. & Ruiz i Altaba, A. In vivo inhibition of endogenous brain tumors through systemic interference of Hedgehog signaling in mice. *Mechanisms of Development* **122**, 223-230, doi:10.1016/j.mod.2004.10.002 (2005).

112 Tabs, S. & Avci, O. Induction of the differentiation and apoptosis of tumor cells in vivo with efficiency and selectivity. *European Journal of Dermatology* **14**, 96-102 (2004).

113 Malhotra, U. Inhibiting the Hedgehog Pathway for Cancer Therapy. Date accessed: 12/05/2015 < http://www.targetedonc.com/publications/targeted-therapies-cancer/2013/oct-2013/inhibiting-the-hedgehog-pathway-for-cancer-therapy>

114 Romer, J. T., Kimura, H., Magdaleno, S., Sasai, K., Fuller, C., Baines, H., Connelly, M., Stewart, C. F., Gould, S., Rubin, L. L. & Curran, T. Suppression of the Shh pathway using a small molecule inhibitor eliminates medulloblastoma in Ptc1(+/-)p53(-/-) mice. *Cancer Cell* **6**, 229-240, doi:10.1016/j.ccr.2004.08.019 (2004).

115 Sporn, M. B. The war on cancer. *Lancet* **347**, 1377-1381 (1996).

116 Liu, C., Kelnar, K., Liu, B., Chen, X., Calhoun-Davis, T., Li, H., Patrawala, L., Yan, H., Jeter, C., Honorio, S., Wiggins, J. F., Bader, A. G., Fagin, R., Brown, D. & Tang, D. G. The microRNA miR-34a inhibits prostate cancer stem cells and metastasis by directly repressing CD44. *Nature Medicine* **17**, 211-215, doi:10.1038/nm.2284 (2011).

117 Croker, A. K., Goodale, D., Chu, J., Postenka, C., Hedley, B. D., Hess, D. A. & Allan, A. L. High aldehyde dehydrogenase and expression of cancer stem cell markers selects for breast cancer cells with enhanced malignant and metastatic ability. *Journal of Cellular and Molecular Medicine* **13**, 2236-2252, doi:10.1111/j.1582-4934.2008.00455.x (2009).
118 Lipinski, R. J., Hutson, P. R., Hannam, P. W., Nydza, R. J., Washington, I. M., Moore, R. W., Girdaukas, G. G., Peterson, R. E. & Bushman, W. Dose- and route-dependent teratogenicity, toxicity, and pharmacokinetic profiles of the hedgehog signaling antagonist cyclopamine in the mouse. *Toxicological Sciences* **104**, 189-197, doi:10.1093/toxsci/kfn076 (2008).
119 Omar, A., Jovanovic, K., Da Costa Dias, B., Gonsalves, D., Moodley, K., Caveney, R., Mbazima, V. & Weiss, S. F. Patented biological approaches for the therapeutic modulation of the 37 kDa/67 kDa laminin receptor. *Expert Opinion on Therapeutic Patents* **21**, 35-53, doi:10.1517/13543776.2011.539203 (2011).
120 Magi, S., Tashiro, E. & Imoto, M. A chemical genomic study identifying diversity in cell migration signaling in cancer cells. *Scientific Reports* **2**, 823, doi:10.1038/srep00823 (2012).
121 Todaro, M., Gaggianesi, M., Catalano, V., Benfante, A., Iovino, F., Biffoni, M., Apuzzo, T., Sperduti, I., Volpe, S., Cocorullo, G., Gulotta, G., Dieli, F., De Maria, R. & Stassi, G. CD44v6 is a marker of constitutive and reprogrammed cancer stem cells driving colon cancer metastasis. *Cell Stem Cell* **14**, 342-356, doi:10.1016/j.stem.2014.01.009 (2014).
122 Dijkgraaf, G. J., Alicke, B., Weinmann, L., Januario, T., West, K., Modrusan, Z., Burdick, D., Goldsmith, R., Robarge, K., Sutherlin, D., Scales, S. J., Gould, S. E., Yauch, R. L. & de Sauvage, F. J. Small molecule inhibition of GDC-0449 refractory smoothened mutants and downstream mechanisms of drug resistance. *Cancer Research* **71**, 435-444, doi:10.1158/0008-5472.CAN-10-2876 (2011).
123 Metcalfe, C. & de Sauvage, F. J. Hedgehog fights back: mechanisms of acquired resistance against Smoothened antagonists. *Cancer Research* **71**, 5057-5061, doi:10.1158/0008-5472.CAN-11-0923 (2011).
124 Rudin, C. M., Hann, C. L., Laterra, J., Yauch, R. L., Callahan, C. A., Fu, L., Holcomb, T., Stinson, J., Gould, S. E., Coleman, B., LoRusso, P. M., Von Hoff, D. D., de Sauvage, F. J. & Low, J. A. Treatment of medulloblastoma with hedgehog pathway inhibitor GDC-0449. *The New England Journal of Medicine* **361**, 1173-1178, doi:10.1056/NEJMoa0902903 (2009).
125 Madison, B. B., Braunstein, K., Kuizon, E., Portman, K., Qiao, X. T. & Gumucio, D. L. Epithelial hedgehog signals pattern the intestinal crypt-villus axis. *Development* **132**, 279-289, doi:10.1242/dev.01576 (2005).
126 Batsaikhan, B. E., Yoshikawa, K., Kurita, N., Iwata, T., Takasu, C., Kashihara, H. & Shimada, M. Cyclopamine decreased the expression of Sonic Hedgehog and its downstream genes in colon cancer stem cells. *Anticancer Research* **34**, 6339-6344 (2014).

9. APPENDIX

APPENDIX A
Cell line data sheets:

DLD-1 (ATCC® CCL-221™)

Organism	*Homo sapiens*, human
Tissue	Colon
Cell Type	Epithelial
Morphology	Epithelial
Culture Properties	Adherent
Biosafety Level	1
Disease	Dukes' type C, colorectal adenocarcinoma
Age	Adult
Gender	Male
Applications	This cell line is a suitable transfection host.
Derivation	DLD-1 is one of two colorectal adenocarcinoma cell lines which were isolated by D.L. Dexter and associates during a period from 1977-1979
Oncogene	myc +; myb + ; ras +; fos +; sis +; p53 +; abl -; ros -; src -
Genes Expressed	carcinoembryonic antigen (CEA) 0.5 ng/106 cells/10 days; colon antigen 3.
Cellular Products	carcinoembryonic antigen (CEA) 0.5 ng/10 exp6 cells/10 days; colon antigen 3; keratin
Tumorigenic	Yes
Effects	Yes, in nude mice (Tumours developed within 21 days at 100% frequency (5/5) in nude mice inoculated subcutaneously with 10(7) cells)

HT29 (ATCC® HTB-38™)

Organism	*Homo sapiens*, human
Tissue	Colon
Morphology	Epithelial
Culture Properties	Adherent
Biosafety Level	1
Disease	colorectal adenocarcinoma
Age	44 years adult
Gender	Female
Ethnicity	Caucasian
Applications	This cell line is a suitable transfection host.
Derivation	The HT-29 line was isolated from a primary tumour in 1964 by J. Fogh using the explant culture method.
Oncogene	myc +; ras +; myb +; fos +; sis +; p53 +; abl -; ros -; src -
Genes Expressed	secretory component of IgA; carcinoembryonic antigen (CEA); transforming growth factor beta binding protein; mucin,myc +; ras +; myb +; fos +; sis +; p53 +; abl -; ros -; src -,Blood Type A; Rh+; HLA A1, A3, B12, B17, Cw5,HT-29 cells are negative for CD4, but there is cell surface expression of galactoseceramide (a possible alternative receptor for HIV).
Cellular Products	secretory component of IgA; carcinoembryonic antigen (CEA); transforming growth factor beta binding protein; mucin
Tumorigenic	Yes
Effects	Yes, in nude mice; forms well differentiated adenocarcinoma consistent with colonic primary (grade I); tumours also form in steroid treated hamsters

SW480 [SW-480] (ATCC® CCL-228™)

Organism	*Homo sapiens*, human
Tissue	Colon
Morphology	Epithelial
Culture Properties	Adherent
Biosafety Level	1
Disease	Dukes' type B, colorectal adenocarcinoma
Age	50 years
Gender	Male
Ethnicity	Caucasian
Applications	This cell line is a suitable transfection host. This line has a mutation in codon 12 of the ras proto-oncogene, and can be used as a positive control for PCR assays of mutation in this codon.
Derivation	SW480 was established from a primary adenocarcinoma of the colon.
Oncogene	myc +; myb + ; ras +; fos +; sis +; p53 +; abl -; ros -; src -
Genes Expressed	carcinoembryonic antigen (CEA) 0.7 ng/10 6 cells/10 days; keratin; transforming growth factor beta,myc +; myb + ; ras +; fos +; sis +; p53 +; abl -; ros -; src -,HLA A2, B8, B17; blood type A; Rh+,The cells are positive for keratin by immunoperoxidasestaining.,The line is positive for expression of c-myc, K-ras, H-ras, N-ras, myb, sis and fos oncogenes.
Cellular Products	carcinoembryonic antigen (CEA) 0.7 ng/10 exp6 cells/10 days; keratin; transforming growth factor beta
Tumorigenic	Yes. Tumours developed within 21 days at 100% frequency (5/5) in nude mice inoculated subcutaneously with 10(7) cells.
Effects	Yes, in nude mice

APPENDIX B

Results: Microscopy controls

Localization of CD133 expression in DLD1 and HT29 cells

A.) DLD1 CD133+

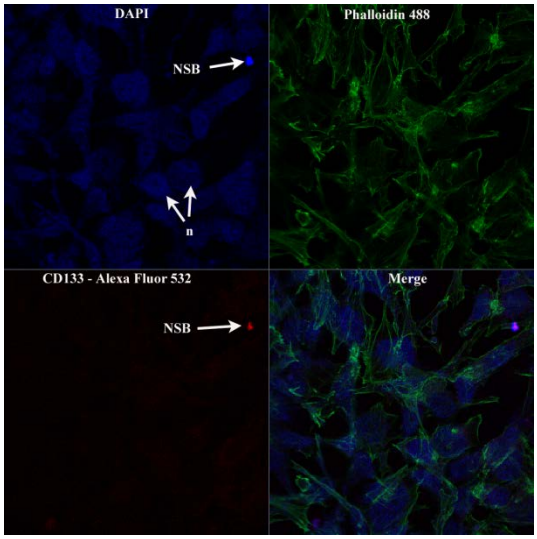
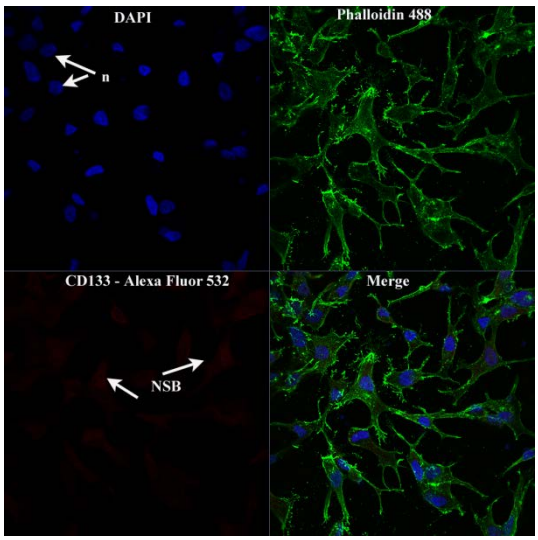


Table A: Corrected Total Cell Fluorescence (CTCF) of DLD1 CD133- cells (non-permeabilized); negative control

	Integrated density	Area of selected cell	Background fluorescence	CTCF
	1414	646	0.111	1342.294
	1472	694	0.111	1394.966
	1571	874	0.111	1473.986
Average CTCF				1403.749

B.) HT29 CD133+



C.)HT29 CD133-

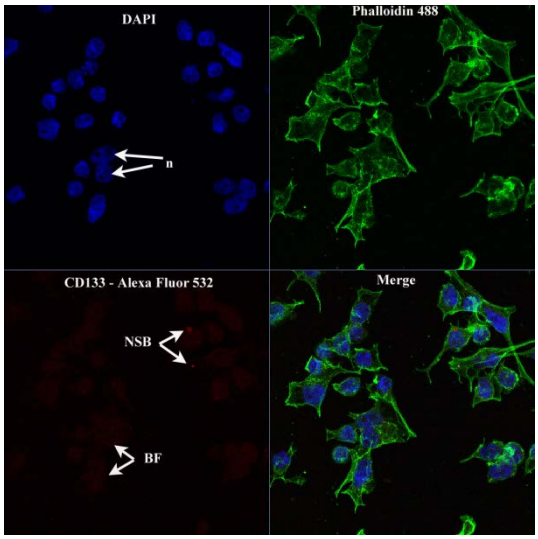


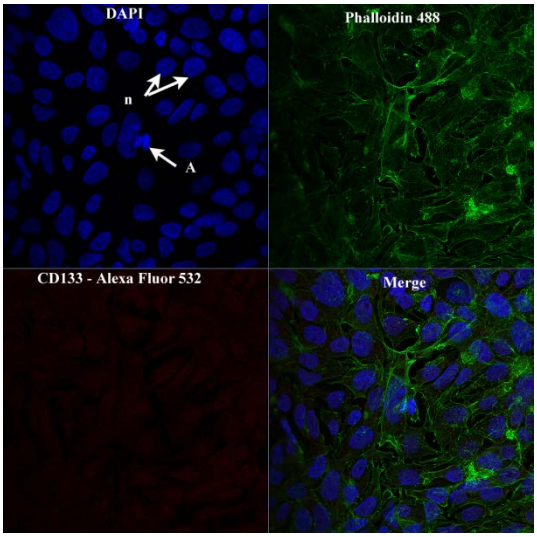
Table B: Corrected Total Cell Fluorescence (CTCF) of HT29 CD133+ cells (non-permeabilized); negative control

	Integrated density	Area of selected cell	Background fluorescence	CTCF
	1270	448	0.011	1265.072
	1069	820	0.011	1059.98
	1176	844	0.011	1166.716
Average CTCF				1163.923

Table C: Corrected Total Cell Fluorescence (CTCF) of HT29 CD133- cells (non-permeabilized); negative control

	Integrated density	Area of selected cell	Background fluorescence	CTCF
	736	340	0.087	706.42
	867	377	0.087	834.201
	705	401	0.087	670.113
Average CTCF				736.9113

D.) DLD1 CD133+



E.) DLD1 CD133-

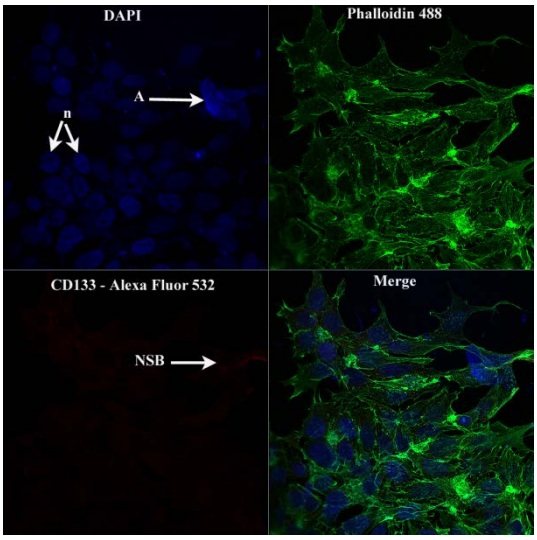


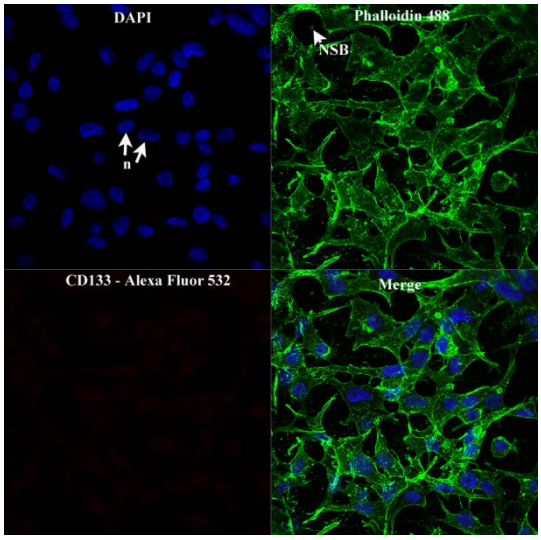
Table D: Corrected Total Cell Fluorescence (CTCF) of DLD1 CD133+ cells (permeabilized); negative control

	Integrated density	Area of selected cell	Background fluorescence	CTCF
	1837	565	0.161	1746.035
	1799	1136	0.161	1616.104
	1682	703	0.161	1568.817
Average CTCF				1643.652

Table E: Corrected Total Cell Fluorescence (CTCF) of DLD1 CD133- cells (permeabilized); negative control

	Integrated density	Area of selected cell	Background fluorescence	CTCF
	658	559	0	658
	641	533	0	641
	613	810	0	613
Average CTCF				637.3333

F.) HT29 CD133+



G.) HT29 CD133-

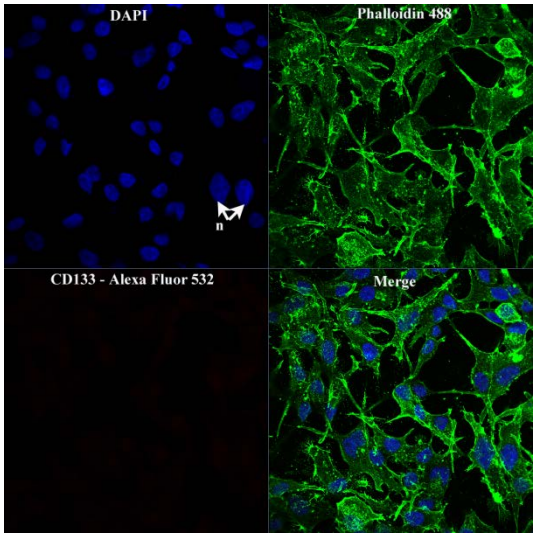


Table F: Corrected Total Cell Fluorescence (CTCF) of HT29 CD133+ (permeabilized); negative control

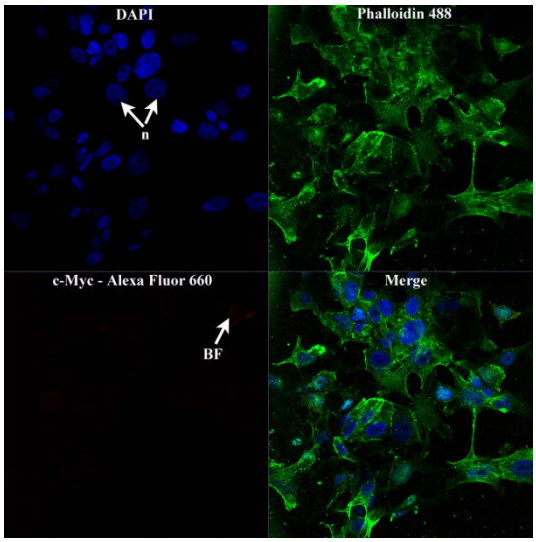
	Integrated density	Area of selected cell	Background fluorescence	CTCF
	519	171	0.033	513.357
	544	334	0.033	532.978
	608	325	0.033	597.275
Average CTCF				547.87

Table G: Corrected Total Cell Fluorescence (CTCF) of HT29 CD133- (permeabilized); negative control

	Integrated density	Area of selected cell	Background fluorescence	CTCF
	221	416	0.028	209.352
	301	472	0.028	287.784
	364	524	0.028	349.328
Average CTCF				282.1547

Expression of c-Myc

H.) DLD1 CD133+



I.) DLD1 CD133-

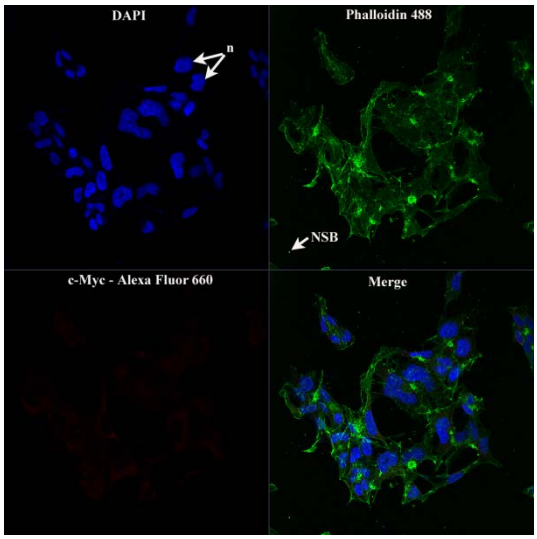


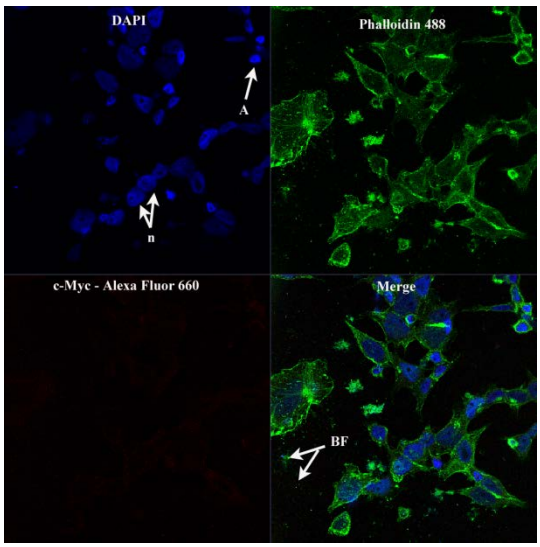
Table H: Corrected Total Cell Fluorescence (CTCF) of DLD1 CD133+ cells; negative control

	Integrated density	Area of selected cell	Background fluorescence	CTCF
	260	447	0.089	220.217
	181	493	0.089	137.123
	165	390	0.089	130.29
Average CTCF				162.5433

Table I: Corrected Total Cell Fluorescence (CTCF) of DLD1 CD133- cells; negative control

	Integrated density	Area of selected cell	Background fluorescence	CTCF
	733	572	0	733
	665	520	0	665
	581	964	0	581
Average CTCF				659.6667

J.) HT29 CD133+



K.) HT29 CD133-

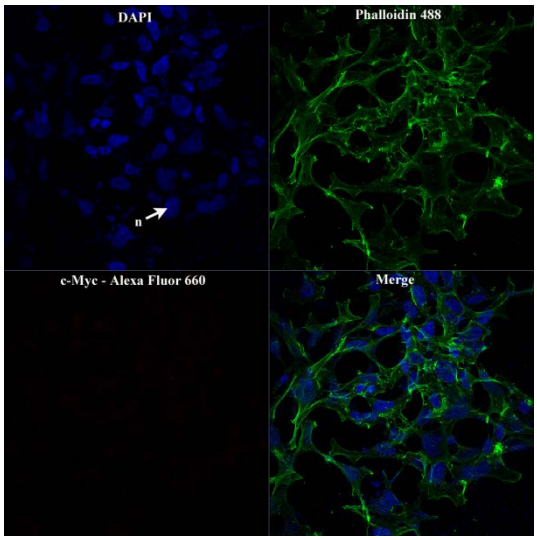


Table J: Corrected Total Cell Fluorescence (CTCF) of HT29 CD133+ cells; negative control

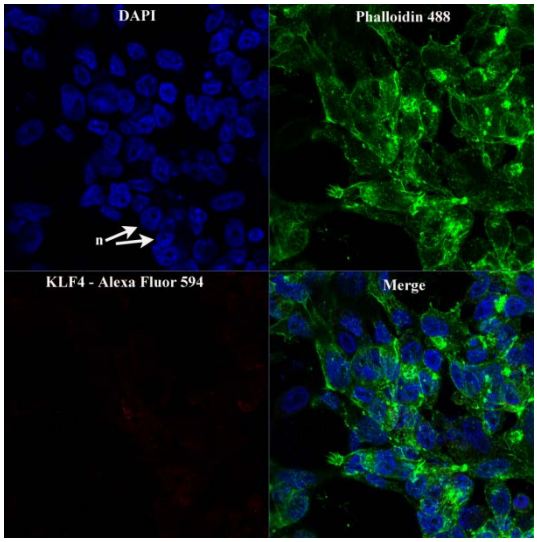
	Integrated density	Area of selected cell	Background fluorescence	CTCF
	402	421	0.168	331.272
	496	703	0.168	377.896
	455	338	0.168	398.216
Average CTCF				369.128

Table K: Corrected Total Cell Fluorescence (CTCF) of HT29 CD133- cells; negative control

	Integrated density	Area of selected cell	Background fluorescence	CTCF
	453	816	0.005	448.92
	403	551	0.005	400.245
	405	547	0.005	402.265
Average CTCF				417.1433

Expression of KLF4

L.) DLD1 CD133+



M.) DLD1 CD133-

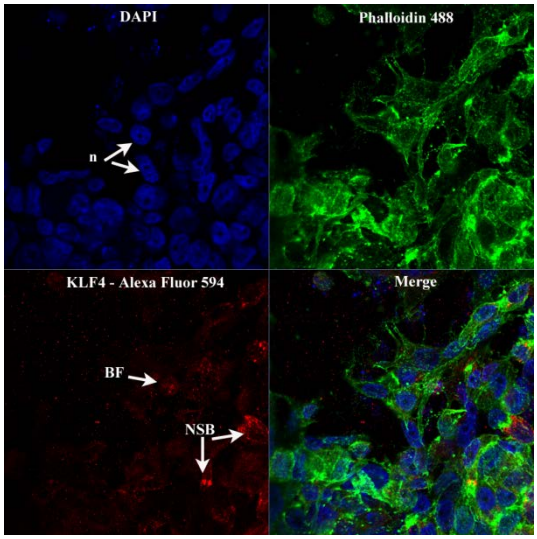


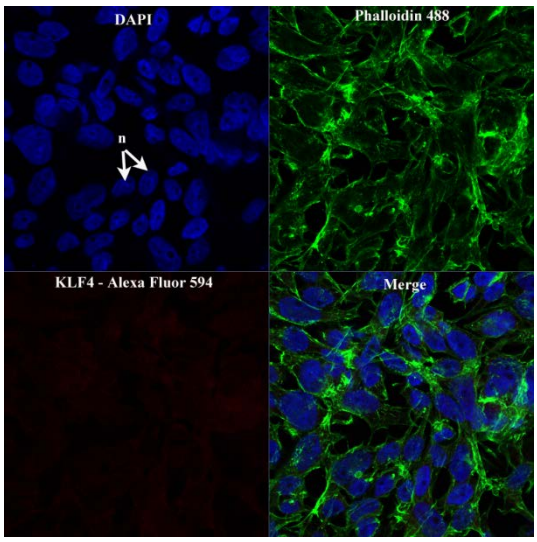
Table L: Corrected Total Cell Fluorescence (CTCF) of DLD1 CD133+ cells; negative control

	Integrated density	Area of selected cell	Background fluorescence	CTCF
	661	618	0.027	644.314
	506	530	0.027	491.69
	523	589	0.027	507.097
Average CTCF				547.7003

Table M: Corrected Total Cell Fluorescence (CTCF) of DLD1 CD133- cells; negative control

	Integrated density	Area of selected cell	Background fluorescence	CTCF
	1597	517	0.519	1328.677
	1649	545	0.519	1366.145
	1666	679	0.519	1313.599
Average CTCF				1336.14

N.) HT29 CD133+



O.) HT29 CD133-

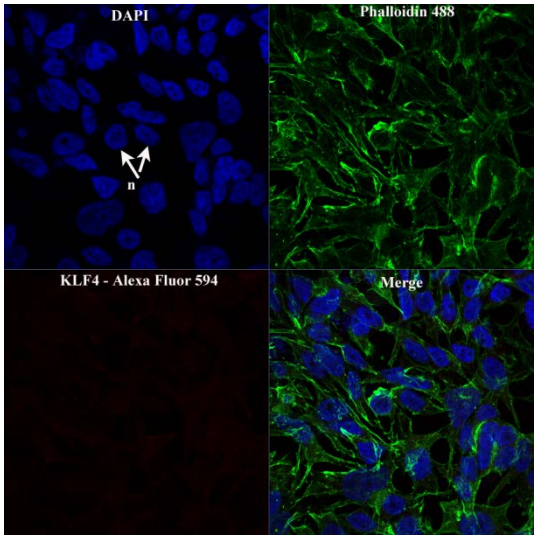


Table N: Corrected Total Cell Fluorescence (CTCF) of HT29 CD133+ cells; negative control

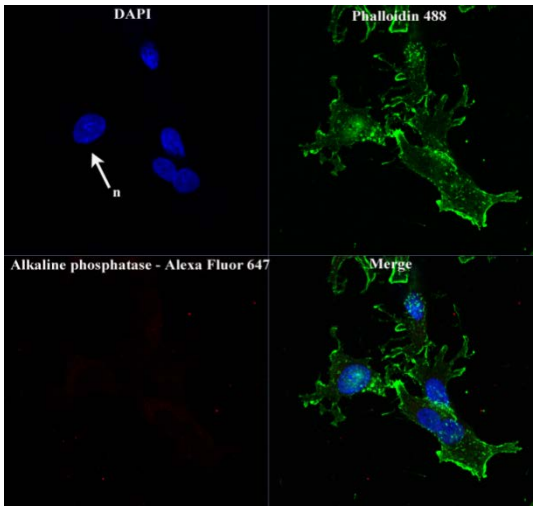
	Integrated density	Area of selected cell	Background fluorescence	CTCF
	1395	779	0.149	1278.929
	1481	547	0.149	1399.497
	1371	612	0.149	1279.812
Average CTCF				1319.413

Table O: Corrected Total Cell Fluorescence (CTCF) of HT29 CD133- cells; negative control

	Integrated density	Area of selected cell	Background fluorescence	CTCF
	581	483	0.092	536.564
	500	546	0.092	449.768
	575	304	0.092	547.032
Average CTCF				511.1213

Expression of alkaline phosphatase

P.) DLD1 CD133+



Q.) DLD1 CD133-

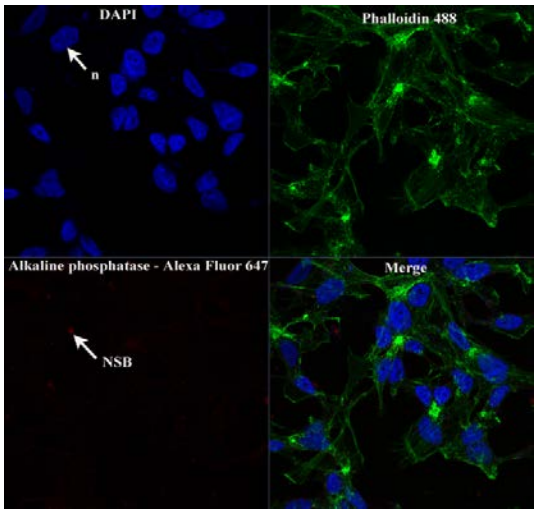


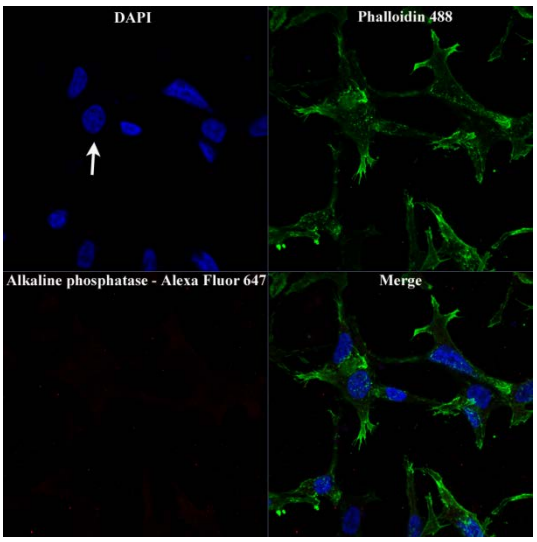
Table P: Corrected Total Cell Fluorescence (CTCF) of DLD1 CD133+ cells; negative control

	Integrated density	Area of selected cell	Background fluorescence	CTCF
	1141	825	0.048	1101.4
	1287	1100	0.048	1234.2
	1268	1554	0.048	1193.408
Average CTCF				1176.336

Table Q: Corrected Total Cell Fluorescence (CTCF) of DLD1 CD133- cells; negative control

	Integrated density	Area of selected cell	Background fluorescence	CTCF
	310	553	0.102	253.594
	348	532	0.102	293.736
	296	626	0.102	232.148
Average CTCF				259.826

R.) HT29 CD133+



S.) HT29 CD133-

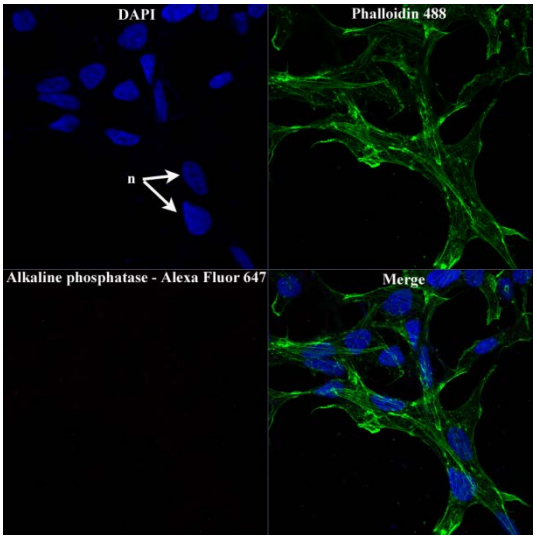


Table R: Corrected Total Cell Fluorescence (CTCF) of HT29 CD133+ cells; negative control

	Integrated density	Area of selected cell	Background fluorescence	CTCF
	681	579	0.141	599.361
	707	543	0.141	630.437
	696	589	0.141	612.951
Average CTCF				614.2497

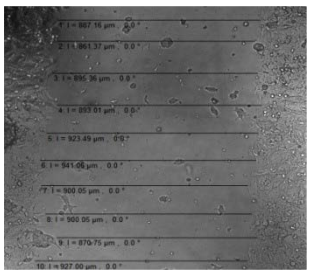
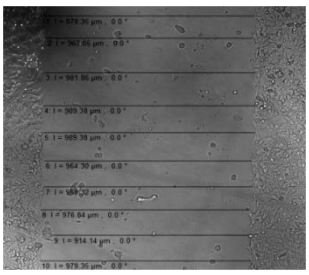
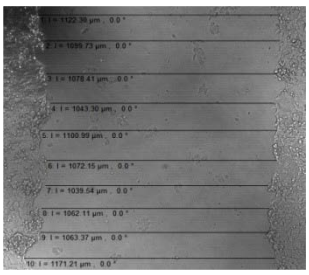
Table S: Corrected Total Cell Fluorescence (CTCF) of HT29 CD133- cells; negative control

	Integrated density	Area of selected cell	Background fluorescence	CTCF
	166	817	0.14	51.62
	175	443	0.14	112.98
	146	393	0.14	90.98
Average CTCF				85.19333

APPENDIX C

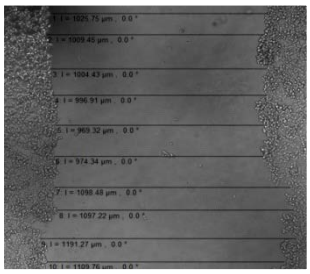
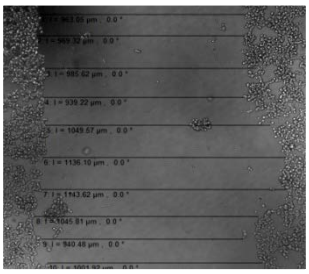
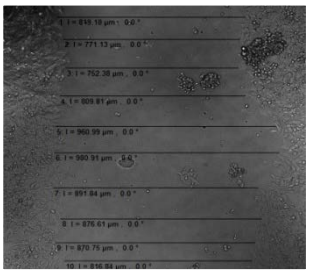
Results: Scratch assay performed with cyclopamine treatment before optimization

DLD1 CD133+ control

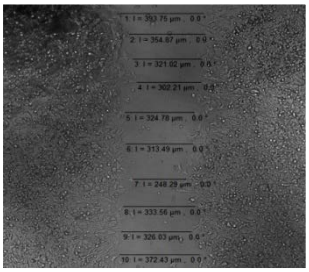
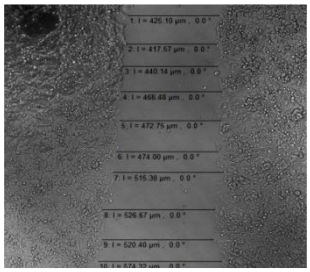
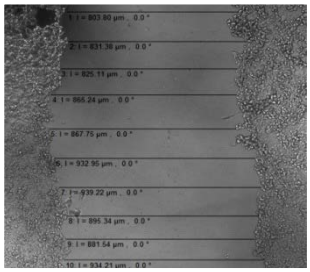
0 hours 6 hours 24 hours

DLD1 CD133+ with cyclopamine

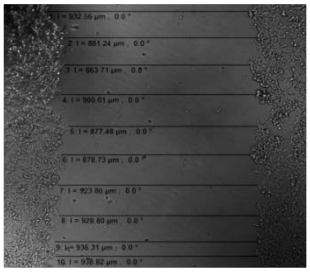
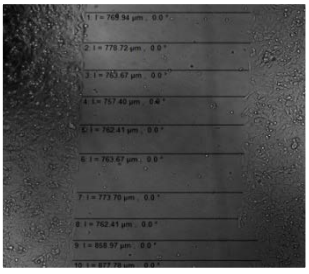
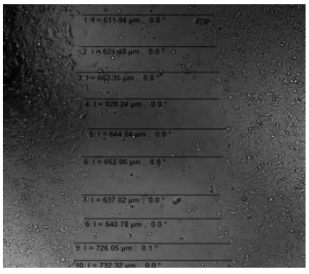
0 hours 6 hours 24 hours

HT29 CD133+ control

0 hours 6 hours 24 hours

HT29 CD133+ with cyclopamine

0 hours 6 hours 24 hours

Scratch assays practiced with implementation of cyclopamine in DLD1+ and HT29+ cell lines over 24 hour period with measurements taken at 0, 6 and 24 hours.

APPENDIX D

Turnitin report:

turnitindraft.docx

by Aadilah Omar

FILE	AADILAH_OMAR_0604004.V_TURNITINDRAFT.DOCX (8.91M)		
TIME SUBMITTED	21-AUG-2015 04:45PM	WORD COUNT	20904
SUBMISSION ID	562672614	CHARACTER COUNT	118012

turnitindraft.docx

ORIGINALITY REPORT

7%	2%	6%	1%
SIMILARITY INDEX	INTERNET SOURCES	PUBLICATIONS	STUDENT PAPERS

PRIMARY SOURCES

1	Sourbier, Carole, Christopher J. Ricketts, Shingo Matsumoto, Daniel R. Crooks, Pei-Jyun Liao, Philip Z. Mannes, Youfeng Yang, Ming-Hui Wei, Gaurav Srivastava, Sanchari Ghosh, Viola Chen, Cathy D. Vocke, Maria Merino, Ramaprasad Srinivasan, Murali C. Krishna, James B. Mitchell, Ann Marie Pendergast, Tracey A. Rouault, Len Neckers, and W. Marston Linehan. "Targeting ABL1-Mediated Oxidative Stress Adaptation in Fumarate Hydratase-Deficient Cancer", Cancer Cell, 2014. Publication	1%
2	Omar, A.. "Anti-LRP/LR-Specific Antibody IgG1-iS18 Significantly Reduces Adhesion and Invasion of Metastatic Lung, Cervix, Colon and Prostate Cancer Cells", Journal of Molecular Biology, 20120525 Publication	1%
3	www.ncp.co.uk Internet Source	<1%
4	www.ableweb.org Internet Source	<1%

APPENDIX E

Ethics waiver:

University
of the Witwatersrand,
Johannesburg

Human Research Ethics Committee (Medical)
(formerly Committee for Research on Human Subjects (Medical))

Secretariat: Research Office, Room SH10005, 10th floor, Senate House • Telephone: +27 11 717-1234 • Fax: +27 11 339-5708
Private Bag 3, Wits 2050, South Africa

Ref: W-CJ-150213-1

15/02/2013

TO WHOM IT MAY CONCERN:

Waiver: This certifies that the following research does not require clearance from the Human Research Ethics Committee (Medical).

Investigator: **Miss A Omar (student no 0604004v).**

Project title: **Inhibition of sonic hedgehog pathway by small molecule inhibitors: targeting colon cancer stem cells.**

Reason: This is a wholly laboratory study using commercial cell lines including HEK293, FHC, HT29, SW480, SW116, Caco2 and DLD1. No humans are involved.

UNIVERSITY OF THE WITWATERSRAND
PROF PE CLEATON - JONES
HREC (MEDICAL)
2013 -02- 15
JOHANNESBURG

Professor Peter Cleaton-Jones
Chair: Human Research Ethics Committee (Medical)

copy: Anisa Keshav / Zanele Ndlovu Research Office, Senate House, Wits